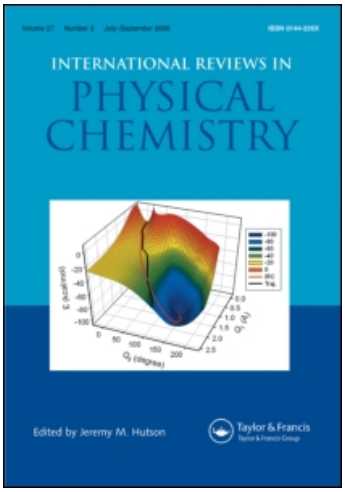

International Reviews in Physical Chemistry
Publication details, including instructions for authors and subscription information:
http://www.informaworld.com/smpp/title~content=t713724383

Growth and characterization of mesoporous silica films

Karen J. Edler; Steve J. Roser

Online publication date: 26 November 2010

To cite this Article Edler, Karen J. and Roser, Steve J.(2001) 'Growth and characterization of mesoporous silica films', International Reviews in Physical Chemistry, 20: 3, 387 — 466
To link to this Article: DOI: 10.1080/01442350118540
URL: http://dx.doi.org/10.1080/01442350118540

INT. REVIEWS IN PHYSICAL CHEMISTRY, 2001, VOL. 20, NO. 3, 387–466

Growth and characterization of mesoporous silica films

KAREN J. EDLER and STEVE J. ROSER
Department of Chemistry, University of Bath, Claverton Down, Bath BA2 7AY, UK

The synthesis of surfactant-templated silicate materials has developed rapidly over the past decade. The uniform controlled pore sizes created in the amorphous silicate framework by this method show promise as catalyst supports, sensors, filtration membranes and in a variety of optoelectronic applications. Formation of these materials in a thin-film or membrane geometry is therefore an active area of research. This review covers the methods currently used to produce thin-film silicate–surfactant composites, with an emphasis on the mechanism of mesostructure formation and the types of composite structure formed in each case. Solvent evaporation methods such as dip coating, spin coating and casting are treated first, followed by methods involving the spontaneous growth of the surfactant–silicate composite as either a self-supporting film or on a substrate such as mica, graphite or silicon.

Contents

International Reviews in Physical Chemistry ISSN 0144–235X print/ISSN 1366–591X online
http://www.tandf.co.uk/journals
DOI: 10.1080/01442350110054910

1. Introduction

1.1. *Porous silicates*

Porous materials have long been of interest in industrial fields as catalytic supports and adsorbents. Many different types of porous material have been used in these applications, ranging from activated carbons to zeolites. More specifically, silica-based systems such as clays, silica gels and zeolites have been used in many catalytic processes and adsorption and separation applications. ZSM-5 is used as a catalyst for conversion of natural gas to motor fuel (Flanigen 1980). Zeolites A and X are used in detergents to soften water by removal of calcium and magnesium ions via ion exchange (Flanigen 1980). Porous silica gels have been used in filtration, chromatography, and thermal and acoustic insulation, and as desiccants (Brinker and Scherer 1990). These, however, each have a range of practical use dictated by the size, shape and selectivity of the pores in the material and each has a distinct manner of preparation to produce the required pore structure.

Microporous materials are those having pore sizes between 5 and 20 Å. The most widely used microporous systems are those with well-defined pore geometries, namely zeolites. Zeolites are crystalline aluminosilicates where the channel structure may be one dimensional (1D) or two dimensional (2D). The channels in these materials are part of the crystal lattice of the material and so are highly monodisperse and have fixed directionality within the crystal. They have a pore size range between about 4 and 7 Å (Flanigen 1980), since the size and shape of these holes are determined by the stability of large rings made up of alternating silicon and oxygen atoms. The widest aperture in conventional aluminosilicate zeolites is a ring of 12

tetrahedral atoms and is 7.4 Å in diameter (Olson 1970, Cheng *et al.* 1995b). The uniformity of the channels in zeolitic systems means that they are extremely selective adsorbents for small molecules of particular molecular geometries and sizes (Flanigen 1980, Suib 1993, Haag 1994) and so make highly selective catalytic supports and adsorbents. However, the narrow range of pore sizes available and the relatively small cross-section of those pores restricts the size of molecules that may escape from or enter the pores to access catalytic or adsorption sites. This limits their use in applications involving larger organic molecules.

Mesoporous materials are defined as those having pores with diameters between 20 and 500 Å (between 2 and 50 nm). Silicate materials with pores in this size range include silica gels, aerogels, xerogels and various types of etched membrane. Porous silica gels are generally prepared via sol–gel methods, in which molecular or colloidal silicate species are dispersed in a solvent and then form a gel, which may lose solvent as the condensation of the silica proceeds. The silica walls in these materials are amorphous, showing no long-range order. The pores in these materials are a result of the process of gelation, which depends upon the reaction conditions (e.g. temperature and pH), and the solvents and reagents used (Brinker and Scherer 1990). Other porous materials include modified layered materials, such as pillared smectite clays and layered double hydroxides, as well as porous glasses. Generally these materials have larger pores than zeolites, but the distribution of pore sizes is also larger, and the pores exist as a disordered network throughout the solid. This lack of uniformity is reflected in a corresponding lack of selectivity in adsorption and catalysis applications. They provide relatively high-surface-area inert supports for catalysts and can be prepared at various densities. Aerogel materials prepared by supercritical drying of wet gels may have densities as low as $0.003\,g\,cm^{-3}$ with porosities of 98% (Hrubesh 1990) and surface areas of more than $1000\,m^2\,g^{-1}$ (Brinker and Scherer 1990). They are used as Cerenkov detectors in particle physics applications and as window and bulk insulation. It has been suggested that aerogels could be used as gas filters or that metal-loaded aerogels could be used as catalyst beds in the petroleum industry (Hrubesh 1990). The distribution of pore sizes in these materials is about 10–500 Å. In xerogels, which are air-dried gels with a surface area of $500–900\,m^2\,g^{-1}$, the pore diameters can range from 10 to 200 Å within the one sample (Brinker and Scherer 1990). Xerogels are used as catalysts and catalyst supports, for the entrapment of sensor molecules, as filtration membranes and in composite formation.

1.2. *Ordered mesoporous silicates*

Ordered mesoporous materials share characteristics of both gels and zeolites. They contain ordered uniform pore systems similar to those of the microporous zeolites, but the pores are larger, allowing larger molecules to diffuse inside. The walls, however, are made up of amorphous silica, similar to that found in xerogels. Ordered mesoporous silicates are the dominant subset of a larger class of ordered mesoporous inorganic materials. These materials are synthesized by using arrays of surfactant molecules rather than single molecules as structure-directing templates around which inorganic species can polymerize. This concept, of surfactant-templated inorganic materials, has spawned a rapidly growing field of research beginning in 1992†

† The existence of a similar preparation in less publicized earlier work was pointed out by Di Renzo *et al.* (1997); however, the extensive research effort on this topic dates from the publication of the work of the Mobil group.

when the work of Beck *et al.* (1992) and Kresge *et al.* (1992) at Mobil was published. In the simplest form these syntheses require a surfactant template that will form lyotropic liquid crystal phases in the solvent used (usually water) and an inorganic species that will interact with the surfactant micelles and polymerize to form a continuous solid network encapsulating the micelles. Ordering in these systems is present only on the mesoscale, arising from the liquid crystalline arrangement of the surfactant micelles within the solid. The inorganic phase is locally amorphous. Surfactants used in these syntheses have been anionic (e.g. sodium dodecylsulphate (SDS) (Huang *et al.* 2000, Huo *et al.* 1994b)), cationic (e.g. alkyltrimethylammonium halides) or neutral (e.g. amines (Mokaya and Jones 1996), poly(ethylene oxide) (EO_x) (Bagshaw *et al.* 1995, Tanev and Pinnavaia 1995a), alkyl poly(ethylene oxide) (Zhao *et al.* 1998b)) with pore dimensions in the resulting surfactant–inorganic composite related to the chain length of the hydrophobic tail of the template. Water-soluble triblock copolymers have been used to create materials with much larger pore dimensions (50–300 nm depending on the chain length of the polymer) than are possible using micelles of smaller surfactant molecules (Zhao *et al.* 1998a). The pore structure, volume, surface area and wall composition can be tailored by careful choice of inorganic source materials, molar compositions, the type of inorganic–template interaction and the polymerization process. Porosity is created in these materials by removal of the surfactant template through liquid extraction, calcination or ozonolysis.

Ordered pore structures corresponding to many different surfactant liquid crystal phases have been synthesized. The most common is the 2D hexagonal phase with *p6mm* symmetry, consisting of close-packed cylinders of surfactants where the cylinder length is many times the diameter. Lamellar phases with alternating layers of silica and surfactant are also frequently reported. These phases are not stable to the removal of the surfactant as the adjacent silica layers collapse together. Various cubic phases have also been reported. The bicontinuous cubic gyroid phase with *Ia*3*d* symmetry is found in alkaline-catalyzed syntheses. This phase with its continuous network of intertwined pores is considered a more suitable candidate than the lengthy channels of the 2D hexagonal phase for applications requiring diffusion of species into and out of the pore network. All the pores in the *Ia*3*d* cubic structure interconnect and connect to the surface of the particles within a relatively short distance allowing more rapid molecular transport. The *Pm*3*n* phase composed of spherical micelles in a cubic close-packed arrangement is found in both acid- and alkaline-catalyzed preparations. The initial work of Beck *et al.* (1992) and Kresge *et al.* (1992) involved only alkaline-catalyzed preparations and materials reported in these papers are referred to as MCM-41 (*p6mm* 2D hexagonal phase), MCM-48 (*Ia*3*d* cubic phase) and MCM-50 (lamellar phase). 2D hexagonal phase mesoporous materials prepared around the same time by Inagaki *et al.* (1993) from surfactant-intercalated kanemite are referred to as FSM-16. Subsequent preparation of materials from acidic preparations produced ordered mesoporous materials with similar symmetries but distinct wall properties. The materials from acid-catalyzed preparations using molecular surfactants are SBA-1 (*Pm*3*n* cubic phase), SBA-2 ($P6_3/mmc$ three-dimensional (3D) hexagonally packed spherical micelle phase) and SBA-3 (*p6mm* 2D hexagonally packed cylinders) (Huo *et al.* 1996). Other surfactant-templated phases include disordered materials with a worm-like network of channels (KIT-1 (Ryoo *et al.* 1996) and MSU-1 (Bagshaw *et al.* 1995)), a well-defined intergrown cubic–hexagonal phase (STAC-1 (Zhou *et al.* 1998)) and ordered non-

ionic alkyl-EO_x-templated materials (e.g. SBA-11, cubic ($Pm\bar{3}m$), SBA-12 3D hexagonal ($P6_3/mmc$) (Zhao *et al.* 1998b)). Using the same methodology, triblock-copolymer-templated materials with much larger pore systems have also been synthesized in acidic systems (e.g. SBA-15 2D hexagonal ($p6mm$) (Zhao *et al.* 1998a) and SBA-16 cubic cage structure ($Im\bar{3}m$) (Zhao *et al.* 1998b)).

1.3. *Structure formation in ordered mesophase silicates*

The surfactant phase which forms in an ordered mesophase material is, to a large extent, dependent upon the relative concentrations of surfactant and the inorganic species, although this is not the only factor. By analogy with surfactants in aqueous solution (where the phase formed is dependent upon the surfactant concentration and its counterion) the surfactant organization may be described by reference to the packing parameter $g = v/al$ where v is the volume of the hydrocarbon chain, a the head-group area and l the maximum effective chain length (somewhat less than the fully extended molecular length of the chain, typically $l = 1.5 + 1.265n$ Å where n is the number of carbon atoms in the chain or one less) (Israelachvili *et al.* 1976, Israelachvili 1985, 1987). For cylindrical micelles, $\frac{1}{3} < v/al < \frac{1}{2}$ whereas, for spherical micelles $v/al < \frac{1}{3}$. The parameter a is known to be sensitive to the surfactant counterion for solution structures. The packing parameter is essentially a measure of the curvature of the structure formed. Generally, at the lowest concentrations, the surfactant will exist as monomers in solution. With increasing surfactant concentration (for the same counterion), it becomes more energetically favourable to form micelles, which initially are spherical. Spherical micelles contain the largest area per head group for any of the surfactant micelle phases. Increasing the concentration further raises the aggregation number in the micelle, reduces the area per head group and may result in elongation of the micelle to form a rod in solution. Still further increases in surfactant concentration lead to agglomeration of the micelles, whether spherical or cylindrical, into a close-packed phase, which, in the case of rod-like micelles is a hexagonal phase. The next level of concentration gives a cubic phase, in which there is one continuous bilayer of surfactant separating two distinct water regions, between which the surfactant forms a cubic gyroid minimal surface. The final phase transition is to a lamellar phase, composed of bilayers of surfactant, separated by a water phase. This phase has the least curvature and the smallest area per surfactant head group. The surfactant liquid crystal phases and a phase diagram for pure cetyltrimethylammonium bromide (C_{16}TAB), a surfactant commonly used as the template molecule for syntheses of ordered mesoporous materials, are shown in figure 1.

The molecular interaction between an inorganic material and a surfactant head group can be understood using conventional reaction schemes. Six different possible molecular reaction pathways (Huo *et al.* 1994a, Tanev and Pinnavaia 1995a, Behrens 1996) which use the principle of surfactant liquid crystal templating (LCT) have been identified: S^+I^-, S^-I^+, $S^+X^-I^+$, $S^-X^+I^-$, S—I and S · I·, where S is the surfactant, I is the inorganic phase, and X is a mediating ion. S—I indicates systems where the inorganic precursor is covalently bonded to the template throughout synthesis, an approach that has been used for some transition-metal oxides (Antonelli and Ying 1996a,b, Antonelli *et al.* 1996). The pathway applicable to a particular synthesis will be dictated by the reagents and synthesis conditions and can influence the physical and chemical properties of the product. The way in which these silica–surfactant composites form the mesophase structures, and the stage in the reaction where the

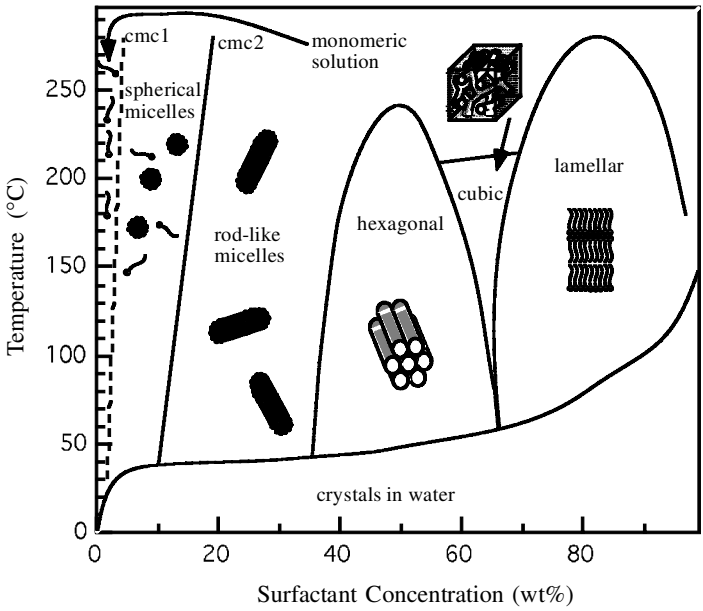

Figure 1. A phase diagram (after Raman *et al.* (1996)) and schematics of the corresponding surfactant liquid crystal phases for C_{16}TAB: cmc1 is the critical micelle concentration (CMC) for the formation of spherical micelles, which has been exaggerated to higher concentrations for the purposes of the illustration; cmc2 is the CMC for the formation of rod-like micelles.

silica–surfactant molecular interactions become important are, however, not yet fully understood.

1.4. *Mechanisms of self-assembly in surfactant–silicate materials*

1.4.1. *Surfactant-driven ordering*

The reaction mechanism, first suggested by Beck *et al.* (1992) is called the LCT mechanism. This proposes that the structure of the channel systems in these mesoporous materials is determined by the surfactant aggregation behaviour, rather than by the condensation of the silica around the template molecule, as occurs for zeolites. Exactly how the silica and surfactant interact in the system is still, however, under debate. Beck *et al.* (1992) proposed two alternative mechanisms in which the surfactant might self-assemble into the observed silica–surfactant composite structures.

The first mechanism (figure 2 (*a*)) posited the existence of a hexagonally ordered concentrated surfactant phase, prior to the addition of the silicate to the system. Upon silicate addition, the anions entered the water regions between adjacent micelles in this pre-existing phase and condensed in these interstitial sites without greatly perturbing the surfactant structure. The second mechanism (figure 2 (*b*)) required only that some surfactant micelles be present in the solution prior to the addition of the silicate anions. It was not necessary that the surfactant already exist in the hexagonal liquid crystal phase observed in the final product. In this case, upon the addition of silica to the system, silicate anions coated the surface of the surfactant micelles by some form of ion exchange with the surfactant counterion.

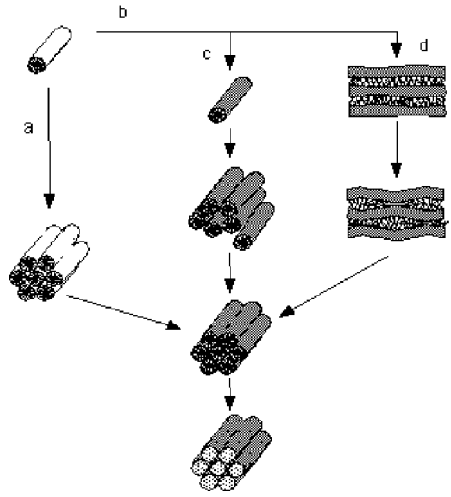

Figure 2. Schematic diagram showing various suggested mechanisms for the formation of MCM-14 as referred to in the text. The change in micelle colour from white to grey indicates the coating of the micelle head groups with silicate oligomers which results in an unperturbed cast of the pre-existing surfactant liquid crystal phase (path a), the formation of silica-coated surfactant species (path b) that form either micelles which then agglomerate to form ordered and disordered arrays (path c) or a lamellar phase which converts into the final hexagonal phase material (path d). The final step, namely calcination, results in an array of hollow, hexagonally packed tubes.

These silica-encased micelles then self-ordered to form the hexagonal phase observed in the final product, and condensation of the silicate occurred to freeze in this structure.

Much work was then carried out to distinguish these mechanisms. In the form of the preparation frequently used to obtain hexagonal phase composite silica–surfactant material, the concentration of the surfactant used (10–26 wt%) is far below the concentration where the hexagonal phase would normally form, even at room temperature. Addition of the silicate anion to the system appears to move the phases that occur normally for the templating surfactant to lower concentrations (Raman *et al.* 1996) despite the fact that the CMC would usually increase for increasing counterion radius and pH. The CMC would, however, be expected to decrease with increases in the valency of the counterions and the ionic strength of the solution (Zhao *et al.* 1996). Evidence from small-angle neutron scattering (Auvray *et al.* 1995, Glinka *et al.* 1996), X-ray scattering (Regev 1996), scanning electron microscopy (SEM) and transmission electron microscopy (TEM) (Cheng *et al.* 1995a), ^{2}H and ^{29}Si nuclear magnetic resonance (NMR) (Kolodziejski *et al.* 1993) and ^{14}N NMR (Firouzi *et al.* 1995) also show that no hexagonal phase surfactant structures exist prior to the addition of the silicate, favouring the second mechanism suggested above. It has also been shown that varying the silicate concentration at constant surfactant concentration will result in the formation of hexagonal, lamellar and cubic phases, implying a prominent structure-directing role for the inorganic silicate anions in this system (Vartuli *et al.* 1994b). Studies on highly alkaline solutions of C_{16}TAB in the presence of dissolved silica species indicated that this system behaved as a lyotropic liquid crystal in the absence of silicate polymerization,

with the silicate anions displacing the bromide counterions at the surface of the surfactant micelle (Firouzi *et al.* 1997). The phase behaviour of the lyotropic surfactant liquid crystal was altered both by the anion exchange process and as a result of the complex silicate chemistry that occurred in response to changes in concentration, pH and temperature, which altered the nature of the silicate anionic species. The results of other workers under similar conditions, however, show little exchange of the micelle-bound bromide or chloride counterions by added silicate and/or hydroxide ions (Zana *et al.* 1999). Likewise, the presence of a large excess of sodium silicate and sodium hydroxide had little effect on the micelle size or shape, leading these workers to doubt the templating role of the surfactant in these syntheses, preferring instead to talk of surfactant-assisted mesoporous silicate formation. They suggested a mechanism based on surfactant binding to the surface of silica prepolymers which eventually precipitate as a mesomorphous surfactant ion-polymerized silicate complex, analogous with observations of systems containing a surfactant with an oppositely charged polyelectrolyte (Frasch *et al.* 2000). In this mechanism, in contrast with the LCT mechanism, the structure formation is initiated by the silicate rather than by the surfactant micelles in solution.

There are, however, a few examples in the literature where very high concentrations of surfactant have been used to create a surfactant liquid crystal phase (Attard *et al.* 1995, 1998, Raman *et al.* 1996) into which monomeric silicate anions were then introduced (figure 2(*a*)). Condensation of the silica in these phases led to the formation of monolithic rigid silica–surfactant composites with structures the same as those of the original surfactant phase. This approach, however, appears only to work with very-high-concentration surfactant systems under conditions where the silicate condensation and consequent release of small molecules do not greatly perturb the existing surfactant structure. Amphiphilic block copolymers have also been used as templates for this type of synthesis, considerably extending the range of templates and structures available that are insensitive to the release of small molecules during silicate condensation (Templin *et al.* 1997, Göltner and Antonietti 1997, Göltner *et al.* 1998a,b, 1999).

In preparations using lower surfactant concentrations, two further refinements of the dilute micellar-assembly mechanism have been suggested. Several groups have observed the formation of a lamellar silica–surfactant phase in the early stages of preparations, which subsequently formed hexagonal phase materials (Monnier *et al.* 1993, Steel *et al.* 1994, Stucky *et al.* 1994, Firouzi *et al.* 1995). This observation led them to propose a 'charge density matching' reaction scheme (Stucky *et al.* 1994, Firouzi *et al.* 1995) (figure 2(*c*)) in which surfactant monomers or micelles in solution become coated with silica oligomers, which act as multidentate ligands for the head groups of the surfactant. The charge on these oligomers will probably cause the surfactant micelle to alter shape during the ion-exchange process. The screening of the electrostatic double-layer repulsion among the aggregates, by the silicate coating, then induces self-assembly of the ordered mesophases. The mesophase formed, by analogy with the surfactant packing parameter discussed above, will be that with the least curvature which is consistent with the surfactant, pH and silicate concentration. These two processes, namely the coating of the micelle and the self-assembly of the mesophase, occur on similar time scales. With the subsequent condensation of the silicate, the inorganic charge density decreases, and lower surfactant charge densities are needed to stabilize the structure; so the head-group area per surfactant molecule increases. This increase in head-group area drives a phase change, for example from

lamellar to hexagonal, which is possible since the incompletely condensed silicate walls are still sufficiently flexible to undergo the thinning that this entails. In this model, the wall thickness is determined by the double-layer potential; silica is only accumulated at the interface to the extent necessary for charge compensation. This results in wall thicknesses of 10–11 Å for lamellar phases, and 8–9 Å for hexagonal phases, as observed (Monnier *et al.* 1993). Post-synthesis treatment in water at 100°C with a pH of 7–10 of various silica–surfactant phases, made with different surfactants, also show phase changes consistent with changes in charge density due to increasing silica condensation and wall reconstruction (Huo *et al.* 1996). A detailed scheme based on the free energy of the various interactions contributing to the synthesis process in this reaction scheme has been proposed (Monnier *et al.* 1993, Huo *et al.* 1994b, Stucky *et al.* 1994).

Other workers, however, did not observe the formation of a lamellar phase as a precursor to hexagonal phase formation (Chen *et al.* 1993, O'Brien *et al.* 1995, Ortlam *et al.* 1996). In fact, at room temperature in one preparation where a lamellar phase is initially present, the subsequent formation of the hexagonal phase does not occur as a direct transformation but proceeds via the dissolution of the lamellar phase followed by crystallization of the hexagonal phase (Matijasic *et al.* 1996). Evidence from TEM, which shows 2D hexagonal phase silicate–surfactant material where a significant proportion of the crystal edges meet at 120°, led Cheng *et al.* (1995a) to propose a different pathway (figure 2(*d*)). In this mechanism, the silicate anion first reacts with the pre-existing surfactant micelle, enabling rods of silicated surfactant species to be formed. These rods then self-assemble directly into the hexagonal phase, via the formation of small hexagonal clusters. These clusters are enormous molecular groups that have faces that may grow at different rates, owing to inhomogeneities in concentration in the surrounding synthesis gel. Adjacent faces are, however, more likely to be in the same solution environment, allowing the 120° angle between the neighbouring edges of the resultant crystal to be preserved. This mechanism allows the formation of both perfect and imperfect crystal shapes, depending on the homogeneity of the reaction medium. Formation of the hexagonal phase via a lamellar phase is unlikely to produce 120° angles between crystal faces.

The formation of a wide range of macroscopic morphologies made up from mesoporous silica in an acidic silica–surfactant system seen using SEM has also been explained by a mechanism consisting of accretion of silicated micelles (Yang *et al.* 1997c). It is suggested that the growth patterns observed are characteristic of a system that is far from equilibrium and not necessarily described by a free-energy function. The range of structures formed in such systems includes toroids, discs, spirals, spheres (Yang *et al.* 1997c) and hollow helicoids (Yang *et al.* 1999a). The formation of these well-defined secondary structures is suggested to arise from the accretion of individual silicate-coated surfactant micelles on to a nucleated silicate seed, and the subsequent freezing in by silicate polymerization of shapes that develop as a result of local solution environments. Solution factors affecting the seed particle predetermine the defect structure, director field pattern, surface mesostructure and charge of the liquid crystal surfactant silicate seed, causing selective anchoring of silicate-coated micelles from solution and growth of a particular resultant particle shape (Ozin *et al.* 1997, Sokolov *et al.* 1999, Yang *et al.* 1999b).

Packing arguments have also been put forwards for this direct assembly of silicated rods mechanism (Vartulu *et al.* 1994a). They suggested that it is difficult to see how a transformation from a lamellar phase to a multidimensional phase such as the cubic phase would occur. All the mesophases can, however, be considered as various forms of packing of silicated rods, the lamellar phase being caused by packing rods directly on top of each other, and the cubic by intertwined rods. Other evidence for the direct formation of hexagonal phase material from silicated rod structures is given by TEM. Micrographs show areas of randomly oriented tubes of the same dimensions as those in hexagonally packed areas within the same surfactant–silicate composite domain. In this case, imperfect packing of the silica-coated rod-like micelles leads to the formation of the randomly oriented phase (Chen *et al.* 1993). Also, work done using cryo-TEM at very early stages of the surfactant–silicate association has detected clusters of highly elongated, partially silicated micelles with dimensions similar to the correlation lengths seen in small-angle X-ray scattering (SAXS) from the same solution (Regev 1996). As the reaction proceeds, silica covers more of each micelle and penetrates into them, causing the decrease in intermicellar distance from about 50 Å to that observed in the 2D hexagonal phase surfactant–silicate composite, about 40 Å. The formation of these micelles from the pre-existing spherical surfactant micelles in solution is explained using curvature arguments, as shown above. The head-group repulsion between surfactant molecules is decreased by the presence of silica anions, which increases the curvature of the micelle by decreasing the head-group area and promotes formation of longer micelles, which then form clusters. These clusters may be initially loosely bound collections of cylindrical micelles but ordering of these was found to be promoted by factors which promote silicate condensation reactions such as higher temperature, decreases in water activity and lowering of the pH during the reaction (Holmes *et al.* 1998, Rathousky *et al.* 1999). Electron paramagnetic resonance studies have also suggested the formation of cylindrical silica-coated micelles, which are then directly incorporated into the final product by aggregation and condensation processes to produce the 2D hexagonal phase (Zhang *et al.* 1997). In this case the lamellar phase was found to form only after several phase changes of the partially condensed material, beginning with the aggregated cylindrical micellar phase.

In this mechanism the driving force for the reaction is both the energetically favourable organic–inorganic interactions and the entropic gain from the binding of the silicate anions to the micelles, which displaces a layer of ordered water surrounding the micelle. It has been predicted that organic species which do not cause the organization of water will not act as templates in this system (Davis *et al.* 1994). *In-situ* ^{14}N NMR has shown no evidence of hexagonal surfactant phases in the synthesis media during surfactant–silicate composite formation. Rather, the results were consistent with randomly ordered rod-like micelles coated with a silica sheath, which did not perturb the motion of the nitrogen-containing surfactant head groups (Chen *et al.* 1993). This result also favours the direct formation of the hexagonal phase from these silicated micelles. Work on the catalytic effect of the surfactant micelles upon silica condensation also suggests the direct assembly of silicated rod-like micelles into the hexagonal phase when monomeric silica at ambient temperatures is used in the preparation. It was, however, also acknowledged that the precise mechanism might strongly depend upon the silica source or reaction conditions (particularly temperature (Cheng *et al.* 1995b)).

1.4.2. *Silica-driven ordering*

It has also been suggested, however, that the silica-coated micelles are not the initial structure-forming species in these preparations but merely a source of silica–surfactant moieties, which add to the growing mesostructured crystal. Zana *et al.* (1999) and Frasch *et al.* (2000) have suggested that, in alkaline syntheses, it is binding of the surfactant ion to preformed oligomers of silica that is the source of mesophase ordering in the system. Di Renzo *et al.* (1999) have suggested that, in acidic syntheses where hydrolysis of the silica source is almost instantaneous, a monomeric coating of silica species forms around micelles. These coated micelles do not interact, by analogy with particles of a stable silica sol under the same conditions. The coated micelles have a low degree of silicate polymerization, rendering them quite soluble so that they act as a reservoir of silica and surfactant monomers for the growth of surfactant-templated silica by mass transfer in solution. In neutral solutions the condensation of silicic acid competes with the interaction with micelles, resulting in the incorporation of larger oligomers and lower amounts of surfactant, producing thicker walls. In alkaline conditions, rapid condensation between surface silanols on silica-coated micelles causes rapid nucleation, and precipitation of a disordered material. The growth of the mesophase composite structure occurs by the growth of more stable silica-coated micelles at the expense of less stabilized micelles in an Ostwald ripening process that converts an initially disordered precipitate into the ordered phase (Galarneau *et al.* 1998). Work on restructuring of the mesophase during ageing at high temperatures in the synthesis solution also suggests that structural evolution of initially precipitated composite materials occurs through the addition of single surfactant and silica moieties. The silica species enter the particle perpendicular to the channels while the surfactant molecules enter along the aggregate cylinders, causing both the channels and the walls to grow in diameter and to become more uniform across the particle with time (Zhou and Klinowski 1998).

1.4.3. *Mesophase formation from layered silicates*

As an interesting comparison, the mechanism of formation of the other hexagonally ordered mesoporous silicate is noted. This material is formed by the intercalation of a surfactant into the layered polysilicate kanemite (Inagaki *et al.* 1994) and is called FSM-16 (from folded sheet mechanism, where the number refers to the length of the carbon chain used in the intercalating surfactant). Kanemite consists of single-layered silica sheets of linked silica tetrahedra with hydrated sodium ions in the interlayers (Kuroda 1996). The first step in FSM-16 formation is the ion exchange of a cationic surfactant ion for the Na^+ between the layers. The second step is the folding and condensation of the silicate into a 3D silicate framework through an interlayer cross-linking process (Inagaki *et al.* 1996). There may be some breaking up of the layers of kanemite at this stage with the occurrence of local reordering of the silica tetrahedra within the layer (Chen *et al.* 1995). The synthetic conditions for formation of FSM-16 are milder than those for hexagonal phase silicate–surfactant materials, occurring at 70°C and requiring only low surfactant concentrations (3.2 wt%). The silicate walls are more condensed in these materials than in MCM-41 and they retain the particle morphology of the initial polysilicate, indicating substantial differences from the LCT materials (Chen *et al.* 1995). Much greater disorder has been seen in the packing of channels in FSM-16, by electron microscopy, than in the MCM-41 type of material. It has been suggested

that FSM-16 may contain pores which are not straight or long but are probably interconnected in a 3D network (Chen *et al.* 1995). No cubic phase has been synthesized from these materials. However, the mechanism is still driven by the aggregation of surfactant ions, which is induced by the higher concentration of ions between the silicate layers. This is similar to the lamellar → hexagonal phase mechanism described above.

One report has been made concerning the heterogenous nucleation of surfactant-templated silicate. In that work, the presence of colloidal particles was shown to promote the formation of hexagonal phase mesopores in a system which otherwise produced amorphous silica (Liu *et al.* 1995). When colloidal silica was used, the colloidal particles formed sites for initial aggregation of silica–surfactant composites. The particle then slowly dissolved and was converted into well-ordered hexagonal phase material, growing in towards the centre of the particle. The presence of more colloidal material induced greater long-range order in the product. When colloidal titania which did not dissolve during the reaction, was used, well-ordered mesoporous silicates again nucleated on the surface. This ordering is probably due to the adsorption of the surfactant species on the particle surface and probably shares some features with the mechanisms of formation of thin films of surfactant templates silicates on mica (Yang *et al.* 1996b) and at the air–water interface (Yang *et al.* 1996a, Aksay *et al.* 1996), which are described in greater detail below.

Much work has been carried out on application of these mesoporous materials to catalysis, either as catalyst supports or by using active inorganic species to create the pore walls. Catalytically active species may be introduced by trapping a species within the pores during or after synthesis, or by functionalization of the pore walls by grafting. It may also be possible to use these materials for molecular-sieving applications utilizing their uniform pores in size exclusion separations. Other applications include their use as supports for sensor molecules, as lightweight insulating materials, in the formation of mesoscale composites and as moulds for the creation and investigation of materials in confined geometries. Applications of mesoporous molecular sieves have been reviewed by several workers (Tanev and Pinnavaia 1995b, Zhao *et al.* 1996, Corma 1997, Moller and Bein 1998, Maschmeyer 1998).

This current review will concentrate on the specific topic of surfactant-templated mesostructured silicate films. Silicate has been used as the starting point in most investigations of the formation and properties of these ordered mesoporous materials and so the greatest body of work at this point in time concerns surfactant–silicate composites. Thin films of these materials are a potentially useful geometry for the creation of membranes for molecular sieving and catalyst support, as well as for surface coatings for sensors, insulation and patterning of mesoscale structures. The rigid brittle nature of the surfactant–silicate composite requires that the desired macroscopic morphology be either grown *in situ* or moulded before the complete gelation of the silicate framework. Initial work on surfactant-templated silicates produced precipitated powders with no well-defined morphologies. However, it has since proven possible to grow the silicate materials as 'single crystals' (Kim *et al.* 1998), monoliths and films with thicknesses ranging from nanometres to millimetres. There are several methods of creating films of mesoporous silicate that will be covered in turn, with a specific focus on the mechanism of structure development in each type of preparation.

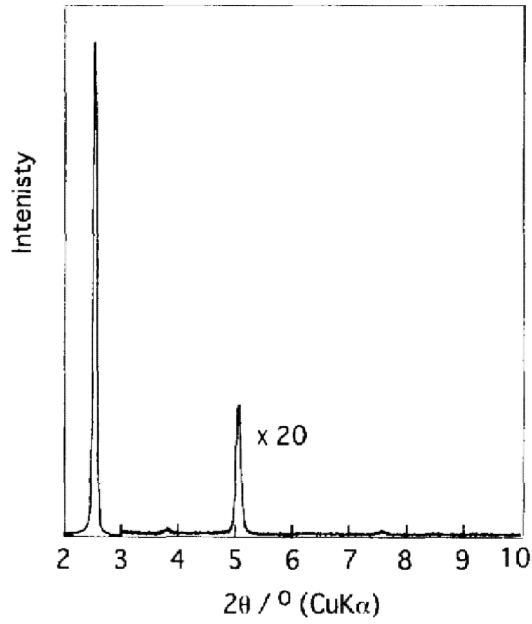

Figure 3. XRD pattern for a layered silica–C_{14}TAB mesophase film, showing two diffraction peaks due to the layered silica–surfactant structure. (Reprinted from Supramol. Sci., 5, Ogawa, M. "Preparation of transparent thin films of silica-surfactant mesostructured materials" 247–251 © (1998) with permission from Elsevier Science.)

2. Solvent evaporation methods

2.1. *Spin coating*

2.1.1. *Layered and two-dimensional hexagonal mesostructures*

The earliest attempt at creating a continuous surfactant–silicate mesostructured film was that of Ogawa (1994). In this work, partially hydrolysed tetramethoxysilane (TMOS) in acid solution (pH 3) and a solution of an alkyltrimethylammonium bromide (C_nTAB, where n is the carbon number in the alkyl chain) were mixed and the solution spin coated on to a substrate and dried at 100°C to remove solvent and to condense the silicate. Transparent thin films were formed on the substrate with thickness controlled by spin rate; however, films thicker than 1 μm were found to peel off the substrate. These films showed two X-ray diffraction (XRD) peaks (figure 3) corresponding to a layered structure organized parallel to the substrate, with the best ordering found for alkyl chain lengths of ten to 16 carbon atoms. Poorly ordered films were formed for C_6 and C_8 chain surfactants. Thinner films were also more ordered. It was concluded from this that the aggregation of the C_nTAB in solution was essential for the formation of layered organization of the silica and C_nTAB. Rapid solvent evaporation also enhanced formation of the layered composites on substrates, as no layered structures were found in the synthesis solution. Evaporation was suggested as the driving force for organization of the C_nTAB into lamellar aggregates, which are then 'frozen in' by the continuing condensation of the surrounding silicate. It is possible that these films in fact had a hexagonal structure, as the diffraction pattern from a well-ordered, hexagonally structured mesophase oriented parallel to the surface of the substrate will also show only the peaks

corresponding to a layered material. Ogawa did not comment in this early work on whether the structure remained in the films after calcination; collapse of the structure would have indicated a true layered structure rather than a hexagonally ordered material. It was, however, noted in a subsequent paper that the *d* spacing increased with increasing tetraethoxysilane (TEOS)-to-C_{16}TAB ratios (Ogawa *et al.* 1997). This increase followed that expected for purely lamellar aggregates for lower ratios but changed slope for a TMOS-to-C_{16}TAB ratio greater than 5, indicating that the silicate wall thickness was increasing but suggesting a transition from an oriented lamellar structure to an oriented hexagonal structure in the films with increasing silica-to-surfactant ratio. A similar change in *d* spacing was also noted for C_{14}TAB-templated films. It was also possible to tune the *d* spacings by using mixed surfactant systems. In cases where the total concentration of surfactant was constant, a change in the proportion of C_{16}TAB to C_{12}TAB or of C_{16}TAB to C_{10}TAB produced spacings intermediate between those of C_{16}TAB and C_{12}TAB or C_{10}TAB alone. In later papers (Ogawa 1998, Ogawa *et al.* 1998) the spin-coated films are shown to retain XRD patterns and to have high surface areas following calcination, indicating the formation of a 3D pore network, suggested to be the hexagonal phase. These materials assemble via the anion-mediated $S^+X^-I^+$ pathway and the presence of the surface promoted ordering in the mesostructure over that formed in the bulk solutions (Ogawa 1998). The use of dialkyldimethylammonium bromide surfactants as templating agents in the mesostructured silicate synthesis was also shown to produce layered structures in both monoliths and when spin coated on to a substrate, although again a greater degree of ordering was present in the thin-film materials (Ogawa 1997). Other work (Ogawa 1995) showed that it was possible to solubilize pyrene molecularly in these layered films, with the pyrene located in the alkyl chain region of the C_nTAB layers. Increasing the amount of solubilized pyrene up to a few weight per cent resulted in an increase in *d* spacing from the XRD pattern of the films due to swelling of the surfactant layer in the surfactant–silicate composite. Other cationic dyes were also introduced into the structure to form coloured transparent films (Ogawa *et al.* 1998).

Another early attempt at spin coating continuous thin films of mesoporous silica on a substrate was made by Anderson *et al.* (1996). This work is one of the few to use an alkaline-catalyzed synthesis for the production of mesostructured silicate thin films. A homogeneous solution of TMOS and the templating surfactant C_{16}TAB in a water–methanol solution at pH 7 was spin or dip coated on to a substrate. This film was stable until exposed to ammonia gas, resulting in a pH switch in the film, causing the rapid formation of periodic mesoporous silica particles as a continuous film on a substrate. A water–methanol solvent was used to enhance TMOS solubility and to increase the homogeneity of the synthesis solution. The optimal time for depositing the neutral solution was found to be 10–60 min after mixing, to allow for partial hydrolysis and oligomerization of the silicate species prior to spinning, increasing the wetting of the solution on the hydrophilic substrate. To obtain a uniform continuous film, it was found necessary to prevent evaporation of the water and methanol until the film had formed by depositing the film under a controlled atmosphere of methanol and water vapour. Electron microscopy revealed these films to be made up of aggregated submicrometre ellipsoidal or spherical particles, within which was a hexagonal array of 3 nm channels. Particle size could be controlled by use of ammonia gas or sodium hydroxide (in films deposited at 0°C to slow the kinetics of composite formation) as the catalyst and film thicknesses were controlled by spin

or dip rate; however, again films thicker than 1 μm tended to crack upon removal of the surfactant template. The mesoporous channels were not uniformly oriented with respect to the substrate; however, the open aggregate structure of these films shown in figure 4 could be useful in applications requiring high-surface-area membranes with accessible pores. The films were developed as high-surface-area size-selective coatings for surface acoustic wave sensors. Further work by the same group (Martin *et al.* 1997) reported similar films made using formamide or ethylene glycol as cosolvents to control evaporation and structure formation in the deposited films. Regions of parallel lines of apparently twisted silica ropes were suggested to result from the interaction of the developing structures with convective rolls owing to uncontrolled evaporation and branched fractal silicate structures were assumed to have formed in the bulk synthesis solutions prior to film deposition.

The first report of a silicate–surfactant film containing a pore structure made up of packed cylindrical micelles was by Liu *et al.* (1996). An acidic solution of cetyltrimethylammonium chloride (C_{16}TACl) and TEOS in water–ethanol was spin coated on to polished silicon wafers, resulting in smooth films 300–600 Å thick. Multiple coating was used to increase the thickness to up to 3000 Å for application as low-dielectric-constant coatings in microelectronic devices. The films showed different interference colours as their thickness increased, indicating uniform thickness and microstructure. TEM showed a randomly packed layer of micellar structures next to the substrate, with ordered structures formed on top of the randomly packed layer. XRD showed two overlapping peaks corresponding to the ordered phase (38 Å) and the disordered phase (54 Å). This XRD structure was maintained after calcination to remove the surfactant, showing that stable 3D structures and not lamellar phases had been formed.

Substituted silica–surfactant mesostructured films have subsequently been formed using spin coating by a number of groups. Shimojima *et al.* (1998) reported the formation of oriented ordered silicate–organic films made from mixtures of alkyltrimethoxysilanes (having between six and 18 carbon atoms in the alkyl chain) with TMOS and no other surfactant present in the system. These solutions were deposited on substrates by spin coating forming transparent films for chain lengths with fewer than 14 carbon atoms. The resulting materials contained alkyl groups ordered in layers between silicate sheets. This reaction is of the S—I class and the degree of ordering was strongly dependent upon the reaction time in the synthesis mixture before spreading. However, ordering was only observed in the spin-coated films and not in the bulk solution even when this was allowed to dry out, again suggesting that the rapid solvent evaporation occurring during film formation enhanced ordering. Ogawa and Kikuchi (1998) have also reported synthesis of silicate–surfactant mesostructured films using vinyltrimethoxysilane and this is discussed further in the context of self-supporting spin-coated films below.

2.1.2. *Mesophase films with other symmetries*

Ogawa and Masukawa (2000) have also published syntheses of transparent cubic and true lamellar films produced by spin coating using C_{16}TACl and C_{18}TACl templates. The synthesis was performed as for Ogawa's work described above but the TMOS-to-C_nTACl ratios were varied. Films about 1 μm thick on glass substrates were prepared and did not crack or peel off the substrate after calcination. For TMOS-to-C_{16}TACl ratios less than 2.3 a true lamellar phase was formed which collapsed upon calcination. For ratios between 2.3 and 6 the 2D hexagonal

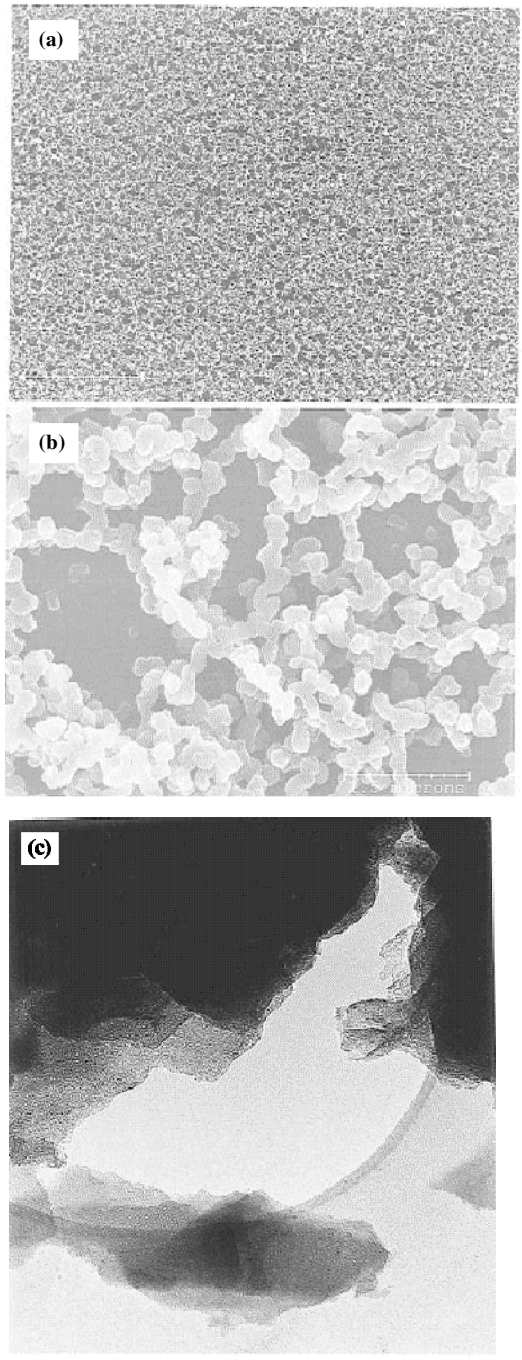

Figure 4. (*a*), (*b*) High-resolution scanning electron micrographs of calcined periodic mesoporous silica films showing an interconnected network of aggregrated 150–500 nm particles that bridge the entire substrate. (The scale bar on (*a*) is 50 nm.) (*c*) Lattice imate TEM of gas-catalysed thin film made using a concentrated methanol–water mixture, showing regions of well-ordered hexagonal phase channels and also randomly arranged pores. (Reprinted in part with permission from Martin *et al.* (1997). © 1997 American Chemical Society.)

mesophase was formed and at a ratio of 8 a pure *Pm*3*n* cubic phase was formed. Between these values, that is at a ratio of 7, a mixture of the hexagonal and cubic phases was observed. This was consistent with silica-to-surfactant ratios for the various phases found in previous work on surfactant templated mesophase structures in acidic solution preparations. Changing the pH from 3.5 to 2.5 or 5 did not significantly affect the structures of the mesophases. The same liquid crystal phases could be formed using C_{18}TACl as the surfactant with the same ratios of TMOS to C_{18}TACl as were used for the C_{16}TACl surfactant; however, gels prepared from the same solutions did not form the cubic phase, indicating an important effect of the rapid evaporation process on the structure formed.

Disordered mesophase silicate–surfactant films have also been prepared by Baskaran *et al.* (2000) using poly(oxyethylene ether) surfactants in an acidic solution of pre-hydrolysed TEOS aged for 20 h before spin coating. The dielectric constant of these films after calcination and various dehydroxylation treatments was measured as a function of ageing time after the treatment. Mesoporous films treated with hexamethyldisilazane (HDMS) by immersion in a solution of HDMS or by spin coating the film with pure HDMS showed constant dielectric behaviour with time while films which were heat treated at 400°C in flowing hydrogen or argon showed an increasing dielectric constant with time because of the re-formation of surface hydroxyls in the pores. Film thicknesses up to 1.2 μm with roughnesses of less than ±50 Å over tens of micrometres could be created by spin coating and the measured elastic modulus was in good agreement with that expected for porous solids.

Further work on dye impregnation in spin-coated surfactant–silicate mesophase films was reported by Honma and Zhou (1998) and Zhou *et al.* (1999). In these papers the surfactant template used was related to C_{16}TAB but contained a ferrocenyl group in the alkyl tail, which was then encased in the tail region of the surfactant micelle in the ordered mesophase composite film. The ferrocenyl-substituted surfactant was the only type of template used in the preparation of the spinning solution, with partially hydrolysed TEOS in an acidic solution as the silicate source. The structure of these films proved to be a lamellar phase, which collapsed after calcination was formed. In uncalcined material, the oriented ferrocenyl-containing bilayers allowed electronic conductivity through the ferrocenyl chain.

The production of liquid crystal phases other than the layered and hexagonal phases has also been reported in two papers by this group (Zhou *et al.* 1999, Honma *et al.* 2000). They described synthesis of hexagonal, bicontinuous cubic (*Pn*3*m*), lamellar and disordered worm-like films using the C_{16}TACl or 11-ferrocenylundecyl-ammonium bromide templates in acidic solutions. The mesophase structure of the film changes systematically with increase in the surfactant concentration relative to TEOS in the spinning solution (figure 5). The *d* spacings for all the various structures are reported to be sensitive to total concentration, as more dilute solutions promoted heterogeneous nucleation on the surface instead of homogeneous nucleation in solution. The solution pH and the anion of the surfactant used also affected the *d* spacing owing to weak $S^+X^-I^+$ charge-matching interactions at the surfactant–inorganic interface. The degree of ordering of the structure was enhanced by suppression of the silicate condensation rate and rapid surfactant enrichment during solvent evaporation. The spinning solutions also contained 1-propanol and 2-butanol which were proposed to act as cosurfactants, altering the packing of the surfactant to allow the formation of the cubic phase.

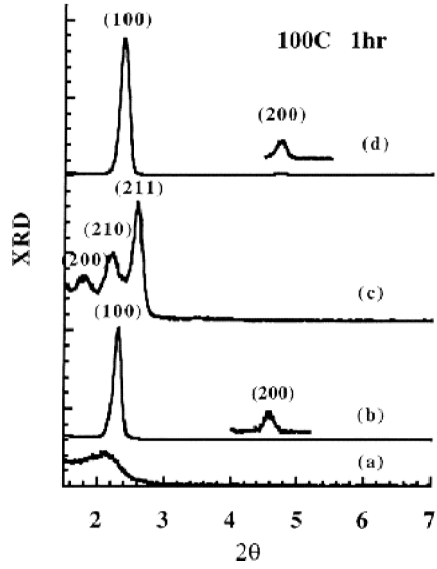

Figure 5. XRD patterns of uncalcined spin-coated films on glass substrates from solutions with C_{16}TMAC-to-TEOS ratios of 0.062 (amorphous mesophase) (curve (a)), 0.093 (2D hexagonal mesostructure) (curve (b)), 0.156 (bicontinuous cubic phase (*Pn*3*m*) (curve c)) and 0.25 (lamellar mesophase) (curve (d)). (Reprinted from J. European Ceramic Soc., 19, Zhou, H. S., Kundu, D. and Honma, I., "Synthesis of oriented meso-structure silica functional thin films" 1361–1364 © (1999) with permission from Elsevier Science.)

Spin-coated C_{16}TAB–silica films with a 3D hexagonal mesostructure having the $P6_3/mmc$ space group were also synthesized by Besson *et al.* (2000a,b). The films were prepared from a polymeric silica sol prepared by prehydrolysing TEOS in an acidic (pH 1.25) water–ethanol mixture aged for various times, at 40 or 60°C. C_{16}TAB was then ultrasonically dissolved in the sol to give a C_{16}TAB-to-TEOS ratio of 0.1 and this solution was diluted with ethanol and spin coated on to a glass substrate. The resultant film thickness was around 1000 nm for all synthesis solutions and shrank to 800 nm upon calcination in air at 400°C. A large contraction of the *d* spacing (23%) was also observed after calcination. XRD also showed a decrease in the *d* spacing with an increased ageing time in the sol from 0.5 to 23 h, in both as-prepared and calcined samples. There was an optimum degree of sol condensation and the formation of well-ordered structure in the film, as shown by the sharpness of the first-order (002) diffraction peak. This optimum ageing time in the sol was temperature dependent, being between 2 and 6 h at 40°C but 0.5 h at 60°C. It was noted that spin coating in air was necessary to produce a mesostructured film, as spin coating in a controlled alcohol atmosphere did not result in an ordered film. The rapid evaporation of the ethanol was a necessity to produce structure. Grazing incidence SAXS studies carried out at different angles α gave information on the structures formed at the air–film interface and that of the film interior (figure 6). At the surface of the film (α equal to the critical angle), Bragg diffraction spots, indexed as the $[2\bar{1}0]$ zone-axis orientation of the 3D hexagonal structure, were observed, confirming a preferred orientation of the channel structure with the *c* axis perpendicular to the film surface. These spots were more pronounced for films produced from sols near the optimum degree of condensation. For well-structured

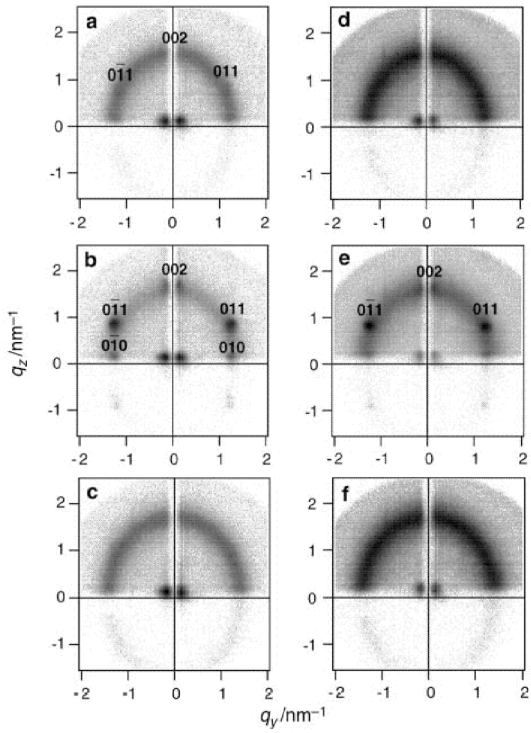

Figure 6. Grazing-incidence SAXS patterns recorded at different incidence angles α for uncalcined mesostructured films prepared from silica sols with different ageing times t at 40°C: (*a*) α equal to the critical angle and $t = 1$ h; (*b*) α equal to the critical angle and $t = 4.5$ h; (*c*) α equal to the critical angle and $t = 23$ h; (*d*) α equal to the critical angle plus 0.5° and $t = 1$ h; (*e*) α equal to the critical angle plus 0.5° and $t = 4.5$ h; (*f*) α equal to the critical angle plus 0.5° and $t = 23$ h. (Reprinted with permission from Besson *et al.* (2000a). © The Royal Society of Chemistry 2000.)

films (ageing for 4.5 h at 40°C for the sol) in the interior of the film (α equal to the critical angle plus 0.5°), diffuse lines were observed between Bragg spots, indicating regions with disorder due to small displacements of the micellar spheres from their nominal positions in the hexagonal lattice. For films produced outside the optimum condensation range, the interior of the film produced a diffuse diffraction halo with an ellipsoidal shape, indicating a distribution of distances between spherical micelles throughout the film although the nearest-neighbour distances in the y and z directions were maintained. These results suggested that the film developed through the growth of ordered domains from the air–sol interface towards the interior of the film. No evidence was seen for the development of an ordered phase at the sol–substrate interface, in contrast with observations made for dip-coated films (discussed below). The degree of condensation of the deposition sol was also reflected in the unit-cell volume, which decreased for increased ageing time of the sol. Increasing dilution of the sol with ethanol for a given degree of condensation also decreased the unit-cell volume and increased the size of ordered domains in the interior of the film but was associated with an increase in anisotropic strain effects during drying. This anisotropy was largely due to a contraction of the silica network along the z direction. These results supported a formation mechanism similar to that proposed

by Lu *et al.* (1997) for dip-coated films. The removal of ethanol preferentially at the air–sol interface increased the concentration of C_{16}TAB, which caused it to exceed the CMC, leading to the formation of spherical micelles and their organization in a 3D hexagonal mesophase oriented by the preorganized air–sol interfacial region. The structure of the sol also has a strong effect on the stability of the mesophase. After hydrolysis, TEOS forms fractal particles in the sol whose size is dependent on the ageing time. During the rapid removal of alcohol, gelation between the fractal silicate particles stabilizes the micellar organization existing in the sol at that moment. The shrinkage on drying of the silicate network is more marked as the ageing time of the sol increases because the size of the fractal aggregates and hence the interwall porosity increases at the point of gelation. When wall formation was prevented by either small fractal units unable to form a percolative network or by large units unable to occupy the space between the spherical micelles, a large distortion in structure resulted. The optimum dilution for the formation of ordered films corresponded to a critical value of film thickness. Below 300 nm, the films were not thick enough to exhibit disorder because domains formed differently at the surface and in the interior, but the extent of 3D hexagonal order was reduced by both the high distortion of the hexagonal structure and the limited dimension along the z direction. This occurred because the film contained long-range 3D hexagonal order, which underwent cooperative contraction during drying, and this contraction was enhanced along the z direction, perpendicular to the substrate plane. In thicker films, disordered regions formed between domains with different orientations, preventing this cooperative shrinkage.

It has also proven possible to create self-supporting films of mesostructured silica–surfactant composite by spin coating of the acidic precursor solution on to a poly(methylmethacrylate) (PMMA)-coated substrate. Upon dissolution of the PMMA film in acetone, the brittle mesostructured film was separated from the substrate and collected as aggregates of small pieces (Ogawa *et al.* 1998, Ogawa and Kikuchi 1998). These pieces retained their hexagonal phase mesostructure after calcination.

Unsupported membranes of mesostructured silicates with controlled thickness size and mechanical strength are required for use as catalysis and separation membranes. In silica films formed using TMOS it was found to be difficult to create thick films (greater than 10 μm) with good ordering and orientation of the pore system because of the competition between the rates of silicate condensation and of the assembling of the surfactant during solvent evaporation. Using vinyltrimethoxysilane in addition to the TMOS as silicate precursors formed thicker well-ordered self-supporting films. The vinyl-substituted species helped to increase the time required for silica gelation, allowing greater ordering of the surfactant-filled pore system during the rapid solvent evaporation step (Ogawa and Kikuchi 1998). The thick films (greater than 10 μm) resulting from this synthesis were also more flexible than those formed from TMOS alone. Calcination caused these films to become brittle but the XRD pattern and TEM showed that the structure was retained, suggesting a 3D pore network rather than a layered structure. From the TEM images a pore system composed of disordered aggregates of cylindrical micelles was suggested, despite the sharp well-defined XRD patterns presented.

The rapid solvent evaporation spin-coating technique has also been extended by this group to incorporate aluminium in the walls of the mesophase (Ogawa *et al.* 2000) by cosolidification of aluminium tris(*sec*-butoxide) (ASTB) with TEOS and

C_{18}TAB in the acidic water–ethanol solution spin coated on to a substrate. Homogeneous films were obtained for ASTB-to-TEOS ratios of up to 0.014, but turbid films were obtained for ratios above this. XRD diffraction peaks grew broader with increasing aluminium content but for all the homogeneous calcined films a single peak indicative of the surfactant-templated mesostructure was observed. An organic photochromic species *p*-(ω-dimethylhydroxyethylammonioethoxy)azobenzene (AZ) was introduced into the films by immersing them in a solution containing AZ. Films containing no aluminium showed very low adsorption of AZ, but AZ was effectively adsorbed into aluminium-containing films owing to an electrostatic interaction between the dye and the negative charge at the substituted aluminium site in the silicate wall. AZ adsorption increased with increasing aluminium content in the film although it was also removed from weakly binding sites by washing. Ultraviolet (UV)–visible adsorption spectra indicated the AZ was dispersed as monomers on the surface of the mesoporous silica irrespective of the degree of loading, and higher concentrations of AZ were achieved in the films than was possible in solution owing to solubility limitations. Calcination of the films at 400°C instead of at 300°C reduced the capacity of the films for AZ adsorption possibly because of the condensation of hydroxy groups on the mesopore surfaces and migration of aluminium from the pore surface into the pore walls at the higher temperatures. It was also shown that the adsorbed *trans*-AZ was capable of undergoing photochemical isomerization upon UV and visible light irradiation, with 90% converted to the *cis* isomer. This photoisomerization occurred for temperatures between 80 and 400 K showing that the mesoporous silica films could be utilized as nanoreaction vessels in a wide temperature range for photochemical reactions.

2.2. *Dip coating*

Dip coating is closely related to spin coating, with substrates being drawn from a homogeneous precursor solution and allowed to drain to a particular thickness. Film thickness is controlled by evaporation rates of the solvent and by the viscosity of the coating solution more directly than for spin coating where the spinning conditions determine thickness to a larger degree. Dip coating is advantageous for the rapid formation of films on nonplanar surfaces. Some of the earliest reports of spin-coated films also refer to dip coating of the same synthesis solutions on to substrates with similar results (Anderson *et al.* 1996, Martin *et al.* 1997). As these syntheses have been discussed in detail above,they will not be mentioned further in this section.

2.2.1. *Fluorescence studies*

An early report of the formation of a silica–surfactant film by dip coating is that of Ferrer and Lianos (1996). Dipping solutions were prepared using prehydrolysed TMOS at pH 3, in water, with no other cosolvents. To this homogeneous solution, either C_{16}TAB or Triton-X-100 (a surfactant with oxyethylene head groups) was added as the templating surfactant. Pyrene and Coumarin-153 (C-153) were solubilized in the surfactant solutions and used as fluorescent probes to probe the film structure. C-153 is sensitive to the polarity of its microenvironment and was found to be solubilized in the surfactant region of the surfactant–silicate composite in an environment similar to that of the surfactant micelles but more rigid. This suggests that the surfactant molecules are more closely packed and better oriented within the film than in solution. Pyrene solubilized in the surfactant micelles gave

similar results, with a lack of eximer formation indicating that diffusion of the pyrene molecules was restricted in the silicate–surfactant films. Further analysis of the luminescence decay of pyrene in the presence of C-153 within the same silicate–surfactant film indicated that the molecular orientations of the probe molecules were also stable and the observed energy transfer kinetics were consistent with a layered system of alternating surfactant bilayers and silicate layers about 10 Å thick as suggested for spin-coated films by Ogawa (1994). Leaching of these dyes from dip-coated silicate–surfactant films made using Triton X-100, C_{16}TAB or SDS is reported in a later paper (Ferrer *et al.* 1997). Hydrophobic dyes such as pyrene and C-153 were leached from the film more rapidly than hydrophilic dyes such as Rhodamine 6G. The hydrophobic dyes were more easily leached as they washed out with the surfactant whereas hydrophilic dyes were trapped in the silicate framework. Films made using Triton X-100 or SDS surfactant were twice as thick as those made using C_{16}TAB and were less damaged by the leaching process. This was related to the gelation rates of the dipping solutions, with sols containing Triton X-100 or SDS gelling after a few hours, while C_{16}TAB-containing sols required a few days under the same conditions. Films made from dip coating C_{16}TAB–silicate solutions that had been aged after mixing of the components were thicker but were less uniform and less transparent. It was also noted that atomic force microscopy (AFM) on films prepared with C_{16}TAB in which the template was removed by calcination rather than by leaching retained a greater degree of linear structure; however, this structure collapsed when the film was placed in contact with water. Triton X-100 and SDS-templated silicate films showed more compact but also more random structures in AFM images. Further studies by the same group on these films showed that the fluorescent probes were confined in 2D layers in the films but not in bulk materials prepared from the dipping solutions (Bekiari *et al.* 1999).

Lu *et al.* (1997) of a New Mexico-based group then published a detailed report on the formation of continuous films by dip coating from a dilute acidic solution of prehydrolysed TEOS in water–ethanol solution under conditions where the siloxane condensation rate was minimized. C_{16}TAB was added as the surfactant template. Films were deposited on silicon (100) by dip coating with the preferential evaporation of ethanol from the entrained film progressively concentrating water, HCl, silicate oligomers and surfactant in the film. A hydrophobic dye (2,6-TNS) was incorporated into the dipping solution in order to observe micelle formation during film deposition. Spatially resolved fluorescence–depolarization measurements indicated a change in the dye environment from freely rotating in solution to incorporation in a micellar environment with decreasing film thickness and increasing distance above the solution reservoir. In solutions containing no templating surfactant the probe environment showed no change from free rotation until above the drying line on the film. This shows that the silica–surfactant micellar structures formed in these films only by virtue of the evaporation of solvent, causing an increase in surfactant concentration. XRD patterns from dry films showed that, by changing the surfactant concentration in the dipping solution, it was possible to create 2D hexagonal (an array of close-packed cylindrical micelles) and lamellar phases oriented parallel to the surface and also, after calcination, phases with cubic and 3D hexagonal order. The 3D hexagonal and cubic phases were observed to develop from lamellar phase films during calcination via a lamellar $\rightarrow$ cubic $\rightarrow$ hexagonal pathway driven by the continuing silicate condensation (figure 7). Cross-sectional TEM on the 2D hexagonal mesophase showed ordered

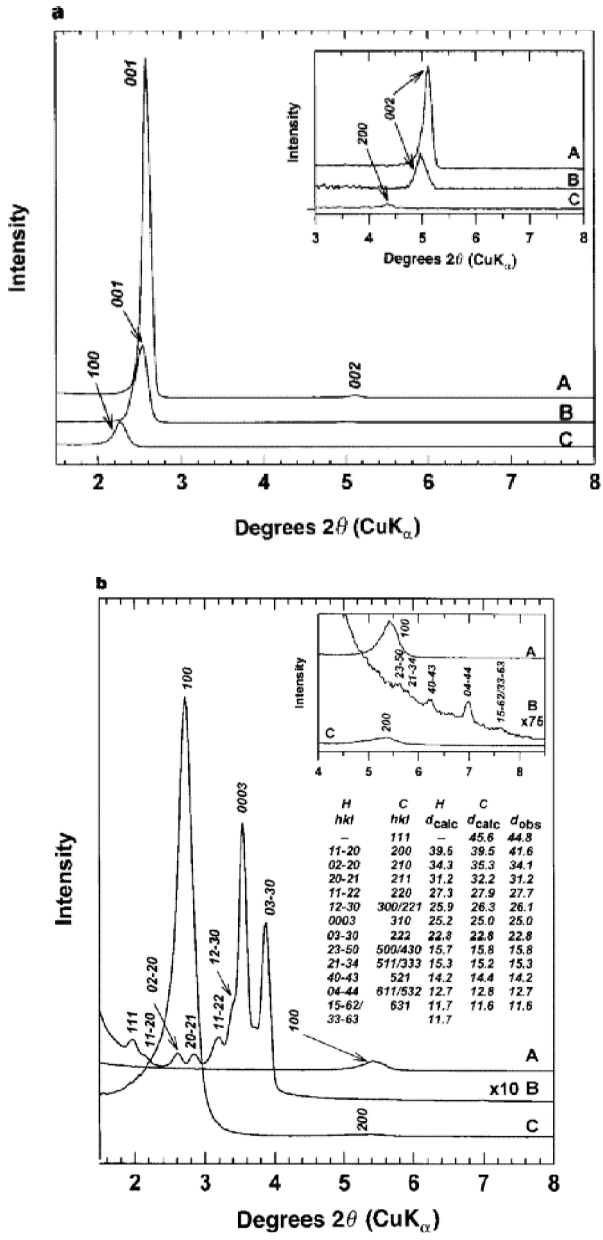

Figure 7. XRD patterns from (*a*) uncalcined films prepared from 5.0 wt% C_{16}TAB (curve A), 4.2 wt% C_{16}TAB (curve B) and 2.5 wt% C_{16}TAB (curve C). The inset is the region where 2θ is between 2.5 and 10° with the intensity scale expanded 115 times, showing that all three spectra contain second-order reflections at half the primary *d* spacing. (*b*) XRD patterns from samples in (*a*) after calcination at 400°C. The inset is the region where 2θ is between 3.5 and 10° with the intensity scale expanded 15 times. Curve A is consistent with a lamellar mesophase that collapses after calcination, curve B initially resembles the mesophase of curve A but upon calcination transforms into a new mesostructure composed of primitive cubic and 3D hexagonal mesophases, and curve C is indicative of a 2D hexagonal mesophase with the channel axes oriented parallel to the substrate surface. (Reprinted with permission from Lu *et al.* (1997). © *Nature* 1997.)

regions at the interfaces parallel to the substrate and to the solution–air interface, with a disordered region of worm-like micellar structures sandwiched in between. A formation mechanism was suggested that involved the cooperative assembly of silica–surfactant micelles at the air–solution and substrate–solution interfaces at an early stage of the deposition process (at or below the CMC of the surfactant) with the ordered regions growing in towards the centre of the film as the surfactant concentration increased with evaporation. Unpublished AFM results were mentioned that indicate the slow spontaneous formation of a silicate–surfactant interfacial structure on a substrate immersed in the dipping solution, confirming that, for the rapid film formation that occurs during dipping, the structure formation is evaporation driven. Nitrogen adsorption isotherms on calcined films showed unimodal porosity with no interparticle macroporosity or mesoporosity and the trans-film flux of the cubic structured films increased 1000 times after calcination, establishing through-thickness pore connectivity.

Another fluorescence study was carried out by Huang *et al.* (1998) on the development of structure in thick (1500 Å) lamellar SDS–silicate films formed from dip coating silicon (100) wafers in a dilute SDS–prehydrolysed TEOS acidic water–ethanol solution. The use of an anionic surfactant as the template in these films is unusual, as most of the published literature on surfactant-templated films concerns cationic or polymeric non-ionic surfactants. Interferometry was used to characterize film thickness with time as each fringe above the solution meniscus was found to represent a decrease in the thickness by about 2200 Å. Simultaneously fluorescence spectroscopy was used to observe the variation in the water-to-ethanol ratio and the formation of micelles. For uniform films the SDS concentration was found to be between 1.0 and 1.5 wt% in the TEOS sol which forms the dipping solution; between 1.5 and 20 wt%, some radial streaks and spots were found (Huang *et al.* 2000). The water content in the dipping solution was about 2% but, by half-way through the film, deposition had increased to about 10% and, by the time that the film has shrunk to almost its final thickness, it was around 60%. The water content was higher at all stages in the SDS-containing film than a film dipped from an equivalent TEOS sol not containing SDS, although the trends observed were the same. This may be due to a greater local concentration of water present in the region of the fluorescent probe to solubilize the mediating sodium ions (Huang *et al.* 2000). Surprisingly, although micelles formed in the film-forming solution just above the solution meniscus, these then broke up about half-way through the process and formed the final lamellar structure only at the end of the drying process. The dipping solution was initially sufficiently dilute that no micelles formed but, after dipping, where the film thickness decreased from about 3–2 μm, the surfactant concentration was increased and the CMC was exceeded. However, after the water concentration had increased to 10%, the micelles broke up, possibly in order to undergo a phase change. At the point where the film had almost reached its final thickness the lamellar phase was formed, but changing pyrene vibronic band intensities indicated that dynamic processes involving continued solvent evaporation or the flexibility of the surfactant in the lamellar state continued for a further 5–15 min. XRD patterns indicated no long-time structural changes occurring during this time, suggesting that the lamellar phase structure was formed at about the time that the final thickness was reached, even though local molecular dynamics persisted for several hours. The formation mechanisms involved in these dip-coated films are summarized in figure 8.

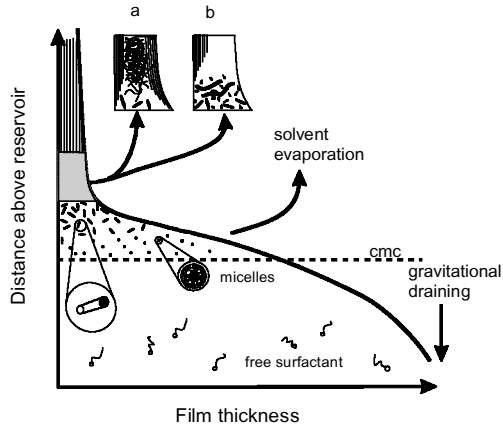

Figure 8. Schematic diagram of the process of mesostructure formation during deposition of mesostructured films by dipping (after Lu *et al.* (1997) and Huang *et al.* (1998)). Inset a corresponds to the mechanism observed by Lu *et al.* (1997) where an ordered phase grows in from the substrate–film and film–air interfaces with a disordered worm-like micellar region at the centre. Inset b corresponds to the process observed by Huang *et al.* (1998) in which micelles broke up during a reorganization process immediately prior to ordered mesophase formation.

2.2.2. *Control of mesophase structures*

Subsequent work by the New Mexico group (Sellinger *et al.* 1998) also made use of the dip-coating process for silica–surfactant mesostructured film formation to prepare nanolaminates that mimic nacre. In these materials, monomeric species were solubilized in the hydrophobic surfactant tail region and self-assembled together with the silicate precursors on to surfaces via solvent evaporation during dip coating. The dip-coating solution contained prehydrolysed TEOS in an acidic water–ethanol solution, a coupling agent (either 7-octenyltrimethoxysilane or methacryloxypropyltrimethoxysilane), C_{16}TAB as the structure directing surfactant, alcohol soluble monomer (dodecylmethacrylate, (DM)), cross-linker (hexanedioldimethacrylate) and initiator (either UV initiated benxoin dimethylether or thermally initiated 1,1′-azobis(1-cyclohexanecarbonitrile)). Subsequent polymerization of the DM fixed the structure while the coupling agent helped to prevent structural collapse after surfactant removal by creating covalent bonds at the organic–inorganic interface. Dip coating provided a mechanism for multilayer construction without the need for repeated deposition steps to build up useful thicknesses. Mesostructures observed in this system were lamellar with an overlayer of isotropic worm-like micelles encased in silicate. The ordered lamellar regions were suggested to have grown from the substrate during deposition, via a continuous interfacially assisted self-assembly process. The thickness of the ordered region was dependent upon the coating rate and the nature of the substrate surface.

Further engineering of the pore structure created by the solvent evaporation during dip coating was carried out by Zhao *et al.* (1998c,d). In these papers the surfactant template used was chosen in order to change the surfactant packing parameter g to favour various liquid crystal phases and to increase the pore size by increasing the size of the template micelles. Large-head-group cationic surfactants (e.g. cetyltriethylammonium bromide (CTEAB)), gemini surfactants $C_{18}H_{37}N(CH_3)_2(CH_2)_3N(CH_3)_3Br$ (C_{18-3-1}) or polymeric surfactants (poly(ethylene oxide)–poly(propylene oxide)–poly(ethylene oxide) ($EO_xPO_xEO_x$) triblock copoly-

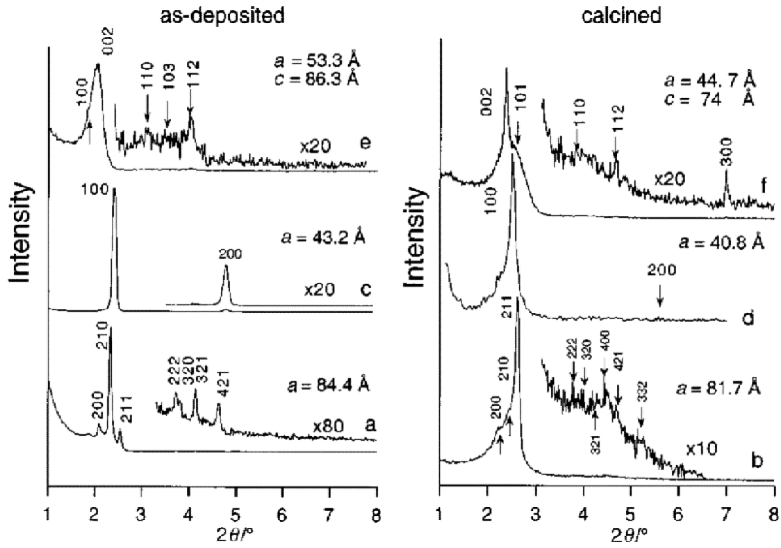

Figure 9. XRD patterns from as-deposited (curve a) and calcined (curve b) 3D cubic (*Pm*3*n*) mesophase silica thin films prepared using CTEAB surfactant, as-deposited (curve c), and calcined (curve d) 2D hexagonal mesophase silica thin films prepared using CTEAB surfactant, and as-deposited (curve e) and calcined (curve f) 3D hexagonal mesophase silica film prepared using gemini $C_{18\text{-}3\text{-}1}$ surfactant. (Reprinted with permission from Zhao *et al.* (1998c). © The Royal Society of Chemistry 1998.)

mers and EO_x non-ionic surfactants) were used. The films were deposited from prehydrolysed TEOS in acidic ethanol–water solutions where the majority component was ethanol. The as-deposited films were heated overnight in deionized water at 80°C. Dip-coated films were transparent and continuous with uniform thickness dependent on the coating solution concentration or coating time. CTEAB-templated films contained *Pm*3*n* cubic mesostructures that were stable to calcination (figure 9). 2D hexagonal phases could be grown from this surfactant by increasing the acid concentration (the reverse of the situation found when depositing films containing this surfactant from aqueous solutions). A 3D hexagonal phase ($P6_3/mmc$) was formed using the gemini surfactant in films deposited from both aqueous and ethanol solutions; however, increasing the acid concentration in the ethanol solutions also resulted in the 2D hexagonal phase with channels parallel to the substrate. C_{16}TAB-templated films deposited from ethanol showed only the 2D hexagonal phase. Polymeric surfactant templates resulted in larger periodic pore and cage structures in the deposited silica–surfactant films. Dipping solutions were made by dissolving the polymeric surfactants in ethanol, and adding this solution to acidic prehydrolysed TEOS sol–gel solutions containing HCl, water and an organic solvent, which was ethanol, methanol, 1,4-dioxane, tetrahydrofuran, CH_3CN or propanol. A triblock copolymer template ($EO_{20}PO_{70}EO_{20}$) was used to produce well-aligned 2D hexagonal silicate–surfactant composites, having a unit cell of 105 Å, with the channels parallel to the substrate and aligned with the dip-coating direction. Calcination produced stable 2D hexagonal mesostructures, which were free of microcracks for films up to 1 μm thick. Block copolymers such as $EO_{17}PO_{85}EO_{17}$ (Pluronic P103), $EO_{20}PO_{30}EO_{20}$ (Pluronic P65), $EO_{26}PO_{39}EO_{26}$ (Pluronic P85) or $EO_{13}PO_{70}EO_{13}$ (Pluronic L64) also were found to produce 2D hexagonal phases

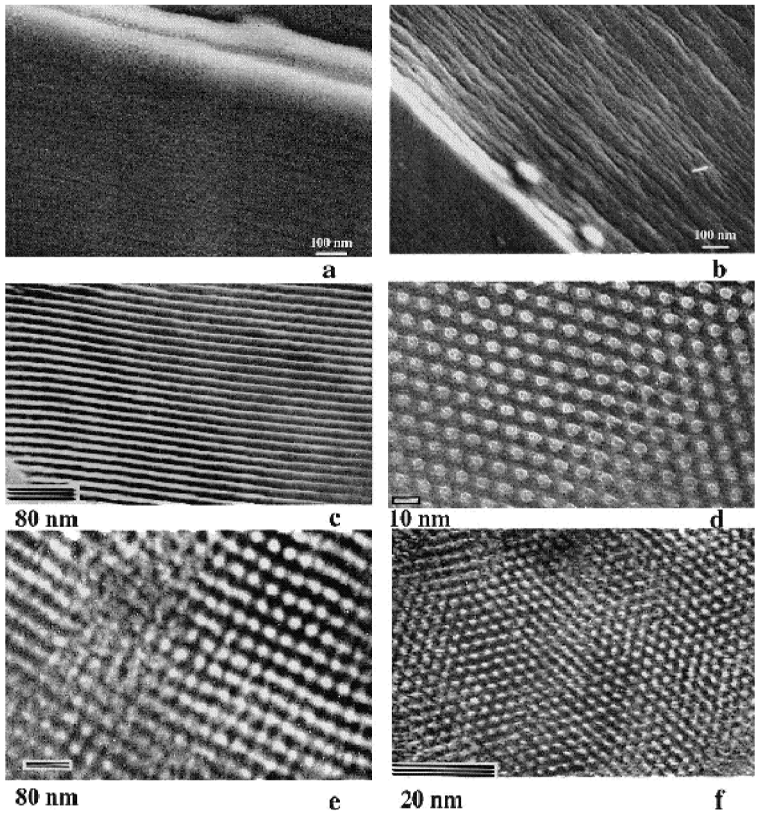

Figure 10. (*a*), (*b*) Scanning electron micrographs of (*a*) as-deposited and (*b*) calcined 2D hexagonal (*p6mm*) mesophase silica films prepared using an $EO_{20}PO_{70}EO_{20}$ block polymer template. (*c*), (*d*) TEM images recorded along (*c*) the [110] and (*d*) the [100] zone axes of a calcined 2D hexagonal film prepared using an $EO_{20}PO_{70}EO_{20}$ block copolymer template. (*e*), (*f*) TEM images recorded along (*e*) the [110] and (*f*) the [100] zone axes of a calcined cubic ($Im\bar{3}m$) mesophase silica film prepared using an $EO_{106}PO_{70}EO_{106}$ block copolymer template. (Reprinted with permission from Zhao *et al.* (1998d). © Wiley–VCH Verlag GmbH 1998.)

over a wide composition range resulting in pore sizes from 40 to 90 Å and porosities from 51 to 75%. Mesoporous silicate–surfactant films with a cubic cage structure ($Im\bar{3}m$) were formed from block copolymers with higher ratios of ethylene oxide (EO) to propylene oxide (PO) (e.g. $EO_{106}PO_{70}EO_{106}$ (Pluronic F127) (figure 10)). The (100) plane was aligned parallel to the substrate in this case. At much higher acid concentrations this surfactant also formed films with the aligned 2D hexagonal channel structure. The lower-molecular-weight alkyl(ethylene oxide) non-ionic surfactants were used to create well-ordered 2D hexagonal oriented films with *d* spacings between those found for polymeric and for small-molecule surfactants (e.g. about 60 Å for $C_{18}EO_{10}$ surfactant). Solution phase preparations, in contrast, are generally much less well ordered for these surfactants (Bagshaw *et al.* 1995). Increasing the acid concentration in this preparation causes the 3D cubic ($Pm\bar{3}m$) phase to form after dip coating, with the (110) plane on average oriented parallel to the substrate (figure 11).

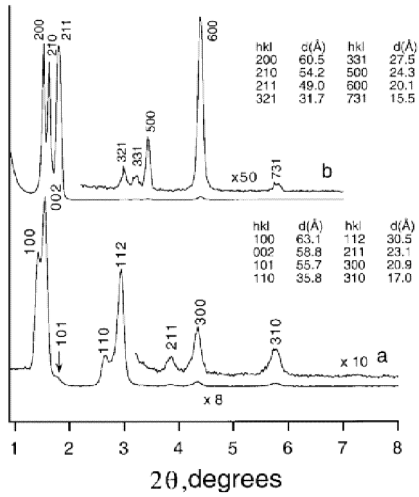

Figure 11. XRD patterns of as-deposited $P6_3/mmc$ hexagonal mesophase silica film prepared using $C_{18}EO_{10}$ as the surfactant template (curve a) and as-deposited 3D cubic ($Pm\bar{3}m$) mesophase silica film prepared using $C_{16}EO_{10}$ (curve b). (Reprinted with permission from Zhao *et al.* (1998d). © Wiley–VCH Verlag GmbH 1998.)

Mesostructured films in which the dye was covalently attached to the silicate framework were prepared by Lebeau *et al.* (1999) using similar methods to those used by the New Mexico group. Dilute prehydrolysed TEOS in an acidic ethanol–water solution formed the silica source but the solution also incorporated an organo-substituted silane (3-(2,4-dinitrophenylamino)propyltriethoxysilane)) in order to attach covalently the organic chromophore into the silicate walls. C_{16}TAB was used as the template and the film deposited by dip coating on to glass slides and aged at 150°C for 24 h. Monoliths of this material were also produced by casting, followed by evaporation of the same synthesis solution. Larger-pore materials were produced by swelling the C_{16}TAB micelles with 1,3,5-trimethylbenzene (TMB). The template was removed by washing in ethanol. XRD patterns indicated the formation of 2D, hexagonally packed cylinders, with no preferential orientation with respect to the substrate. The TMB-containing composite was much less well ordered than the unswollen materials. NMR, Fourier transform infrared (FTIR) and UV–visible measurements confirmed the presence of the intact dye within the mesopores after surfactant extraction.

2.2.3. *Patterning of mesostructures on substrates*

The interesting recent work of Doshi *et al.* (2000) made use of molecular photoacid generators and Brij 56 surfactant ($C_{16}H_{33}(OCH_2CH_2)_{10}OH$) as templates in dip-coated silicate films where the surfactant ordering during solvent evaporation trapped the photoacid generator within the mesophase as a cosurfactant. Condensation of the silicate in the precursor solution was suppressed by prehydrolysis of TEOS under conditions designed to minimize siloxane condensation, in order to promote silica–surfactant supramolecular assembly during film deposition. When exposed to UV light, through a mask, localized acid-catalyzed siloxane condensation occurred, solidifying the surfactant silicate composite (figure 12 (*a*)). Unexposed regions could then be selectively etched, leaving patterned areas of low-dielectric-

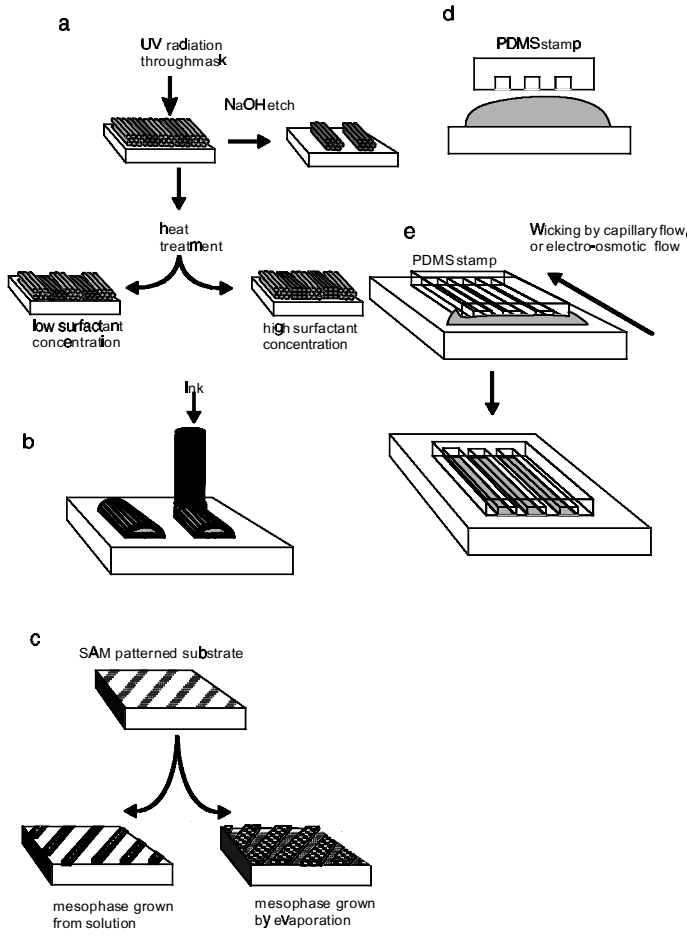

Figure 12. Schematic diagrams showing various methods of patterning mesophase silica–surfactant composites on to substrates. The silica–surfactant precursor solution is shown as grey. (*a*) The method of Doshi *et al.* (2000) using a mesophase doped with a photoacid generator which is activated by irradiation with UV light, causing silica wall polymerization to occur in the regions exposed through a mask to the light. Unexposed regions can be removed by a sodium hydroxide etching process or left in place to form a continuous film with a structure and refractive index which is dependent upon the local patterned degree of silica polymerization. (*b*) The micropen method of Fan *et al.* (2000) where the precursor solution is deposited as an ink on the substrate and mesostructure formation occurs as the solvent evaporates. (*c*) Patterning through use of SAMs stamped on to the substrate can be achieved in two ways. Spreading of a dilute aqueous solution over the patterned hydrophobic–hydrophilic surface results in dewetting from the hydrophobic SAM-covered regions and mesophase formation in the hydrophilic areas on the substrate (Fan *et al.* 2000). However, spontaneous growth of a mesophase from solution on to a patterned substrate results in mesophase formation on the hydrophobic areas of the surface (Yang *et al.* 1997b, Coombs *et al.* 1997). (*d*) Patterning using a stamp can also be obtained by using the stamp itself to displace a drop of precursor solution from the substrate surface, provided that the solution will dewet the substrate to allow good contact between the poly(dimethyl siloxane) (PDMS) stamp and the substrate (Yang *et al.* 1998d). (*e*) Finally a patterned PDMS stamp with open ends in contact with a substrate surface can be used to pattern the mesophase on to a substrate. The recursor solution is drawn into the channels of the pattern by capillary flow (Yang *et al.* 1998d) or through electro-osmosis (Trau *et al.* 1997).

constant mesophase film. The reaction could also be used for creating graduated changes in refractive index within the film, for patterning of pore size, pore connectivity, surface area and wetting behaviour and for optically defining a mesophase transformation from hexagonal to tetragonal within the film. Graduations in refractive index resulted from variations in UV dose, resulting in different silica densities in different parts of the irradiated film. At higher surfactant concentrations, irradiation of the film changed the charge density of the framework relative to that of the EO head groups, resulting in a hexagonal to tetragonal (distorted cubic) phase change through an undulating intermediate structure. The structural transformation was explained as an effective increase in surfactant head-group area to maintain charge-density matching at the silica–surfactant interface. Increasing the surfactant head-group area reduced the surfactant packing parameter g, favouring formation of the higher-curvature lower-density mesophase.

Evaporation-driven self-assembly has also been put to use by this group to create a self-assembling ink, which can be patterned using micropen lithography (figure 12(*b*)) and ink-jet printing (Fan *et al.* 2000). The dilute acidic prehydrolysed TEOS sol in an ethanol–water solution was prepared at a pH that would minimize the silicate polymerization rate, and surfactant was added at an initial concentration well below its CMC value to form a stable ink. After the pattern of ink was metered on to a surface, the preferential ethanol evaporation caused the CMC of the surfactant–silicate composite to be exceeded and self-assembly into micelles resulted in the formation of mesostructures, nucleated at the liquid–vapour interfaces. The mesostructures grew inwards along compositional trajectories established by the steep 3D evaporation-induced concentration gradient. Organo-substituted silanes were also included in the oligomeric silica sol to prepare mesostructures with walls functionalized on a molecular scale as well as having mesoscale and macroscale organization. The amphiphilic nature of the organosilanes caused them to behave as a cosurfactant, locating the reactive siloxane group at the micelle surface, and caused the organic tail to remain attached to the pore surface when the surfactant template was removed. This cosurfactant nature also caused changes in the symmetry of the mesostructure formed during the solvent evaporation. Alcohol-soluble dyes such as rhodamine B could be included into the surfactant–silicate composite films by segregation into the tail region of the surfactant micelles as ethanol evaporation took place. The thickness of the lines drawn by the micropen lithography method varied from microns to millimetres depending on pen dimension, wetting characteristics, evaporation rate, ink viscosity, substrate speed, surface tension and the ratio of the rate of ink supply to the rate of withdrawal. The use of micropen lithography together with different combinations of surfactant and functionalized silane resulted in the ability to create functionalized films patterned on arbitrary surfaces and the ability to print different functionalities at different locations. Micropen lithography is best suited to writing continuous structures; however, ink-jet printing could be used to print patterned macroscopic arrays of discrete mesostructures with resolution comparable with that achieved using standard ink. Dip coating of the same solutions on to hydrophilic–hydrophobic surfaces patterned with self-assembled monolayers (SAMs) through microcontact printing or electrochemical patterning also resulted in patterned mesophases (figure 12(*c*)). In this case the evaporation of the ethanol from the solution resulted in an enrichment of the water content, causing selective dewetting in the hydrophobic regions and ensuring self-assembly of the silica–surfactant mesophases exclusively on the hydrophilic regions. This approach

enabled the printing of arbitrary shapes having uniform mesostructures within seconds. Slow nucleation and spontaneous growth of thin film mesophases on to patterned SAMs suspended in solution were observed to produce inhomogeneous globular morphologies unsuitable for fluidic or photonic applications. It was also noted that in this case the mesophase grew on to the hydrophobic regions of the patterned surface.

2.2.4. *Structural studies on dip-coated films*

Detailed structural studies of dip-coated films have been carried out by Klotz *et al.* (2000a) on the static solid films. This group used a similar TEOS solution aged for 3 h prior to deposition. This preparation method was developed in an earlier paper (Klotz *et al.* 2000b) where deposition from TMOS in a methanol–water solution was compared with deposition from TEOS in an ethanol–water solution. The surfactant was added at various ageing times after preparation of the silica sol and subsequently also aged before deposition. The best results were obtained for TEOS solutions aged for a total of around 200 min prior to deposition (being the sum of ageing times for hydrolysis prior to surfactant addition and further ageing after surfactant addition). This corresponded to the greatest number of Q_1 species in the sol from ^{29}Si NMR measurements. When the Q_3 species appeared in the sol, hexagonal ordering in deposited films was lost, indicating that too large a condensation of silicate oligomers prevented the formation of the ordered composite. However, if the solution was not sufficiently condensed when deposition occurred, preferential evaporation of the alcohol solvent caused the formation of localized drops on the substrate, as water had a low surface tension with respect to the substrate. The 2D hexagonal film structure was well defined and maintained after calcination for surfactant volume fractions in the final material of between 0.5 and 0.65 when TMOS was used as a silicate source and slightly lower volume fractions when TEOS was used, corresponding to the hexagonal regions found in the CTAB–water phase diagram. Use of shorter-chain surfactants resulted in a shift of the hexagonal phase to higher volume fractions of surfactant to silica, as was also expected from the surfactant–water phase diagrams, but calcination-stable well-ordered phases were found only for C_{12} and longer-alkyl-chain surfactants. The pore diameter in the deposited films could be tailored by adjusting both the chain length and the surfactant volume fraction. The *d* spacing of the system was observed to increase as the surfactant volume fraction in the deposited film decreased and this phenomenon was explained as a swelling of the silicate region by an increase in the volume fraction of the aqueous phase. The shrinkage of the swollen phases upon calcination was greatest for those having the largest water volume fraction, and therefore lowest silica content in the walls, which were presumed to form as a sol–gel in the interstices between micelles (Cot *et al.* 2000) rather than by specific interaction with the surfactant head groups. The wall densities measured for these materials are rather lower than for bulk amorphous silica, being 1.75 g cm^{-3} for TMOS and 1.69 g cm^{-3} for TEOS gels (Klotz *et al.* 2000b). The addition of nanoparticle silica or magnetic maghemite seeds to these dip-coated films destroyed most of the in-plane orientational order for the maghemite particles and all the oriented domains for the larger silica nanoparticles (Klotz *et al.* 2000a). Attempts to produce ordered porous films of alumina or titania via the same method resulted in ordered composite gels which were, however, not stable to calcination (Cot *et al.* 2000). A membrane prepared from C_8TAB and TMOS showed preferential adsorption of ethanol over cyclohex-

ane into the 10 Å micropores in this film, owing to interaction with surface hydroxyl groups on the silica walls.

Detailed structural work on these dip-coated films was carried out using 2D transmission XRD to observe ordering aligned with the substrate (Klotz *et al.* 2000a). The structure of a C_{16}TAB–TEOS film proved to be distorted in the *b* direction, being a centred rectangular rather than a true 2D hexagonal phase. A Pluronic F127 ($EO_{106}PO_{70}EO_{106}$)-templated film also showed a centred rectangular structure although with larger *d* spacing and greater eccentricity than the C_{16}TAB-templated film. The centred rectangular structure was ascribed to greater shrinkage of the hexagonal structure in the perpendicular direction relative to the substrate that occurred during solvent evaporation from the top surface of the deposited film. A similarly 1D shrinkage was observed after calcination. The films were powders in the (a, b) plane and all the films prepared showed some disorder in the orientation of the cylindrical pores parallel to the interface, although large areas of very-well-ordered film were created in most cases.

Detailed static structural work on C_{16}TAB–TEOS dip-coated films was also carried out by Grosso *et al.* (2000) using 2D transmission XRD, ellipsometry and TEM. This group synthesized films from acidic (pH 2) prehydrolysed TEOS in an ethanol–water solution with a C_{16}TAB template, with the dipping solution stirred for 48 h prior to deposition. The structural studies indicated the formation of large areas of packed ellipsoidal micelles with 3D hexagonal ($P6_3/mmc$) ordering extending the entire width of the film. This was the first report of formation of this particular structure using C_{16}TAB as the template, although it had been reported for gemini surfactants (Tolbert *et al.* 1997) and for alkyl poly(ethylene oxide) surfactant templates (Zhao *et al.* 1998d). These domains show no preferential ordering in the (a, b) plane (parallel to the substrate) corresponding to the direction of withdrawal from the dipping solution. After template removal a contraction of the network was observed, but only in the direction normal to the substrate. Various low-temperature treatments were applied to remove the surfactant and to avoid damage to possible included species by calcination at high temperatures. Soxhlet extraction in ethanol after heat treatment to increase wall condensation resulted in the least unit-cell contraction and the same porosity as calcination while treatment with ammonia followed by Soxhlet extraction caused a decrease in unit-cell spacing similar to that in calcined films. TEM images suggested the possibility of connections between the ellipsoidal pores in these films.

2.2.5. *Applications of dip-coated films*

Recently it has been reported by Chia *et al.* (2000) that by using the principles of surfactant–silicate organization it is possible to create hexagonal arrays of spherical living cells via dip coating of a silicate-cell solution. The silica interacts with the lipid species of the cell membranes in the same manner as with surfactants, and the cells themselves pack to form a 2D hexagonal network embedded in the silica film.

Dip-coated films of surfactant-templated silica have also been used by Plyuto *et al.* (1999) to synthesize silver nanoparticles within the mesostructured channels. A 2D hexagonal phase film 100 nm thick, using a C_{16}TAB template, was deposited by dip coating from a TEOS–ethanol–water solution on a glass substrate. The films were calcined, next impregnated with an aqueous solution of $[Ag(NH_3)_2]NO_3$ in water, dried and then treated in a hydrogen–nitrogen flow at various temperatures for the reduction of silver. This produced a colour change in the film from clear to

yellow, and an adsorption peak at 410–435 nm was characteristic of the surface-plasmon resonance of silver nanoparticles. No nanoparticles were observed in films deposited without the surfactant. TEM showed the distribution of nanoparticles to be bimodal with one diameter centred around 3 nm and the other around 6–7 nm, possibly owing to defects such as locally merged pores in the film. Successive silver impregnation treatments caused the particles to grow up to 5 and 11 nm respectively.

Dip coating of surfactant-templated silicate films has been used by Wirnsberger *et al.* (2001) to produce films with pH-sensitive dyes covalently anchored to the silicate wall using a method similar to that of Lebeau *et al.* (1999). These films were produced by introducing a hydrolysable unit on to the dye molecules, which allowed the surfactants to be removed, leaving a porous matrix with the anchored dye molecules. In this case, fluorescein isothiocyanate was derivatized with 2-aminopropyltriethoxysilane, and this dye was incorporated into a solution of the triblock copolymer Pluronic F127 ($EO_{106}PO_{70}EO_{106}$) in acidified water with TEOS as a silicate source. This solution was refluxed for 1 h and used to prepare films by dip coating, resulting in films 900 nm thick although with considerable variation in thickness along the dipping direction. Spin coating of the same mixture resulted in more homogeneous but thicker films (1500 nm). XRD patterns showed peaks indexable in the $P6_3/mmc$ space group, indicating that the film consisted of a hexagonally packed network of cages, although a small amount of cubic $Im3m$ impurity phase was also present. This phase was formed from the same silica–polymer mixture in the absence of dye and so was attributed to areas in the film where no dye was incorporated. Increasing the concentration of dye did not result in ordered film mesostructures owing to the pH increase caused by the basic amine. It was possible to remove the templating surfactant using hot ethanol without cracking the film only when the films were aged for 10 days at room temperature and afterwards for 3–5 days at 70°C. The extraction procedure resulted in less shrinkage of the unit-cell constants than calcination of a similar film, and even after prolonged treatment in ethanol the optical transparency and all the reflections in the XRD patterns of as-synthesized materials were retained. The response time of photoluminescence of dye incorporated in the films to a change of pH was fast because of the porosity of the film. This compared favourably with that observed for the same dye incorporated in sol–gel-based sensors.

2.3. *Casting*

Cast films are those in which the synthesis solution is merely dropped on to a substrate and left to solidify. This method results in much thicker films and the boundary between a film and a monolith is largely defined by the viewpoint of the researcher. For the purposes of this review some of the recent papers on thin cast structures resulting from solvent evaporation processes are covered, but the reader should be aware that many other papers on cast monoliths exist (see for example Dabadie *et al.* (1996), Ogawa (1996), Göltner *et al.* (1999) and Lebeau *et al.* (1999)).

2.3.1. *Control of mesophase structures*

Casting of a mesophase silica–surfactant film was briefly mentioned by Attard *et al.* (1995) in work on using concentrated liquid crystal phases as templates for mesoporous silica. In this report, non-ionic octaethylene glycol monododecyl ether ($C_{12}EO_8$) or octaethylene glycol monohexadecyl ether ($C_{16}EO_8$) were used as templates with a TMOS silica source. The required surfactant phase (in this case

the 2D hexagonal phase) was prepared by dissolving the surfactants in water at pH 2 with a 50% ratio of surfactant to water. TMOS was added such that the final amount of TMOS was not more than 0.25 mol equivalent with respect to water. Methanol from TMOS hydrolysis was removed from the system using gentle vacuum, causing the disrupted hexagonal phase to reform. Thin films of this optically birefringent mixture were heated to 45°C and formed solid films after 2–3 h with no visible alteration of the optical properties. TEM, nitrogen isotherms and XRD confirmed the formation of the 2D hexagonal structure that was retained on calcination. Thin films of *Ia*3*d* cubic and lamellar mesostructured silica were also prepared in this manner using more concentrated surfactant solutions.

Another early report by Ryoo *et al.* (1997) concerned the formation of films and monoliths up to 0.5 mm thick. The synthesis solution was an acidic TEOS solution in an azeotropic mixture containing molar ratios of 2 ethanol:3*n*-heptane:0.5 H_2O with a small amount of HCl. The surfactant used was cetylpyridinium chloride. In later work, other azeotropes with ethanol such as acetonitrile, toluene and chloroform were also used, and various quaternary ammonium bromide and gemini surfactants were used as templates (Ko *et al.* 1998). These solutions were refluxed for 1 h and then concentrated on a rotary evaporator under vacuum at 333 K. The resulting viscous solutions were coated on to slide glass, pulled into fibres through a nozzle or cast into Petri dishes and then dried in an oven at 313 K to complete solvent evaporation. Films could be dried rapidly without cracking but monoliths up to 0.5 mm thick required drying for several hours while partially covered to slow solvent evaporation. The use of binary azeotropes of ethanol helped to control cracking during drying by reducing the surface tension of the solvent while still allowing sufficiently high boiling points to permit silicate polymerization at reasonable rates (Ko *et al.* 1998). The films and monoliths were repeatedly exposed to alternating TEOS vapour and vacuum at 423 K in order to reinforce the structure and then calcined. Films and plates created in this manner were optically clear and crack free over the centimetre size range and showed uniform birefringence under crossed polarizers. XRD showed two peaks ascribed to hexagonally packed cylindrical channels oriented parallel to the substrate or to the top and bottom faces of the monoliths; powder XRD on a ground specimen showed the expected hexagonal diffraction pattern. It was observed by *in-situ* XRD that the mesoscale structure did not develop until the completion of the solvent evaporation step.

The structure of these cast films was highly dependent upon synthesis conditions: the nature of the solvents, the drying temperature and time, the convection conditions in the oven, the sample size and the surface roughness of the sample container were all identified as important factors (Ko *et al.* 1998). Films synthesized with different amounts of water in the synthesis solution or different reflux times in the azeotrope gave only one broad peak in the mesophase region of the XRD pattern and were isotropic under crossed polarizers, indicating a disordered arrangement of interconnected worm-like channels. Films created with lower TEOS-to-surfactant, water-to-TEOS or HCl-to-TEOS ratios and shorter refluxing times had low degrees of silica polymerization at the point of casting and showed segregation of the surfactant from the silicate, resulting in opaque materials. Films dried at high temperatures for extended periods of time also developed increasing disorder because of continuing silicate condensation, and XRD patterns showed differences between the top and bottom surfaces. Argon adsorption isotherms gave high surface areas (1250 $m^2 g^{-1}$) for both ordered and disordered films, showing that the pore

volume was accessible throughout the film (Ryoo *et al.* 1997). It was observed that ordered film formation occurred even for very low TEOS-to-HCl ratios and that no mesoscale organization was observed when the degree of silicate polymerization was too low or too high. On the basis of this it was suggested that the mesoscale organization occurred not as a result of $S^+X^-I^+$ interactions as is generally assumed to be the case in highly acidic syntheses, but via multiple weak non-bonded or hydrogen-bonded interactions between the template surfactant and the growing silica oligomers. These non-bonded interactions were too weak to allow mesostructure formation in solution but were sufficient to enable ordering after the solvent had been removed by evaporation as observed by *in-situ* XRD. Silica oligomers larger than the preferred wall thickness disrupted the mesoscale ordering in the growing films.

Cast films using poly(isoprene-b-ethylene oxide) block copolymer templates were reported by Templin *et al.* (1997) using (3-glycidyloxypropyl)trimethoxysilane ($(CH_3O)_3Si(CH_2)CHCH_2$-O) and aluminium *sec*-butoxide ($Al(OBu^t)_3$) as the inorganic precursors. In the absence of inorganic species the block copolymer used (which was about 15% EO_x by volume) formed a microdomain structure of spheres packed in a bcc lattice. The inorganic precursors were prehydrolysed in the presence of HCl and a stoichiometric amount of water required for complete hydrolysis of the metal alkoxide groups for 1.5 h then added to the block copolymer solution in $CHCl_3$ and tetrahydrofuran. Films 0.5–1.0 mm thick were cast in Petri dishes at 333–343 K from this solution after stirring for 2 h. The solvents were allowed to evaporate and the composite then treated at 403 K in vacuum for 45 min to complete the inorganic condensation. SAXS patterns of these materials showed lamellar and 2D, hexagonally packed cylindrical structures having d spacings of about 40 nm, with the planes oriented parallel to the film interfaces. The inorganic species were segregated into the EO_x regions of the block copolymer, suppressing the crystallization so that no T_g was observed, while the T_g for the polyisoprene block remained unaffected.

2.3.2. *Macroscale patterning of cast surfactant–silica films*

Patterning of mesostructured membranes simultaneously on the macroscale has been recently reported by Zhao *et al.* (1999) who cast films consisting of mesoscopically ordered block copolymer–silicate phases that macroscopically phase separate from an electrolyte phase. This results in a composite with different characteristic length scales that can be independently adjusted. The membranes were prepared by casting of prehydrolysed acidic TEOS in an ethanol solution containing $EO_xPO_xEO_x$ triblock copolymers and inorganic salts such as NaCl, LiCl, KCl, NH_4Cl and $NiSO_4$ in water. The solutions were dried at room temperature, washed to remove residual inorganic salts and calcined to remove the polymer. The resulting membranes can be varied to be between 10 μm and 5 mm thick and they have a 3D sponge-like, macroscopically porous structure with the network made up of struts (about 1 μm thick) consisting of continuous interconnected rope-like mesoporous silica (figure 13). The mesostructure is composed of 2D, hexagonally packed cylinders (*p6mm* symmetry) for lower-molecular-weight $EO_xPO_xEO_x$ copolymers and *Im*3*m* cubic structures for higher-molecular-weight templates, with d spacing also dependent on template size. The macropores are not well ordered but have shapes reflecting the sizes and structures of the aqueous salt droplets and crystals that grow from these droplets. Droplet size depends upon the rate of ethanol evaporation and the rate of silicate condensation; high evaporation rates cause large

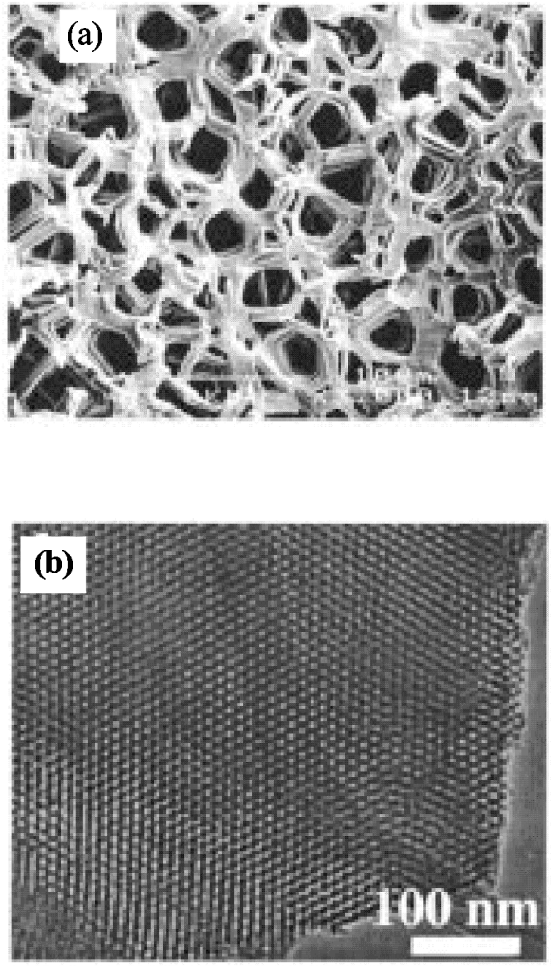

Figure 13. (*a*) SEM image of as-synthesized and washed meso-macrostructural silica membranes prepared using a P123 ($EO_{20}PO_{70}EO_{20}$) block copolymer template in sodium chloride solution. (*b*) TEM image of the mesostructured silica struts from the calcined material from the same preparation as (*a*). (Reprinted in part with permission from Zhao *et al.* (1999). © 1999 American Chemical Society.)

droplets to form which cannot coalesce due to the high viscosity of the silica sol. Crystallization of the inorganic salts was affected by the block copolymers, resulting in various unusual crystal morphologies around which the silica framework formed. The macrostructure formed was due to non-equilibrium interactions with the surface energies and forces at the strong electrolyte-triblock copolymer–silica interface. Both the polymer template and the inorganic salts were easily removed from the silicate framework by washing, indicating that there was only a weak interaction between the silicate walls and both kinds of template.

Similar macrophase templating but without mesophase porosity has been carried out by Karthaus *et al.* (1999). This group created microphase honeycomb structures in a titanium dioxide film by casting a chloroform solution of the alkoxide with double-chain surfactants (either didodecylphosphate or ditetradecyldimethylammo-

nium bromide) in a humid atmosphere. Condensation of water droplets on to the chloroform solution results in a hexagonally ordered array of spherical microemulsion droplets stabilized by the surfactant. Evaporation of the chloroform, followed by the water, leaves spherical 2D ordered arrays of voids 500 nm diameter in the titania film. Similar films could be formed using niobium ethoxide as the inorganic precursor. Lateral flow of the solution, achieved by tilting the substrate during solvent evaporation, led to the formation of a void structure with orthorhombic symmetry as well as some regions with elongated water pores.

2.3.3. *Domain structures in cast monoliths*

Detailed analysis of the structure of a cast monolith (1–2 mm thick) was carried out by Melosh *et al.* (2000) showing the existence of several phases within the one structure (figures 14 and 15). These materials were prepared using block copolymer ($EO_xPO_xEO_x$) templates, dissolved in water–ethanol solution. TEOS was added and the solution tightly sealed for 12 h and then left open to gel (3–4 days). The vial was then sealed and allowed to age at room temperature for 6 weeks; it was then uncovered and stored at room temperature to allow the evaporation of excess solvent. 2D XRD patterns taken of the monoliths through two perpendicular directions indicated 2D, hexagonally packed cylindrical aggregates lying parallel to the air–sample interface with a d spacing of 111.9 Å for the $EO_{106}PO_{70}EO_{106}$ triblock copolymer template used. The sharpness of the diffraction spots and the constancy of the pattern as the sample was translated, indicated that a single-crystal sample had been formed in the 1.5 cm × 1 mm × 1 mm volume that had been cut from the prepared sample. Typical domain sizes were about 0.5 cm^2 × 1 mm and were ascribed to the slow annealing process used to produce the monoliths. Average deviations in alignment from a perfect hexagonal array in the (a, b) plane were only $\pm 1^\circ$ over the 1 mm^3 sample volume probed by the X-ray beam and only $\pm 6^\circ$ along the length of the cylinders in the same volume. Calcination caused the structure to become opaque because of microcracks in the silicate framework and a slight increase in the disorder of the hexagonal orientational order (an increase in the FWHM from 2° to 8° for the (10) peak). Diffuse scattering appearing between the strong diffraction peaks was suggested by analogy with scattering observed for low-molar-mass thermotropic mesogens to be due to localized defects, such as dislocations of the hexagonal lattice. Two additional rows of weak reflections, which did not belong to the hexagonal mesophase, were suggested to be due to a small amount of an epitaxially related oriented cubic structure. TEM indicated that the sample contained some areas that appeared as a modulated cylinder–layer structure where the silica walls separating the cylindrical channels had thickened preferentially along the hexagonal (10) planes. This produced a structure that appeared as hexagonally spaced pores interspersed with silicate lamellae, a structure which has also appeared in the hexagonal → cubic → lamellar phase transitions in liquid crystal systems. The denser planes of the hexagonal structure become the layers of the lamellar structure but, as the periodicity and hexagonal arrangement of the channels are unaffected, the diffraction patterns overlap with those of the bulk hexagonal phase. Large areas of very-well-ordered cubic phase were also found in the same sample, occurring near the outer edges of the monolith, with a similar degree of order to that observed for the hexagonal phase (FWHM for the (100) peak less than 3°) although the lattice spacing was smaller at 97 Å. This order was also preserved, with some shrinkage, upon calcination. In the as-synthesized materials the cubic phase was found to exist

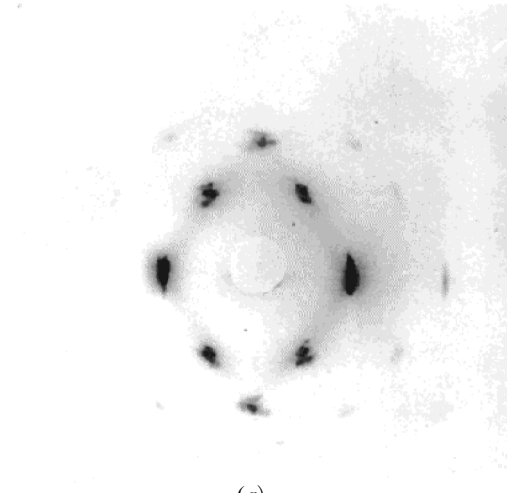

(*a*)

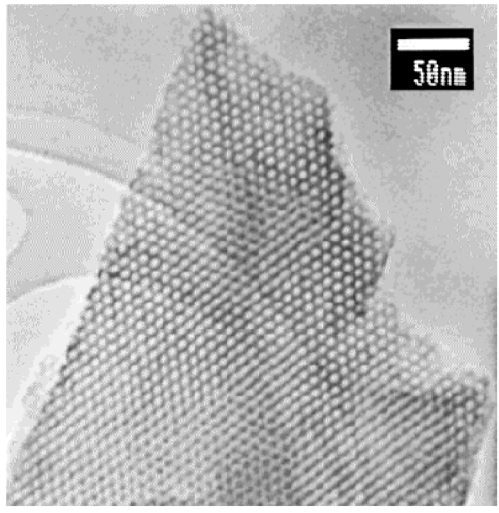

(*b*)

Figure 14. (*a*) 2D XRD pattern from a hexagonally ordered mesostructure silica material following calcination. The reflections are (10), (11), (20), (21) and (30), giving a lattice constant of 107.7 Å, and the sharp diffraction spots and higher order peaks indicate that the structure is predominantly a highly ordered single domain. (*b*) TEM image from the same calcined sample as in (*a*). The preferential thickening of some of the silica layers between the hexagonally packed cylinders visible in the lower right of the image shows the deformation responsible for the two significantly more intense XRD reflections visible in (*a*). (Reprinted in part with permission from Melosh *et al.* (2000). © 2000 American Chemical Society.)

in a thin layer (less than 0.1 mm) at the air–sample interface and also in a region 1–2 mm wide at the outer edge of the disc. A mixed region 1 mm thick of epitaxially related hexagonal and cubic phases was found to connect the cubic and hexagonal regions with the hexagonal cylinder director axes in registry with the cubic (111) direction. Cubic regions with reduced ordering were found in the highly curved meniscus regions and attributed to the large gradients in solvent concentration that

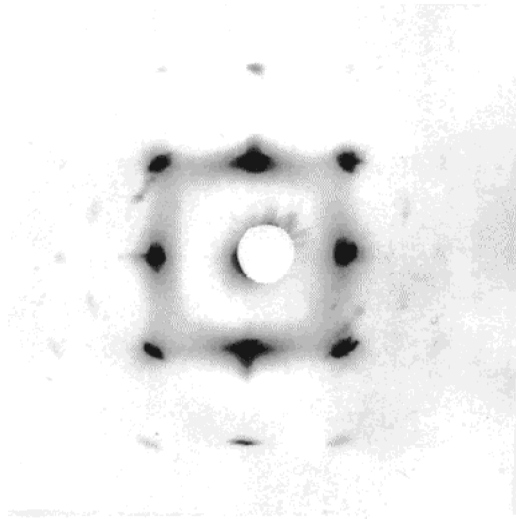

(*a*)

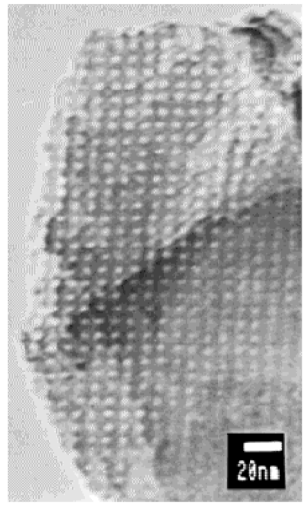

(*b*)

Figure 15. (*a*) 2D XRD pattern of the cubic domain obtained from the meniscus region of a calcined 50 wt% $EO_{106}PO_{70}EO_{106}$–silica composite. The sharp reflections indicate uniform long-range cubic mesostructural ordering characterized by $d_{100} = 93.1$ Å and a full width at half-maximum (FWHM) of 4°. (*b*) TEM image of the calcined cubic material from (*a*). The structure appears to be composed of spherical pores (about 30 Å in diameter) arranged on a cubic lattice. The cubic lattice appears to be slightly rectangular owing to imperfect alignment with respect to the incident electron beam, but the cubic symmetry is unambiguously established by XRD. (Reprinted in part with permission from Melosh *et al.* (2000). © 2000 American Chemical Society.)

are expected to exist at the air–monolith surface, which lead to spatially varying rates of block copolymer self-assembly, structural annealing and silicate polymerization. This pattern of structure formation in the monolith is suggested to arise from rapid solvent evaporation and silica polymerization near the surface of the solution, forming the cubic phase which is typical of the block copolymer template at low concentrations and which has been found for rapidly dried films using this template

(Zhao *et al.* 1998d). In the interior of the monolith, the slow transport of the water and ethanol to the evaporation surface causes the solution to cross over into the hexagonal concentration regime of the copolymer and silicate polymerization rates are low, permitting annealing and structural rearrangements creating large well-ordered domains.

Functionalized thin-film mesophases have also been produced by Dag *et al.* (1999b) through the use of salt LCT. In this work a lithium triflate–silicate–oligo(ethylene oxide) surfactant mesophase was cast on to a glass slide after the removal of methanol generated by the hydrolysis of the TMOS silicate source. As the film dried, an aligned 2D hexagonal phase was observed to form by optical polarization microscopy and XRD. Within the film the $LiCF_3SO_3$ was found to be dissociated into free lithium and triflate ions in the oligo(ethylene oxide) head-group region of the surfactant assembly within the mesoporous silica channels. This nanocomposite material was shown to be a fast lithium-ion conductor at room temperature, having possible applications in the field of polymer electrolytes and battery technology.

3. Films grown spontaneously from solution

3.1. *Films grown at a solution–substrate interface*

Rather than impose order by spreading of the film-forming solution on a substrate, it is also possible for the ordered silicate–surfactant composite to develop spontaneously at an interface submerged in the synthesis solution. Macroscopic films of this type grow only from acidic solutions, with the best ordering found for dilute synthesis mixtures.

3.1.1. *Spontaneous film growth on untreated substrates*

Surfactant silicate films formed spontaneously from an acidic synthesis medium on to mica substrates were first reported by Yang *et al.* (1996b) from Toronto. These films were grown from a solution containing molar ratios of 100 H_2O:7.4 HCl:0.11 C_{16}TACl:0.13–0.24 TEOS at 80°C for periods of 1–2 h up to 1 week, with the freshly cleaved mica substrate arranged to lie horizontally in the polypropylene bottle containing the synthesis mixture. The films formed were approximately 0.2–1.0 μm thick and grew on the bottom side of the horizontal mica substrate. As-synthesized films were washed with water. SEM images showed that separated small oriented crystals nucleated on the mica surface with a preferred alignment direction. These crystals grew in size and eventually coalesced to form a continuous mesophase film. SEM images showed that calcination at 540°C for 4 h in air did not destroy the macroscopic integrity of the film and argon adsorption isotherms as well as FTIR spectra of adsorbed benzene, perdeuterobenzene and tris-isopropylbenzene indicated the retention of porosity in the films. TEM images of epoxy-embedded and microtomed samples showed that the films were composed of surfactant-filled channels running parallel to the mica surface, with good adhesion to that surface. Scanning electron and optical micrographs suggested that the macroscopic crystalline domains of channels are co-aligned preferentially with the hexagonal unit-cell axes of mica. The TEM images also suggested that film nucleation began at the solution–mica interface. Some of the images showed 'brick-like' lateral distortions of the mesopores close to the film–mica interface and at the surface of the film mesoscopic steps suggested the multilayer deposition of surfactant–silica micellar

building blocks. XRD patterns showed two peaks, assigned to the (100) and (200) reflections from the aligned hexagonal mesophase. These were retained after calcination. It was also reported to be possible to remove the oriented films intact from the mica substrate. A formation mechanism was suggested that began with the nucleation of silica–surfactant micelles on the freshly cleaved mica surface. The cleaved surface of mica is atomically flat, containing aluminosilicate six-ring sites giving the surface hexagonal symmetry. Under acid conditions, potassium ion exchange with protons produces reactive Si—OH sites, which are available to bind to the silica–surfactant micellar precursors. The elongation of nucleated surfactant–silicate domains along the hexagonal cell axis of the mica implies that the crystal growth is regulated by charge and structure matching at the surface.

This report was followed quickly by a report by Schacht *et al.* (1996) of the formation of mesoporous silicate fibres, spheres and thin sheets at the oil–water interface. These preparations combined long-range ordering imposed by oil–water interfaces with the shorter range cooperative assembly of silica and surfactants to create ordered composite mesophases that were also macroscopically structured. The syntheses were made in acidic preparations where the interaction between silica and surfactant is mediated by the halide counterions of the surfactant through weak hydrogen-bonding forces. This allowed the surfactant molecules, coordinated to organic surfaces through van der Waals interactions, to maintain that structure during the mesophase self-assembly process. TEOS was used as the silica source, in the presence of auxiliary organics such as n-hexane, benzene, toluene or mesitylene to form an oil-in-water emulsion. The TEOS was dissolved in oil droplets that were surrounded by an acidic aqueous solution with surfactant concentrated in the interface. The TEOS was hydrolysed just at the oil–water interface and so there formed the mesostructure, encapsulating the oil droplet within the solidifying inorganic material. In the preparations, solutions of C_{16}TAB in water were acidified with HCl and the auxiliary organic and TEOS were added slowly over 30 min at room temperature with stirring. The rate of stirring determined the morphology of the silica–surfactant product. Slow stirring produced rope-like fibres made up of smaller intertwined fibred with mesophase channels oriented parallel to the fibre axis. Increasing the stirring rate produced more spherical morphologies that decreased in size with increasing stirring rate. These spheres proved to be hollow shells, having XRD patterns with *p6m* (2D hexagonal) symmetry, although $P6_3/mmc$ and $Pm3n$ phases could also be made using gemini surfactants.† Self-supporting membranes were produced at a static interface between an aqueous and an organic phase with the same chemical composition as was used for the emulsion preparations. About 5 min after the dropwise addition of the organic phase on top of the aqueous phase, formation of a patchy thin film was observed with the naked eye. After further growth time a coherent solid sheet was formed, with a thickness of about 0.5 μm. TEM on a piece of calcined film formed at the water–decane interface showed that the pores were predominantly hexagonally ordered and perpendicular to the plane of the film. Some pores were less ordered but also appeared to be perpendicular to the

† Extensive further work on discrete structures such as spheres, ropes and gyroids, formed as precipitates in acidic TEOS–C_{16}TAB preparations without the addition of auxiliary organics, has been carried out by the Toronto group (Yang *et al.* 1997c, 1998c, 1999b) but discussion of this is beyond the scope of this review.

film. XRD showed one or two small-angle peaks from these films. SEM showed that thicker films consisted of agglomerated particles but were relatively crack free; thinner films showed cracks due to handling and it was not clear whether these films also contained pores larger than the mesophase surfactant-templated channels.

Further growth of mesostructured surfactant–silica films on solid substrates was reported by Aksay *et al.* (1996) at Princeton. This group synthesized surfactant–silicate composite films from dilute acidic TEOS solutions containing an excess of C_{16}TACl on mica, graphite and silica substrates. Dilute solutions were used to decrease the rate of homogeneous nucleation such that thermodynamically favoured heterogeneous nucleation was dominant. Initial studies using AFM on the various substrates in the presence of the surfactant solution in the absence of TEOS showed the formation of one or two layers of cylindrical micelles on the substrate surface. The first layer of these micelles was dependent on the nature of the substrate. Adsorbed hemimicellar arrangements were observed on poorly orienting amorphous substrates such as silica while aligned tubular structures were found on more strongly orienting crystalline surfaces such as mica and graphite. The orientation of adsorbed surfactant occurred through anisotropic attraction (either van der Waals or electrostatic) between the crystalline substrate and the surfactant molecule. In the case of graphite the surfactant tails adsorb horizontally to the surface, causing the formation of rigid half-cylinder structures.

In the presence of TEOS, mesophase films formed on the substrates, having distinctly different surface textures on length scales between 0.5 and 10 μm. Oriented tapes were observed on mica and graphite substrates, with the film on mica appearing much smoother than that grown on graphite. On silica the film was initially uniform, but spiral structures about 10 μm diameter grew out into solution at the film–solution interface. AFM images showed meandering surfactant-filled tubules of 6.2–6.8 nm spacing oriented parallel to the substrate–solution interface. Tubules were initially aligned along one of the three next-nearest-neighbour directions of the mica oxygen lattice and this orientation was preserved for reaction times less than 7 h as the tubules continued to assemble and grow away from the interface. For long reaction times, aligned tapes and steps appeared on the film surface with macroscopic grain boundaries of 60° and 120° resulting from the registry of the surfactant tubules with the underlying mica lattice. XRD analysis indicated a distorted hexagonal stacking of surfactant tubules that lie parallel to the surface and TEM revealed hexagonally stacked tubules with a slight elliptical distortion of the tubules, suggesting that the films were compressed in a direction normal to the substrate.

On the hydrophobic graphite surface the AFM showed tubules aligned parallel to the substrate along one of three symmetry axes of the hexagonal carbon lattice. These tubules did not meander but formed rigid parallel stripes owing to the strong orientation effect of the large contact area between surfactant molecule and hydrophobic surface. After long reaction times, edges with macroscopic angles of 60° and 120° were also observed. Film formation on mica and graphite was therefore suggested to occur by a sequential mechanism beginning with surfactant self-assembly on a surface followed by intercalation and polymerization of inorganic material to form the mesostructured composite. Further surfactant self-assembly then occurred on the fresh silicate surface. The assembly of the first surfactant layer defined the structure of the subsequent film.

On amorphous silica, periodic dimples were observed rather than ordered stripes, suggesting an orientation of the tubules away from the interface. Similar dimpled structures were observed for C_{16}TACl-only solutions, which suggested the formation of roughly spherical surfactant aggregates that acted as starting points on the surface for the growth of cylindrical tubules into the solution. XRD analysis confirms a distorted hexagonal packing of the tubules. The dimpled pattern suggested a twisting arrangement of locally hexagonally packed tubules attached to the interface at one end and spiralling into solution at the other. The ordering ability of the silica surface was clearly less than that of the mica or graphite, so that the tubules were not constrained to the plane of the surface. This also suggested that only a little energy was required to bend the tubules along their long axes, and this was explained in terms of a Helfrich bending energy model of the tubule surfactant layer. On silica, once film thicknesses exceeded approximately 0.5 μm, the ordering influence of the substrate was no longer important, and accumulated strain energy within the film led to hierarchical structures with bundles of tubules wrapping around each other in three dimensions on several length scales. On mica and graphite for films that reached similar thicknesses, worm-like features described as 'swirling tubes' or 'hooks' were observed growing out into solution. These were attributed to the release of the strain caused in the film during growth by epitaxial mismatch with the surface that was released once the film became thick enough that the ordering influence of the substrate no longer existed. This was also discussed in a later paper by this group (Yao *et al.* 2000) where it was suggested that the substrate–solution interface imposes physical and/or energy constraints on the first micellar layer, confining it to the plane of the interface. This may be due to a combination of Helfrich-type bending energy effects and electrostatic or other surface–micelle interactions. The Helfrich bending energy model predicts that micellar structures possess a spontaneous curvature in three dimensions; however, the presence of a surface restricts micellar motion, creating an energy incentive for in-plane confinement of the structure.

Yang *et al.* (1997d) also reported the growth of mesoporous silicate films on graphite. This synthesis was carried out using C_{16}TACl in a dilute acidic TEOS solution with molar ratios of 100 H_2O:7 HCl:0.11 C_{16}TACl:0.1 TEOS under quiescent conditions at 80°C. The graphite substrate was positioned by floating at the surface of the solution and film formation commenced within minutes and was allowed to continue for up to 24 h, forming films with thicknesses around 0.5–0.6 μm. The films were washed with water and calcined at up to 540°C for 4 h in air. Powder XRD showed the two peaks assigned to a hexagonal phase oriented parallel to the substrate (*d* spacing, 37–39 Å), and this was confirmed by TEM. SEM images of the film surface showed similar aligned domains to those reported by Aksay *et al.* (1996), with filaments having sharp edges meeting at 60° or 120° occurring at the edges of the film. Triangular pits occurred in the films, having both straight and convex edges. The edges of the triangles were exclusively aligned with respect to each other as well as with the domain edges of the film. AFM indicated the occurrence of a multilayer step structure in the central regions of the film, as well as on the walls of the triangular pits and on the filamentary growth fronts of the film.

This group also reports formation of a hemimicellar layer of C_{16}TACl cylindrical micelles adsorbed at the graphite–solution interface prior to the addition of TEOS. AFM images indicated the presence of well-defined parallel stripes on the graphite surface with a periodicity of about 53 Å and a thickness of up to 500 Å, implying the

existence of up to ten layers of cylindrical surfactant micelles organized in layers at the interface. The images also showed the presence of domains within which parallel arrays of cylindrical micelles met at 60° or 120°, indicating that the liquid crystal overlayer, as well as the first hemimicellar layer was aligned with the hexagonal unit-cell axes of the graphite surface. They put forward a similar mechanism to that described by Aksay *et al.* (1996) involving initial assembly of the surfactant hemimicelles on the graphite surface with geometrical matching of the methylene groups in the all-*trans* alkane chain with the aromatic carbon six-membered rings in the planar graphite surface favouring a head-to-head and tail-to-tail arrangement of the surfactant along the hexagonal symmetry axes of the graphite. The assembly process was driven by hydrophobic electrostatic ion pair and image dipole forces between the C_{16}TACl and the conducting graphite surface. This initial assembly then acts as a template for further adsorption of the surfactant from solution so that for solutions above roughly 9 mM in surfactant, a film thickness of about 500 Å is formed. The film still contained 50 Å stripes, however, implying that it was a multilayer of close-packed cylindrical micelles, organized in registry with the graphite surface. In the presence of TEOS, nucleation of the mesophase silica–surfactant film was initiated by polymerization of the silicate species in the head-group region of the aligned liquid crystal film, producing a solid composite structure with the channels retaining the alignment imposed upon the surfactant micelles by the graphite surface.

3.1.2. *Larger-scale patterning of deposited films*

This group then went on to report the growth of patterned mesostructured silicate–surfactant films on gold surfaces that had been modified with SAMs of hexadecanethiolate (Yang *et al.* 1997b, Coombs *et al.* 1997) (see figure 13 (*c*)). Lines of hexadecanethiolate in methanol were deposited on the gold using a PDMS stamp with a range of 3–10 μm size lines. The substrate was floated horizontally at the surface of a quiescent solution with molar ratios 100 H_2O:7 HCl:0.11 C_{16}TACl:0.1 TEOS. At 80°C, deposition of mesostructured silica–surfactant composite was observed within minutes. The deposition process was allowed to proceed for up to 2 days, following which the films were rinsed with deionized water. SEM images showed that the mesophase silica–surfactant composite was deposited preferentially on the SAM-covered regions of the surface and formed disc and ribbon-shaped morphologies. In the absence of the SAM it was also possible to deposit the composite on the gold surface but clearly the adhesion of the surfactant–silicate material was better on the SAM-covered regions of the surface. Energy-dispersive X-ray analysis indicated that greater than 80% of the deposited mesophase silica was located on the SAM delineated regions of the substrate. XRD showed one intense (100) reflection and a second weaker peak assigned to the (200) reflection of aligned, hexagonally packed cylindrical channels with a *d* spacing in the range 35–38 Å. TEM confirmed that the cylindrical channels ran substantially parallel to the gold surface. The preferential formation of the mesophase composite on the SAM-covered regions of the substrate was suggested to be due to hydrophobic interactions between the SAM and the alkane tail regions of the templating surfactant causing the formation of an alkanethiol surfactant heterobilayer. The charged head groups of the surfactant in the heterobilayer were exposed to the aqueous solution phase and acted as reactive sites for further preferential accretion and organization of the mesophase structure.

Microscopic patterning of the deposited surfactant–silicate film was also described by Trau *et al.* (1997). In this case, growth of the tubules was guided by the infiltration of the reaction fluid into the microcapillaries of an elastomeric mould in contact with a substrate. The synthesis fluid contained typical molar ratios of 1 TEOS:1.2 C_{16}TACl:9.2 HCl:1000 H_2O. This was intentionally very dilute in TEOS concentration in order to prevent homogeneous nucleation of the composite in the solution and to promote surface film growth. The PDMS stamp, possessing designed relief features on its surface was placed in contact with the substrate and the reaction solution placed in contact with the edge of the mould and transferred into the channels by 'wicking' (figure 12 (*e*)). Film growth began immediately on contact with an interface on to which the surfactant could adsorb; however, the dilute solution meant that the reactants were quickly depleted. Also, growth of the film only at the edge of the mould, where fresh reaction solution was available, sealed the capillaries, preventing diffusion of reacting species to the interior of the mould. An electric field applied tangentially to the surface within the capillaries was used to induce electro-osmotic flow to ensure a uniform concentration of reactants within the capillaries during growth and also had the effect of enhancing the rate of silicate polymerization by localized Joule heating. The electric field also caused alignment of the surfactant tubules and these three effects acted synergistically to guide the formation of the silicate mesostructures within the microcapillary reaction chambers. Electrolysis of the water in the reaction solution, causing bubble formation, occurred at the electrodes but did not disturb the growth of the silicate within the capillaries.

Continuous patterned mesostructured silicate–surfactant films 0.5 μm thick were grown on a silica substrate under an applied dc field of about 0.1 kV mm^{-1} for 1–5 h. In the absence of an applied field, films 0.5 μm thick could be grown in 24 h but the lines showed depressions or discontinuities because of incomplete filling. TEM and electron diffraction showed the surfactant–silica film to be made up of hcp cylindrical tubules parallel to the substrate with a nearest-neighbour spacing of 5 nm, having a slight (4%) deviation from perfect hexagonal in the case of films prepared under an applied field. No distortion from hexagonal packing was observed for films prepared with no applied field, so the distortion was suggested to be due to the accelerated polymerization caused by localized heating when the field was applied.

The uncalcined structures were highly sensitive to the TEM electron beam, converting into amorphous-like structures after illumination for 30–50 s. XRD indicated the presence of a minority (10%) lamellar phase with a repeat distance of 2.9 nm. In the uncalcined samples the tubules were highly aligned along the surface-normal direction, having a mosaic spread of less than 1.7°, but were less aligned in the plane parallel to the surface with a mosaic width of 20°. The structure was retained upon calcination although it underwent shrinkage by 25%. The long-range orientation of tubules was contrasted with the disordered meandering tubule arrangement found in films grown on unconfined surfaces. The alignment was due to either the confined growth conditions or the application of the applied field. The formation of surfactant micelle end caps has been shown to be a high-energy process; so the mesostructure will minimize the number of end caps by elongation along the capillary rather than truncation at the capillary walls. For field-induced alignment, tubules positioned parallel to the capillary walls would minimize the overall electrostatic energy, provided that a difference exists between the dielectric constants of the inner and outer volumes of the tubule.

A similar method of patterning surfaces with mesostructured oxides was published by a different group (Yang *et al.* 1998d). This study used a combination of micromoulding, polystyrene sphere templating and surfactant templating using amphiphilic triblock copolymers to structure silica, niobia and titania on discrete length scales from nanometres to micrometres. The precise structure generated in each case could be tuned by choosing the mould pattern, the type of latex sphere and the block copolymer used. For materials with two-scale ordering, a patterned PDMS mould pressed against a drop of precursor solution on a substrate was used (figure 12(*d*)). The precursor solution was required to dewet the substrate surface in order to permit contact between the PDMS mould and the substrate in the areas where no mesostructured material was desired. The patterned surface of the mould was typically 1–5 cm^2, with moulded features of sizes in the micrometre range. The precursor solution had molar ratios of 0.008–0.018 $EO_nPO_mEO_n$:1 TEOS: 20–60 ethanol:0.01–0.04 HCl:5–10 H_2O, resulting in a cubic mesophase for $EO_{106}PO_{70}EO_{106}$ (Pluronic F127) and a hexagonally packed cylindrical mesophase for $EO_{20}PO_{70}EO_{20}$ (Pluronic P123). Gelation of the mesophase occurred within hours, but the mould was left undisturbed for at least 12 h to allow increased cross-linking of the inorganic network. The patterned material was calcined at 400°C for 5 h to remove the block copolymers. XRD confirmed the formation of the cubic and hexagonal phases in the mesoporous silica thus generated. The smallest line feature obtained by this method was 100 nm. The formation of surfactant end caps is not energetically favoured and so the highly confined geometries of the PDMS micromoulds were expected to lead to highly oriented mesophase aggregates aligned parallel to the walls of the micromoulds. This method was also used to prepare micromoulded mesostructures of Nb_2O_5, TiO_2, ZrO_2, WO_3, $AlSiO_{3.5}$ and $SiTiO_4$ by slowing the rate of hydrolysis of the inorganic chloride precursor species in alcohol solutions.

Latex-sphere templating was combined either sequentially or concurrently with the micromoulding and cooperative silica–surfactant assembly process to obtain materials patterned on three length scales. In this case the ends of the mould were left open and capillary flow used to fill the micrometre-scale channels in the mould with the polymer latex suspension (figure 12(*e*)). The solvent was evaporated at room temperature, leaving the latex spheres organized into a close-packed array within the confinement of the micromould. A drop of the sol–gel block copolymer solution was then placed at the end of the mould and was similarly drawn into the latex sphere filled micromould by capillary action. After 12 h to allow for inorganic polymerization to occur, the mould was removed and the resulting materials calcined at 450°C in air for 2 h to remove the organic templates. TEM images showed that ordered structures with features on length scales of 10, 100 and 1000 nm had been formed. Some effect of the microscale pattern size on the packing of the latex sphere templates was observed, with narrow areas having larger edge effects, resulting in different packing sequences than more open larger-scale features. It was also possible to combine the latex sphere templates with the sol–gel block copolymer solutions (1:1 ratio) and to use the first stamping method described above to create isolated surface pattern features with the same hierarchical ordering on three length scales.

This micromoulding approach was then used to create mesostructured waveguides for mirrorless lasing by the incorporation of the dye rhodamine 6G into the mesophase channels (Yang *et al.* 2000). The 2D hexagonal phase mesophase silica templated with block copolymer P123 (refractive index, 1.43) was deposited on a

silicon wafer coated with mesoporous silica. For waveguiding to occur, the waveguiding medium must have a higher refractive index than its surroundings. The underlying mesoporous silica layer was found to make excellent cladding as it was mechanically and hydrothermally stable and had a low refractive index of only 1.15. The cylindrical channels in the micropatterned copolymer-templated mesophase were shown to run parallel to the substrate and were partially aligned along the axes of the microchannels. They proved efficient as high-quality waveguides in both straight and curved microstructures, with no scattering of helium–neon laser light observed along the waveguides and strong emission from the ends. Dye molecules introduced into the synthesis solutions were incorporated into the films uniformly. Optical pumping of the dye-doped waveguide array by a frequency-doubled neodymium-doped yttrium aluminium garnet laser perpendicular to the film substrate produced a broad photoluminescence spectrum from the ends of the waveguides. The photoluminescence spectrum showed amplified spontaneous emission at low thresholds, demonstrating that lasers with coherent emission could be made if mirrors were incorporated to provide feedback. The mesostructured waveguides enhanced the emissive properties of the dyes contained within them over that of dyes in similar sol–gel systems with no surfactant templating, by preventing concentration quenching.

3.1.3. *Preferential alignment of mesostructures through shear*

A different approach to producing greater preferential organization of the mesostructured channels in surfactant-templated films grown on substrates was reported by Hillhouse *et al.* (1997, 1999, 2000). In this work a continuous-flow cell was used to impose a shear field upon the precursor solution, resulting in elongation of the ordered domains as well as preferential alignment within those domains in addition to the ordering effects of the substrate. The films were grown on borosilicate glass substrates from solutions with molar ratios of 1 TEOS:41.1 HCl:0.61 C_{16}TAB:555 H_2O at 80°C for times from 1 h to 1 day. In the absence of flow, disc-like particles and some tape-like features formed on the glass surface and, with increasing deposition time, intergrown domains spanned the surface of the substrate. The surface texture of the discs showed tubules oriented parallel to the substrate surface and the observation that the discs were wider at the bottom and narrower as they grew away from the interface suggested that growth proceeded by layer-by-layer deposition. XRD patterns showed only one peak, which was retained on calcination. For films grown under the continuous-flow condition a similar solution was pumped through a glass capillary in an 80°C water bath for 1 h. The aligning shear rate at the surface was approximately 450 s^{-1} and the resulting film was 200 nm thick. The film morphology was dominated by tape-like features running along the flow direction, and the films showed less frequent indentations due to grain boundaries. The tape-like domains were similar to those found for films grown on mica but were induced by the fact that the flow field hindered bending of the mesostructures in directions normal to the direction of the flow field. End-cap formation was therefore reduced and growth proceeded more along the flow direction than in the transverse direction. This effect was observed only for early stages of growth; thicker films deposited for longer times (greater than 2 h) did not show evidence of preferred orientation, possibly because the flow field became disturbed by increasing surface roughness, or the depletion of reactive species in solution.

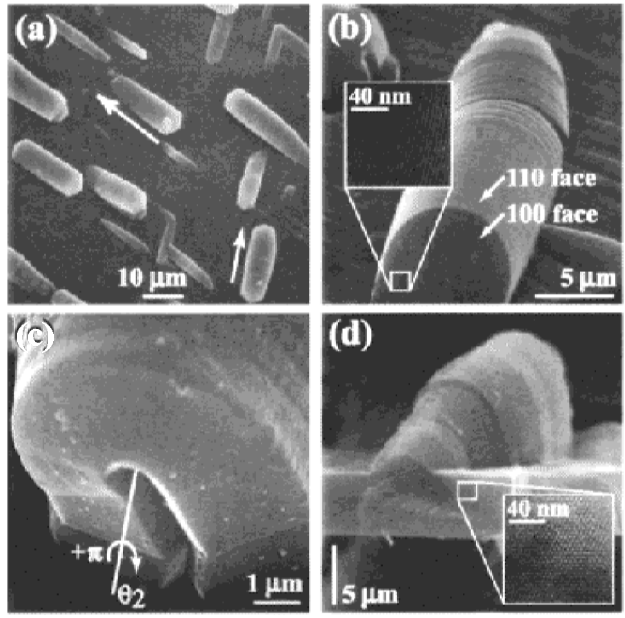

Figure 16. Electron micrographs of a mesostructured film synthesized epitaxially on mica substrates in an applied flow field. (*a*) Top view SEM image showing two discrete orientations of elongated structures. The white arrows indicate the *c* direction of the mesostructure in regions of the film beside the elongated structures as determined by polarized optical microscopy and TEM. (*b*) Side-view SEM image with a TEM image inset from a reflection of the film similar to that indicated by the box. The TEM image shows channels oriented perpendicular to the substrate. (*c*) Side-view SEM image, showing the location of a $+\pi$ disclination about the transverse twofold axis θ_2. (*d*) Cross-sectional SEM image with a TEM inset from a region of the film similar to that indicated by the box, showing a hexagonal array of pores oriented parallel to the substrate. (Reprinted with permission from Hillhouse *et al.* (2000). © 2000 American Chemical Society.)

A greater degree of ordering was subsequently induced by deposition of the silica films epitaxially on mica under the shear flow (Hillhouse *et al.* 2000). This method produced 2D XRD patterns that were 'single-crystal-like' exhibiting sixfold *p6mm* symmetry that was rotationally invariant over the entire film. By rotation of the film in the X-ray beam, it was also found that there were both a component having channels perpendicular to the substrate surface in this case, and a component with the channel axis parallel to the substrate. The component with perpendicular channels was found to consist of about 50% of the channels, and three mesophase orientations (separated by 60°) were found with channels parallel to the substrate and rotationally oriented with the longer transverse axis (through the centre of adjacent pores, rather than through the wall region) also parallel to the substrate. These three orientations were due to the chemical equivalence of these directions on the surface lattice of the muscovite mica at the cleavage plane, but the ratios of these horizontal orientations was unbalanced with a ratio of about 20:5:1, possibly owing to the applied flow field. SEM and TEM images showed horseshoe-shaped structures protruding out of the plane of the film and also extending below the film surface. In these structures the channels were oriented perpendicular to the substrate. The structures are also elongated and oriented in one of three discrete directions

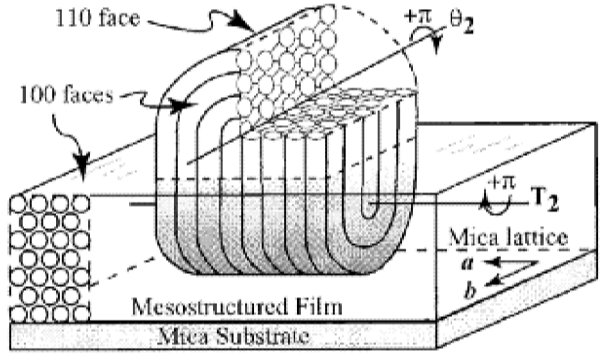

Figure 17. Topology embedded in the mesoporous film that may be generated by an orthogonal pair of $+\pi$ disclinations. A disclination along the T_2 axis combined with the disclination along the θ_2 axes generates the dual-horseshoe structure shown. Note that for this topology the (110) crystal face (next-nearest-neighbour arrangement) is exposed on the top curved surface while the (100) crystal face (nearest-neighbour arrangement) is present on the bottom. The different growth rates of these crystal faces exposed to the nutrient solution could lead to the anisotropy of the structures observed in figure 17(*a*). (Reprinted with permission from Hillhouse *et al.* (2000). © 2000 American Chemical Society.)

correlated to the underlying crystalline mica lattice (figure 16). The *c* direction of the surrounding mesostructure was coincident with the direction of elongation. The topology of the elongated structures possibly arose from two orthogonal $+\pi$ disclinations (figure 17), although other such defect combinations common to hexagonal liquid crystal systems could produce similar structures. It was noted that films grown in a similar manner on glass substrates also showed $+\pi$, $-\pi$ and $+2\pi$ disclinations; however, the growth and channel orientation remained in two dimensions parallel to the substrate, suggesting that the observed morphologies on crystalline substrates were due to the epitaxial nature of the growth. It was also possible that homogeneously nucleated particles from solution were adhering epitaxially to the growing film surface; however, SEM on particles precipitated from the synthesis solutions showed wide ranges of shapes and defect structures not reflected in the protruding structures in the films. Alternatively, defects in the film may have been produced dynamically during growth owing to reaction-induced stresses or epitaxial mismatch. Polarized optical micrographs showed that films grown under the flow field had much smaller domain sizes than identical syntheses in quiescent solutions, suggesting that the effect of the flow field was to increase mass transfer and as a result also to increase the number density of nuclei on the surface and hence the film growth rate.

In other work (Hillhouse *et al.* 1999) the flow field method was extended to produce an optically anisotropic mesostructured coating of tungsten oxide–surfactant composites showing a 3D hexagonal structure with surfactant-filled channels oriented parallel to the substrate and aligned in the direction of the shear flow. The periodicity of the wall structure in the *c* direction is due to the Keggin ion structural unit of the tungsten oxide precursor, which remains intact in the wall material. The most ordered deposits were obtained from a precursor suspension composed of 0.35 $(NH_4)_6W_{12}O_{39}$:8 C_{16}TACl:1000 H_2O at 70°C for 1 h under a shear rate greater than 50 s^{-1}. It was necessary to dry the deposited films quickly to prevent structural

rearrangement from altering the fibrous surface observed in the most highly oriented films. Films deposited at lower temperatures and lower concentrations showed a higher degree of curvature, resulting in poorly defined fibres and smaller, irregularly shaped domains. This suggests that the shape of the fibres was kinetically controlled, with increased rates of assembly at higher temperatures and concentrations allowing extended growth in a given direction. A suggested formation mechanism for this film was composed of several steps:

(1) formation of the primary hexagonal structure immediately after mixing the reagents;
(2) formation of a gel network of particles composed of $x\mathrm{C16TA}^{+}[(\mathrm{NH_4})_{6-x}\mathrm{W_{12}O_{39}}]^{x-}$ species;
(3) irreversible disruption of the gel by stirring to form a low-viscosity precursor suspension of gel fragments;
(4) shearing the precursor suspension resulting in aggregation, deposition and morphological rearrangements of particles on the substrate surface;
(5) rapid drying of the film to prevent structural rearrangement.

Interestingly, films of the tungsten oxide–surfactant composite could not be deposited under quiescent conditions, implying that collisions between precursor particles play an important role in layer formation, as is also observed in colloidal systems. The tungsten oxide clusters did not condense with each other during the synthesis; so the films were not stable to calcination.

3.1.4. *Preferential alignment of mesophases through interactions with the substrate*

In studies to discover the factors controlling the mesophase structure in films on substrates, work by Manne *et al.* (1997) using gemini surfactants adsorbed on surfaces showed that there was a distinct difference between surfactant behaviour when adsorbed on mica and surfactant behaviour when adsorbed on graphite. The surfactants used were of the form $(\mathrm{C}_m\mathrm{H}_{2m+1})[\mathrm{N}^{+}(\mathrm{CH}_3)_2](\mathrm{CH}_2)_s[\mathrm{N}^{+}(\mathrm{CH}_3)_2](\mathrm{C}_n\mathrm{H}_{2n+1})\cdot 2\mathrm{Br}^{-}$, (hereafter $\mathrm{C}_{n\text{-}s\text{-}m}$ for short), having different packing parameters g dependent on the relative sizes of the charged head-group and hydrophobic tails. The cleavage plane of mica was negatively charged and interacted electrostatically with the head groups of the cationic gemini surfactants. Aggregates of surfactant on the surface varied according to surfactant geometry. Asymmetric gemini surfactants C_{n-3-1} formed globular aggregates arranged in a hcp pattern with its symmetry axes aligned with the underlying mica symmetry axes on average, although some dislocations were observed. The aggregate lattice had a nearest-neighbour spacing of about 50–80% over the expected micelle diameter. Symmetric gemini surfactants $\mathrm{C}_{12\text{-}4\text{-}12}$ and $\mathrm{C}_{12\text{-}6\text{-}12}$ formed parallel cylindrical aggregates similar to those formed by $\mathrm{C_{16}TAB}$ with a measured stripe spacing slightly over twice the length of the dodecane tail groups. The cylinders were on average oriented parallel to the mica symmetry axes, although more so for $\mathrm{C}_{12\text{-}4\text{-}12}$ than for $\mathrm{C}_{12\text{-}6\text{-}12}$. The gemini aggregates on mica seemed to show closer registry with the underlying mica lattice than conventional quaternary ammonium surfactants because of the presence of two binding head groups giving the gemini surfactants a larger interaction area with the mica lattice. Both the spherical and the cylindrical aggregates were assumed, by analogy with well-studied conventional quaternary ammonium surfactants, to be slightly flattened on the bottom to conform to the mica plane. Gemini surfactants with a short spacer, $\mathrm{C}_{12\text{-}2\text{-}12}$, formed flat bilayers on the mica surface.

The results indicated that the interfacial self-assembly was dominated by head-group–surface electrostatic interactions, resulting in flattened but full micellar aggregates with only head groups exposed to the solution and surface. This electrostatic interaction precluded formation of multilayers at concentrations below the first solution mesophase boundary as the second layer must overcome the electrostatic repulsion of the first layer. In comparisons with the solution behaviour of these surfactants, it was shown that aggregates on mica favoured a lower curvature than the corresponding free aggregates in solution, as well as being much closer together than in solution, resembling a concentrated bulk phase in two dimensions. This was probably because the electrostatic binding to the surface allowed a closer packing of head groups at the surface than is found in free micelles. Comparisons with the phase formed by each surfactant in bulk mesophase silicate preparations indicated that the phase formed on the mica surface was the 2D analogue of that formed in the bulk surfactant–silicate composite, indicating similar binding mechanisms operating between the surfactant head groups and the silicate surfaces. Work on gemini surfactant-templated films formed at the air–water interface and also on mica surfaces (Tolbert *et al.* 1997), discussed in the section below, confirms this finding for the surfactant–silicate structures as well as the pure surfactant aggregates. The aggregates on mica were also observed to be fairly insensitive to counterion exchange, and counterion concentration, possibly because the mica surface already acted as a highly charged counterion.

On the hydrophobic cleavage plane of graphite, however, interfacial aggregates of all the gemini surfactants were observed to be parallel half-cylinders oriented perpendicular to an underlying symmetry axis of graphite. This self-assembly was driven by strong tail-group–surface interactions with the bottom row of tail groups aligned parallel to a graphite symmetry axis, and surfactant geometry played a very minor role, even for very concentrated surfactant solutions. The tail-group–surface interaction was stronger than the interactions between neighbouring tail groups. This surface interaction proved strong enough that it was possible to grow surface films of surfactant-templated silica with the same oriented cylindrical geometry from both acidic TEOS–C_{18-3-1} precursor solutions and from alkaline TEOS–C_{18-3-1} precursor solutions. Such linear structures were not observed for the same solutions nucleated from acidic solutions on mica surfaces (Tolbert *et al.* 1997). This is the only report of an aligned film grown on a substrate from an alkaline solution, although these workers raised the question of how far normal to the surface the cylindrical morphology would persist, since the spherical 3D hexagonal morphology was favoured for this surfactant in bulk solution.

One other brief report of a mesoporous surfactant-templated silica membrane grown from alkaline solution is that by Nishiyama *et al.* (1998). In this case, cubic MCM-48 was grown in the pores of a stainless steel support at 90°C for 96 h from a solution with molar ratios of 0.6 C_{16}TAB:1.0 TEOS:0.5 NaOH:60 H_2O. This preparation produced both an MCM-48 powder precipitate and a coating on the stainless steel support. This silica coating was about 0.5 mm thick but this was removed by polishing prior to calcination, leaving only MCM-48 particles that had nucleated inside the support. Permeance measurements of nitrogen through the membrane confirmed that the MCM-48 particles completely filled the pores of the support, preventing gas permeation prior to calcination. After calcination, XRD patterns showed the cubic structure was maintained although some shrinkage in the structure had occurred and the calcined membrane was permeable to nitrogen. In

this case there was no preferential alignment of the silicate mesophase with respect to the pores of the support.

A different approach to alignment of silica–surfactant films grown on substrates was taken by Miyata and Kuroda (1999a,b,c, 2000). In the first paper, aligned mesostructured surfactant–silica films were again observed to grow epitaxially, this time on a silicon (110) surface, although not on the silicon (100) and (111) surfaces. The solutions used had molar ratios of 0.10 TEOS:0.11 C_{16}TACl:100 H_2O:10.5 HCl and the silicon substrate was held horizontally between two Teflon discs, in the reaction solution with the polished surface downwards, open through a window in the Teflon disc to the solution. The reaction was carried out at 80°C for 1 day to 1 week. The resulting films were glossy and continuous, 0.1–0.2 μm thick, although the film thickness was not linear with reaction time. Samples were washed with water and calcined at 540°C for 10 h. Calcination caused a shrinkage in the *d* spacing observed in XRD patterns by 0.3 nm, and also an increase in disorder in the mesophase structure; however, this did not cause the film to crack. XRD showed two peaks assigned to the (100) and (200) reflections of a hcp cylindrical mesophase aligned parallel to the substrate. On the silicon (100) and (111) substrates a winding striped contrast was observed over the whole of the film by SEM, similar to that found on a silica substrate, whereas on silicon (110), an aligned ellipsoidal texture was reported, similar to that observed on mica. In-plane XRD scans of the (110) peak of the silicate mesophase indicated a Gaussian-type distribution of in-plane alignment of the mesochannels, with a FWHM of 29°. The orientation of the cylinders was parallel to the [001] direction of the silicon lattice owing to the anisotropy in the arrangement of silanols along this direction on the (100) surface. The hexagonal packing of the cylindrical channels in the mesophase was distorted by 11%, as the in-plane distance between adjacent micelles was longer than the distances along the other two axes (i.e. the distances to micelles above and below). The positions of the (110) peaks in in-plane XRD on the as-prepared and calcined films were identical, indicating no shrinkage in the horizontal direction, despite the shrinkage noted in the direction normal to the plane of the substrate. The strong adhesion of the film to the substrate prevented the film from undergoing horizontal shrinkage, and the degree of alignment of the mesochannels was unchanged.

To improve the observed degree of alignment of the silicate–surfactant film this group then used a rubbing method that had previously been successful in aligning liquid crystals (Miyata and Kuroda 1999a). This required the deposition of a thin layer of polyimide on to a silica glass substrate by spin coating of the monomer and polymerization, followed by rubbing with a nylon buffing wheel. The mesoscopic silicate surfactant was deposited as described above with the substrate immersed horizontally with the rubbed surface downwards in the reaction vessel. To obtain good alignment the substrate was covered with another silica glass with a approximately 0.2–1 mm spacing. SEM showed that the mesophase composite nucleated on the polyimide film was composed of elongated particles aligned with the rubbing direction. The maximum aspect ratio of the fibre-like particles was approximately 100 and the particles were 0.2–0.3 μm thick. Particles grown on a similar polyimide film that had not been rubbed were small disc-like particles. XRD patterns showed two peaks assigned to a cylindrical hexagonal phase aligned parallel to the substrate, and this pattern degraded slightly upon calcination, indicating shrinkage and disordering of the mesophase structure. In-plane XRD confirmed this structure. It was also noted that calcination removed the polyimide layer without

destroying the mesostructure and also caused the particles to become firmly attached to the glass substrate, whereas the particles were easily removed from the surface of the as-synthesized sample. The exact mechanism for alignment of liquid crystals on rubbed surfaces is uncertain but a number of physical and chemical effects may be responsible such as the morphological effect of microgrooves or orientation of the polymer chain. The film deposited on the rubbed polyimide surface was not continuous, indicating a low nucleation density on this surface. If the density of particles was increased by preparing the film without the glass cover, the degree of uniaxial orientation was reduced. Improvements in continuity were made in a later paper by changing the polymer and rubbing conditions used (Miyata and Kuroda 2000) (see below). An attempt was also made to align the surfactant–silicate film on a substrate treated with an obliquely deposited silicon monoxide evaporated film. Such films consist of column-like structures and are also known to align liquid crystals owing to a morphological effect. However, mesophase silica–surfactant films did not show preferential alignment on obliquely evaporated silicon monoxide films deposited at 10° and 30°, indicating that molecular-scale interactions between the initial silicate–surfactant liquid crystal seed and the surface are essential to impose preferential ordering on the films.

Ordering of the molecular structure of the polymer substrate was therefore attempted in the next paper (Miyata and Kuroda 1999b) where a polyimide film was deposited as a Langmuir–Blodgett (LB) film on a substrate and used to orient the silicate–surfactant structure. The polyimide film was prepared by spreading a monomolecular layer of polyamic acid monomer units on a pure water subphase and depositing 30 layers as an LB film on silica glass or silicon substrates. The polyimide film was then obtained by thermal imidation of this film. Polarized FTIR spectra showed the polymer chains to be aligned along the withdrawal direction of the film and showed a high degree of uniaxiality. Silica–surfactant mesostructured films were deposited upon the substrate as described above for deposition on silicon. SEM of the as-prepared films showed uniaxially aligned elongated particles, which formed a disconnected film, confirmed by the lack of a (110) peak in the in-plane XRD patterns. High-resolution SEM showed periodic stripes of approximately 4 nm spacing along the long axis of each particle. Conventional XRD showed the two peaks assigned to the (100) and (200) reflections of a hexagonally packed cylindrical structure aligned parallel to the substrate with a d spacing of 3.74 nm. This morphology was similar to that found on the rubbing-treated polyimide layer but the alignment in this case was normal to the withdrawal direction of the LB film, whereas previously the particles were aligned parallel to the rubbing direction. This alignment normal to the deposition direction of the LB film suggested that the hydrophobic chain of the surfactant interacted with the polymer chain such that the surfactant molecules were accommodated parallel to the axes of the polyimide chains. As the long axis of the cylindrical micelle is perpendicular to the long axis of the individual surfactant molecule, the resultant silica–surfactant mesophase is oriented normal to the polyimide chains. This result indicated that it is possible to align the surfactant-templated silicate materials through chemical interactions with organic materials alone, without the necessity for physical interactions as are additionally present in the rubbing case. Calcination caused no changes in the morphological arrangement of the mesostructured silica particles and, although some broadening of the peaks and shrinkage was observed, the two diffraction peaks were retained. The adhesion of the particles to the substrate was improved by

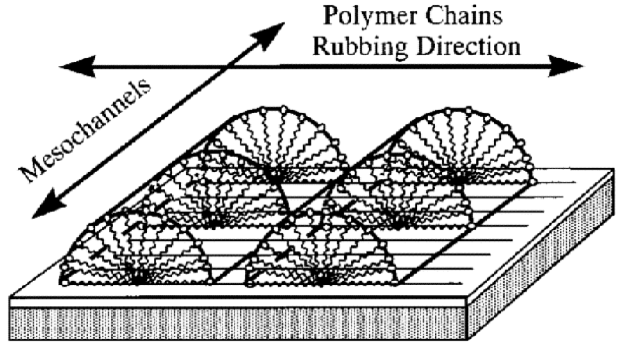

Figure 18. Schematic illustration of the alignment of surfactants and mesochannels on the rubbing-treated polyimide film. (Reprinted with permission from Miyata and Kuroda (2000). © 2000 American Chemical Society.)

removal of the LB film, probably owing to partial bonding between the silica substrate and the particles through dehydration of silanol groups. As LB films can be deposited on many types of substrate, that is metals, semiconductors and glasses, this method offers the possibility of creating oriented mesophase films on many different materials.

Further work on alignment via the rubbing method was successful in producing an aligned continuous film by changing the molecular structure of the polymer used (Miyata and Kuroda 2000). The results from the LB film study suggested that the hydrophobic surfactant chain interaction with the polymer surface was important for the alignment of the surfactant micelles. Previously the polyimide chain contained a phenylene group in the chain, which after the rubbing treatment nucleated a non-continuous film with particles elongated and aligned in the rubbing direction. Substitution of the phenylene group for an unbranched hexamethylene chain to give a more hydrophobic surface resulted in a continuous film with the alignment of channels normal to the direction of rubbing. The polyimide film was prepared and rubbed as described above, and the mesostructured silicate–surfactant film prepared using a silica glass spacer held 0.2 mm from the substrate in order to obtain a uniform film as used previously. The glossy continuous film formed was 0.3–0.5 μm thick and XRD confirmed that the hexagonally packed cylindrical channels ran parallel to the substrate normal to the rubbing direction with a d spacing of 3.6 nm (figure 18). The morphology was unchanged after calcination and no cracks were induced; however, the intensity of the XRD peaks was greatly reduced and some shrinkage in the d spacing was observed. In-plane XRD measurements and high resolution TEM indicated distortions of the hexagonal lattice from the ideal hexagonal channel structure of 18%, a larger distortion than observed for films grown epitaxially on mica or silicon (110) (figure 19). However, the Gaussian distribution in mesochannel orientation is 12.6°, which is narrower than that found for films grown on silicon (110) substrates. The high degree of alignment on this rubbed polyimide film and the continuity of the mesostructured film were ascribed to the more hydrophobic nature of the polyimide used in this case than was used previously. The hexamethylene group provided a larger interaction area with the surfactant molecules, possibly increasing the number of nucleation sites and promoting the growth of each silica–surfactant seed. The change in structure may also have made the polymer more susceptible to the rubbing treatment, with the

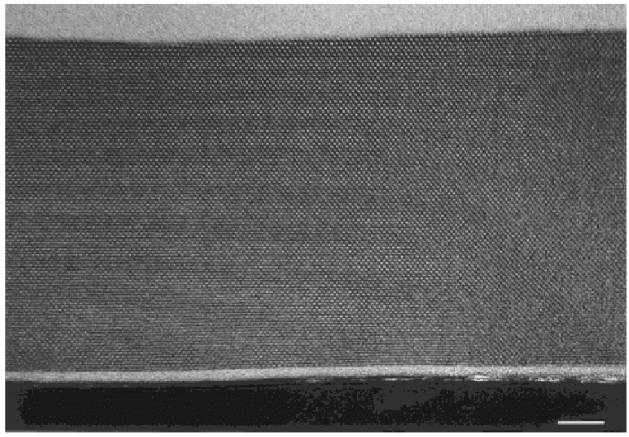

Figure 19. Cross-sectional TEM image of the as-synthesized mesostructured silica film grown on the rubbing-treated polyimide film. The sample was sliced perpendicular to the long axis of the mesoporous silica domains (scale bar, 50 nm). (Reprinted with permission from Miyata and Kuroda (2000). © 2000 American Chemical Society.)

more flexible hexamethylene group more easily stretched and so aligned in the rubbing direction than the phenylene ring. The linearity of the polymer chain, with respect to both the straight main chain and an absence of side chains, was also considered to be important for good uniaxial alignment of the mesostructured silicate. This corresponded to requirements for good alignment of thermotropic liquid crystals on rubbing-treated polymers. As a test of this requirement, mesostructured silica was grown on a rubbing-treated film of a polyimide containing a folded main chain structure and a long alkyl group as a side chain in the repeating structure. A continuous mesostructured film was formed as the polymer was highly hydrophobic; however, only a small amount of alignment was observed, parallel to the rubbing direction of the film and not normal to it as was the case for the straight-chain polyimide used before. This weak alignment was probably due to physical microgrooves left in the polymer by the rubbing process and not by the alignment of the polymer chains which caused alignment of the surfactant micelles.

To avoid problems with structure degradation and cracking of mesophase surfactant-templated silicate films upon high-temperature calcination, Hozumi *et al.* (2000) studied the low-temperature photocalcination of mesoporous silicate films using vacuum ultraviolet light. The films were prepared on silicon wafers coated with octadecyltrimethoxysilane in the manner described for mesoporous film formation on silicon by Miyata and Kuroda (1999c), although the substrate was suspended in the solution without the aid of a Teflon holder. The calcination method was based on the photochemical decomposition of organic molecules under irradiation in a vacuum with UV light of 172 nm wavelength. The dried as-prepared films were irradiated for 0.5–3 h at room temperature and compared with films calcined at temperatures between 373 and 773 K for 1 h. FTIR spectroscopy confirmed that the template surfactant had been totally removed from the films by photocalcination and by thermocalcination. The proportion of Si–OH groups was lower on the thermocalcined materials because of increased condensation of the silica walls at the higher temperatures used in this process. XRD indicated a much higher degree of structure retention in the photocalcined materials than in the thermocalcined materials, with

two orders of diffraction remaining in the photocalcined film, compared with one broad reflection in the thermocalcined film. The observed shrinkage in *d* spacing was also less in the photocalcined films.

3.1.5. *In-situ observation of film growth*

Direct observation of the growth of silica–surfactant films at the silicon–liquid interface using neutron reflectivity was reported by Holt *et al.* (2000). These experiments were carried out using the polished (100) face of silicon, clamped downwards in a cell 2 mm deep and held at room temperature with scans of the developing pattern taken over 30 min intervals. The silicon surface was treated prior to use to result either in an oxide coating or a covalently attached trimethylchlorosilane hydrophobic layer. Both types of coating were flat and amorphous, so that only the hydrophobic or hydrophilic effect on the film growth was observed. Solutions for the synthesis of surfactant–silicate films had molar ratios of 0.0016 C_{16}TAB or C_{16}TACl:1.0 D_2O:0.013 HCl:0.0014 TEOS; the final solutions were 60 and 70 mM in the chloride and bromide counterions respectively. Solutions of the same concentration without the TEOS were also prepared to study the interfacial adsorption of the surfactants on to silicon from low-pH solutions.

The C_{16}TAB or C_{16}TACl surfactants gave similar interfacial structures, which differed on the two types of substrate. The hydrophobic interface had a thicker overall structure, requiring two layers of adsorbed material to fit the reflectivity data, whereas only one adsorbed layer was required for the hydrophilic surface. The surfactant structure on the hydrophilic interface was suggested to correspond to the adsorption of a layer of complete cylindrical micelles, slightly flattened by their interaction with the surface. Adsorption on the hydrophobic interface was suggested to be composed of half-micelles. The fitted scattering length densities for the C_{16}TACl surfactant were consistently lower than those for the C_{16}TAB, possibly owing to the greater amount of water present in the C_{16}TACl preparations (since the C_{16}TACl was supplied as a 25 wt% solution in water, whereas the C_{16}TAB was a dry powder). The fact that the subphase H_2O-to-D_2O ratio affected the observed scattering length density of the surfactant structure indicated the incorporation of the subphase solution to an appreciable extent in the adsorbed surfactant layers at the interface.

The mode of surfactant adsorption on the hydrophobic and hydrophilic surfaces appeared unchanged by the addition of TEOS to the solution mixture. Film formation at the solid–liquid interface occurred in a different manner from that found for films grown at the air–solution interface (discussed below). During the induction period a fringe appeared in the reflectivity that was fitted to the same structure as the layers found in the pure surfactant solutions. At the end of the induction period for the solid–liquid interface the first-order diffraction peak of the hcp cylindrical mesophase appeared superimposed upon the fringe structure observed, whereas for the solution–air interface the fringe itself increased in amplitude during the induction period, ultimately forming the diffraction peak. This difference was reflected in the physical properties of the films formed; those formed at the solid–liquid interface were grainy and easily rinsed off the surface with water, but films formed at the air–solution interface were much more robust.

At the air–water interface there was found to be a steady accumulation of material at the interface, forming alternating micellar and silicate–ionic layers during the induction period (Brown *et al.* 1997, 1998). On the solid surface, however, the

initial surface structures appear unchanged for all the induction period, with perhaps one or two extra layers forming just prior to diffraction peak development. Solution processes appeared to dominate during the induction period, possibly because of a lack of evaporation drying the film at the interface as occurred in the air–solution case. As the film developed over time a second-order diffraction peak also became visible, suggesting that the near-surface structure on both the hydrophobic and the hydrophilic interfaces was a layered structure oriented parallel to the interface, unlike that suggested by Aksay *et al.* (1996) on silica where micelles adopted a variety of morphologies growing out into solution with only the initiating end tethered to the substrate. It was also noted that the film development and structure were the same for C_{16}TAB and C_{16}TACl and were also independent of the hydrophilic or hydrophobic nature of the surface, except that the induction periods for both were slightly reduced on the hydrophilic surface. A strong variation in induction time with anion was noted, being about 2.5 times longer for the C_{16}TACl-templated film than for the C_{16}TAB-templated film. This was suggested to be due to the requirement for a sphere-to-rod transition to occur in solution prior to rapid film growth, as was suggested in earlier work on air–solution interface grown films (Ruggles *et al.* 2000) (discussed below).

3.2. *Films grown at the air–water interface*

3.2.1. *Formation of two-dimensional hexagonal phase films and their secondary structures*

The first report of free-standing silicate–surfactant films grown spontaneously from solution at the air–solution interface was that by Yang *et al.* (1996a) following shortly after their report of films grown at the solution–mica interface (Yang *et al.* 1996b). The films were grown from a dilute acidic solution of TEOS using C_{16}TACl as the templating surfactant at 80°C for reaction times between minutes and days. The films formed at the air–solution interface had thicknesses of between tens of nanometres up to about 0.5 μm. SEM images showed that, after transfer on to a copper grid, the films were continuous, while polarizing optical microscopy images suggested that the films were optically isotropic. TEM images showed hcp cylindrical channels with a centre-to-centre distance of about 50 Å oriented parallel to the solution–air interface. XRD showed two peaks for film samples removed on to a substrate but showed three peaks corresponding to the 2D hexagonal lattice when powdered. AFM images showed parallel surface features with a periodicity of about 50 Å that appeared to have a spheroidal texture. The observed, approximately 2–3 Å rms roughness of the smooth film surface at the air–water interface suggested a growth mechanism involving the deposition of silica–surfactant micellar solution precursors at a surfactant overstructure localized at this interface. The observed rms roughness was consistent with the surface structure of C_{16}TACl solutions, where a surface profile consisting of wave-like hemimicellar structures was reported, rather than a close-packed planar structure as found for insoluble surfactants at the air–water interface. Evidence for localized hexagonal phase formation near the surface of C_{16}TACl solutions had previously been observed and this phase was suggested to facilitate the formation of the smooth mesophase film at the interface. Silicate film formation was proposed to occur via the polymerization of silicates in the surfactant head-group regions of a hexagonal mesophase that was concentrated at the liquid surface overstructure. The film surface growing into the solution showed meso-scopic-scale roughness, which was interpreted as evidence of the deposition of silica-

Figure 20. Laser scanning cofocal microscopy image of a mesoporous silica film synthesized at the air–water interface (scale bar; 25 μm). (Reprinted with permission from Yang *et al.* (1997a). © The Royal Society of Chemistry 1997.)

coated micelle structures at the lower surface of the film. The mesostructure in the films was stable to calcination and SEM showed that the films were resilient to bending and could be transferred on to substrates with various shapes.

Further work by the same group (Yang *et al.* 1997a) on the channel patterns that appear in mesophase silicate–surfactant films grown at the air–water interface suggested a more detailed mechanism for film growth. The approximately 25 Å channels observed in the films were found to be aligned parallel to the air–solution interface, but to form curved swirling patterns including concentric circles, herringbones, fingerprints and hairpins in the plane of the film. These were suggested to be a frozen record of the growth of the aggregated channel structure out from 50 nm seed particles consisting of approximately 50 Å micellar rods constrained in two dimensions by the air–solution interface. TEM images of the film at early stages of growth show a morphology consisting of roughly micrometre-scale-sized domains with voids between them. These consolidated after further reaction time to give the impression of a continuous film. Reaction–diffusion processes and defects in the rod packing, as

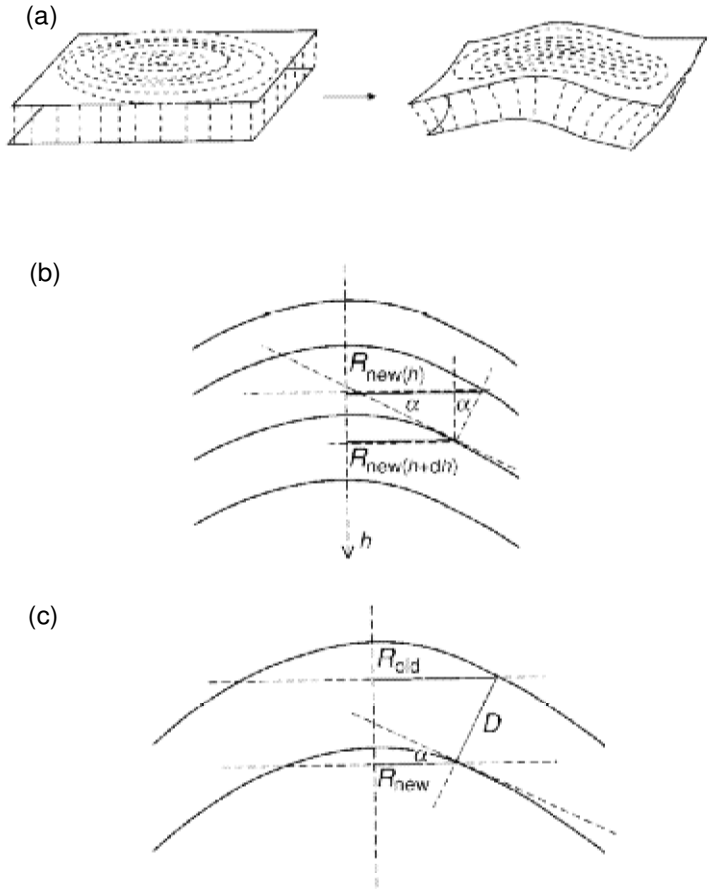

Figure 21. (*a*) A sketch of the film contraction induced by radial stress. (*b*) Various degrees of bending inside the film due to differential radial stresses. (*c*) Uniform bending of the entire thickness of the film for the linear contraction model. (Reprinted with permission from Yang *et al.* (1997a). © The Royal Society of Chemistry 1997.)

well as interactions between growth fronts from neighbouring seeds, contributed to the development of curved channel patterns in the films. Radial stresses due to the contraction of the silica network with increasing polymerization were suggested to cause differential contraction between the top and bottom of the film and so to produce micrometre-scale mounds in the film at the air–film surface (figure 20), which appeared to reflect the channel design within the film. Warping of the film in this manner was observed for films grown at room temperature and at 80°C and also was observed in both wet and dried films. The film maintained constant thickness within 20% in the areas of the mounds. A model based on differential stress between layers (figure 21), owing to a higher rate of polymerization closer to the solution interface, was shown to describe the majority of the features observed by AFM using a single value of a linear radial contraction coefficient. The fact that all the observed mound features were protruding outwards into the air rather than in towards the solution was ascribed to the lower-energy elastic deformation pathway for bending motion into the air rather than into solution. The warp patterning of the films

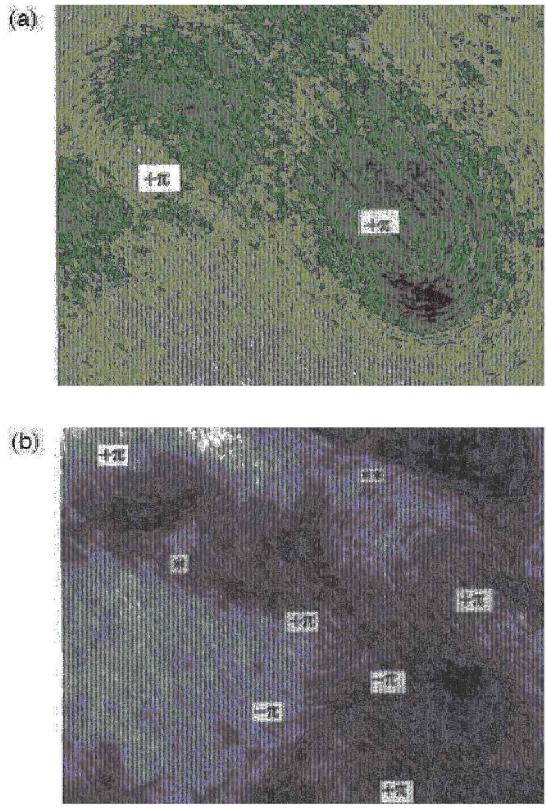

Figure 22. TEM images of defect structures in ultrathin hexagonal mesophase silica films: (*a*) a pair of $+\pi$ defects; (*b*) a collection of defects (edge dislocation and wall structures may exist at the regions denoted by a single asterisk and a double asterisk respectively). (Reprinted with permission from Yang *et al.* (1998b). © Wiley–VCH Verlag GmbH 1998.)

therefore was considered to be intrinsic to the growth rather than to drying processes in the materials.

The role of defects in the formation of channel structures and warp patterning in silica–surfactant mesophase films formed at the air–water interface (Coombs *et al.* 1997, Yang *et al.* 1998b) was discussed by analogy with those found in precipitated particulate forms of mesophase surfactant-templated silicate materials (Feng *et al.* 1997). The channel architecture of the mesophase composites resembled that of the director field patterns in hexagonal organic liquid crystals that are associated with common line defects such as $+\pi$, $-\pi$ disclinations, pairs of $+\pi$ disclinations (due to bending of the director field which points along the channel length), edge dislocations, bending and wall defects. As the size of the defects in liquid crystal structures in the silica–surfactant systems is much larger than ordinary solid-state crystals, the energy required to stabilize the defects is much less than is required in solid crystals. This lower energy allows the formation of defects with stronger distortions of the director fields that are reflected in the morphologies observed in the films. Surface interactions are also important for the stabilization of certain kinds of defect in liquid crystals and so can play a role in the growth processes of the silicate–

surfactant composites. The patterns of stable director fields depend on the bulk and surface elastic constants, anchoring strengths at the polar surface (i.e. planar and homeotropic interactions), magnitudes of applied fields and the surface-to-volume ratio of the liquid crystal. These patterns are reflected in the textures seen in liquid crystals when viewed between crossed polarizers and in the channel patterns seen in TEM images of ultrathin films. Defects such as pairs of $+\pi$ disclinations, $-\pi$, $+\pi$ disclinations and $+\pi$ disclinations and dislocations were identified in TEM images of silica–surfactant films (figure 22). Combinations of defects were presumably generated because of the requirement that higher-energy defects tend to split into several lower-energy defects. Wall structures appeared at the boundary regions, especially around $-\pi$ disclinations. A large variety of highly curved morphologies occurring as precipitated particles in similar preparations were also identified and could also be described using the defect-initiated growth concept applied to the films above.

It was also found to be possible to create thicker films by reducing the acidity of the synthesis, producing films up to 10 μm thick (Yang *et al.* 1998a). These films show either a fan-type texture in polarized optical micrographs, diagnostic of a hexagonal lyotropic organic liquid crystal H_1 phase or discrete birefringent patterns. The texture observed depended upon the rate and time of stirring prior to quiescent film growth, with a greater amount of agitation leading to the fan-type texture. This texture remains after surfactant template removal, and thermal annealing of the films, implying that the optical birefringence is due to the mesoscopic channel organization within the silica. Differential scanning calorimetry measurements showed a lack of thermal events that could be associated with crystal–liquid crystal or isotropic melting transitions of the included surfactant up to 250°C also indicate that the observed texture does not arise from the surfactant component of the film. XRD patterns from these films show two reflections, assigned to be the (100) and (200) reflections of an oriented hexagonally packed cylindrical phase, as XRD of powdered films show also the (110) and (210) hexagonal phase peaks.

These thicker films showed a greater shrinkage in *d* spacing upon calcination, attributed to a lower degree of condensation in films grown under lower-acidity conditions relative to those from more acidic preparations. Films that were vacuum dehydrated prior to calcination shrank as a result of this dehydration but retained a greater degree of mesostructural ordering after calcination, pointing to the retention of water in the as-prepared films. Thermogravimetric analysis of the as-synthesized film showed the expected weight changes due to loss of water below 100°C, surfactant template around 270°C and water from condensation of framework hydroxyls around 360 and 600°C. The total weight decrease was around 60–70%, which is high compared with bulk mesoporous silica preparations, presumably because of low framework condensation and higher relative amounts of surfactant incorporation. ^{29}Si NMR also pointed to low degrees of framework condensation in the thicker films compared with that of thinner films from more highly acidic preparations. TEM of microtomed sections of films indicated that the orderings of the film were approximately the same at the top and bottom interfaces. However, films formed from synthesis mixtures with a shorter mixing period had a rougher surface, showing varied thickness as well as a domain structure. These differences were suggested to arise from two modes of film formation, one initiated by silicate liquid crystal seeds at the air–water interface which grow and coalesce, and the other involving formation of a continuous silicate liquid crystal surface film, with a

gradual array of intermediate structures forming as the degree of stirring, and thus the homogeneity of the initial solution increased.

The thicker mesoporous silica films could also be grown on substrates such as glass and mica. On glass surfaces, discrete birefringent patterns instead of the fan-type textures were observed in the polarized optical micrographs even for longer mixing times, owing to local nucleation and growth of concentrically aligned tubules. On mica, light, grey and dark areas were observed in polarized optical micrographs, corresponding to areas of tubules aligned along the hexagonal *a* and *b* axes of the mica surface.

Films grown at the air–water interface were also functionalized with silicon clusters through a mild chemical vapour deposition treatment using disilazane on the as-prepared film, that is with the surfactant template intact in the channels (Dag *et al.* 1999a). The low degree of silica polymerization in the walls of this film enabled the adsorption of disilyl precursors into the walls where anchoring on the high population of SiOH sites occurred. Silicon clustering reactions were confined to spaces between surfactant molecules, producing silicon clusters at temperatures around 100–140°C. The resulting films were bright yellow and showed yellow–orange photoluminescence. As well as photoluminescence analysis, the FTIR, Fourier transform Raman and ^{29}Si NMR data suggested that non-oriented silicon clusters with a size below 2 nm had been formed within the channels of the mesoporous silicate film.

3.2.2. *Formation of three-dimensional hexagonal films*

Silicate–surfactant films grown at the air–water interface consisting of hcp interconnected ellipsoids, having $P6_3/mmc$ symmetry, were reported by Tolbert *et al.* (1997). These films were produced from dilute acidic TEOS solutions at room temperature or 80°C, using a gemini surfactant with a C_{18}, C_{20} or C_{16} alkyl chain connected to a dimethyl quaternary ammonium that was attached via a three-carbon chain spacer to a trimethylammonium head group. The large, highly charged head group altered the packing parameter of the surfactant micelles to favour the 3D hexagonal structure. XRD patterns showed only one or two peaks assigned to the (002) peak of the $P6_3/mmc$ phase, but TEM images show hexagonal symmetry perpendicular to the *c* axis and a cubic (minor) orientation observed in thin sections of the film near edges. Films were also grown on mica and showed the (200) and (400) diffraction peaks in XRD patterns. SEM images showed the early stages of growth to consist of overlapping circular or hexagonal domains of micelle-templated silica for films formed using the gemini surfactant template, reflecting the hexagonal packing of spherical micelles within the structure. In contrast, a film templated with C_{16}TAB, which forms films with 2D hcp symmetry (cylinders), formed elongated domains. AFM of the gemini surfactant adsorbed on mica in the absence of TEOS showed hcp spherical micelles, which were suggested to serve as nucleation points for the growth of the mesophase silicate composite. As the films grown on mica were synthesized at 80°C, they showed much less shrinkage (8%) upon calcination than was observed for the room-temperature air–water interface films. However, as the films on mica were bonded to the mica substrate, this shrinkage caused some cracking that was not observed for the air–water interface films despite their larger degree of shrinkage. SEM images of the film–solution interface of dried films templated with gemini surfactant grown at the air–water interface showed a similar hexagonal domain structure to that observed for the gemini-templated films grown

on mica. It was suggested that the weak interaction between the surfactant micelle and the silicate cation in acidic syntheses, mediated by the counteranion of the surfactant (in this case Cl^-) enabled the surfactant self-assembly at interfaces to be energetically significant compared with the stabilization resulting from mesophase assembly. This allowed surfactant surface assemblies as observed by AFM on the mica surfaces to remain intact as an array of hcp spherical micelles, despite the presence of silicate ions, and to act as nucleation sites for the formation of oriented silicate–surfactant films with 3D hexagonal symmetry. The porosity in these 3D hexagonal films was likely to retain a component perpendicular to the plane of the films, allowing diffusion normal to the plane of the film, making them potentially more useful as membranes than the aligned cylindrical pores of the 2D hexagonal mesophase films.

3.2.3. *Formation through accumulation of surfactant–silica micelles at the interface:* in-situ *studies*

A more direct series of *in-situ* studies on the growth of mesoporous silicate–surfactant films at the air–water interface has been carried out using X-ray reflectometry by Brown *et al.* (1997, 1998), Holt *et al.* (1999) and Ruggles *et al.* (1999, 2000). An initial X-ray reflectivity study indicated that the formation of the mesostructured film occurred after a lengthy induction period at room temperature for a dilute acidic aqueous TEOS solution using C_{16}TAB as the surfactant template. In a covered static solution kept at constant humidity, film formation did not occur for 10 h. Diluting the synthesis solution delayed film formation for almost 23 h. Following this induction period the X-ray reflectivity pattern showed the rapid development of peaks assigned to the ordered mesophase structure with a repeat distance of 44 Å. These peaks reached saturation values of the intensity after 3 h. During the preceding induction period, the initial air–water interface was reported to have a fringe in the reflectivity with a maximum that was close to the wave-vector of the first strong maximum in the diffraction from the subsequently crystallized film. Fitting of the reflectivity indicated the formation of a layered structure at the interface, although it was noted that it was not possible to distinguish a layer of cylindrical surfactant micelles oriented parallel to the surface from a bilayer structure using only specular reflectivity. In later work, grazing-incidence synchrotron X-ray diffraction was used to show that the structure did in fact contain oriented cylindrical micelles (Holt *et al.* 1999). A 2D hexagonal diffraction pattern representing the in-plane ordering of the first two to three layers of film was observed to form at the interface at the end of the induction period. The (10), (01) and $(\bar{1}1)$ diffraction peaks were observed to develop out of weak diffraction streaks indicating a transition from a disordered to ordered phase at the surface. The (20), (02) and $(\bar{2}2)$ reflections were observed to form after further reaction time. A structure consisting of bundles or domains several hundred nanometres across, of surface-oriented hexagonally packed cylindrical micelles was proposed, although the possibility of an hcp spherical micellar structure was not discounted. After long-term film growth, the development of weak broad bumps in the positions corresponding to the (10) and $(1\bar{1})$ reflections was suggested to correspond to diffraction from the small fraction of the surface domains that was oriented non-parallel to the interface and so did not satisfy the diffraction condition for those spots.

Further work on this system by the same group using a combination of X-ray and neutron specular reflection (Brown *et al.* 1998) reported the development of a

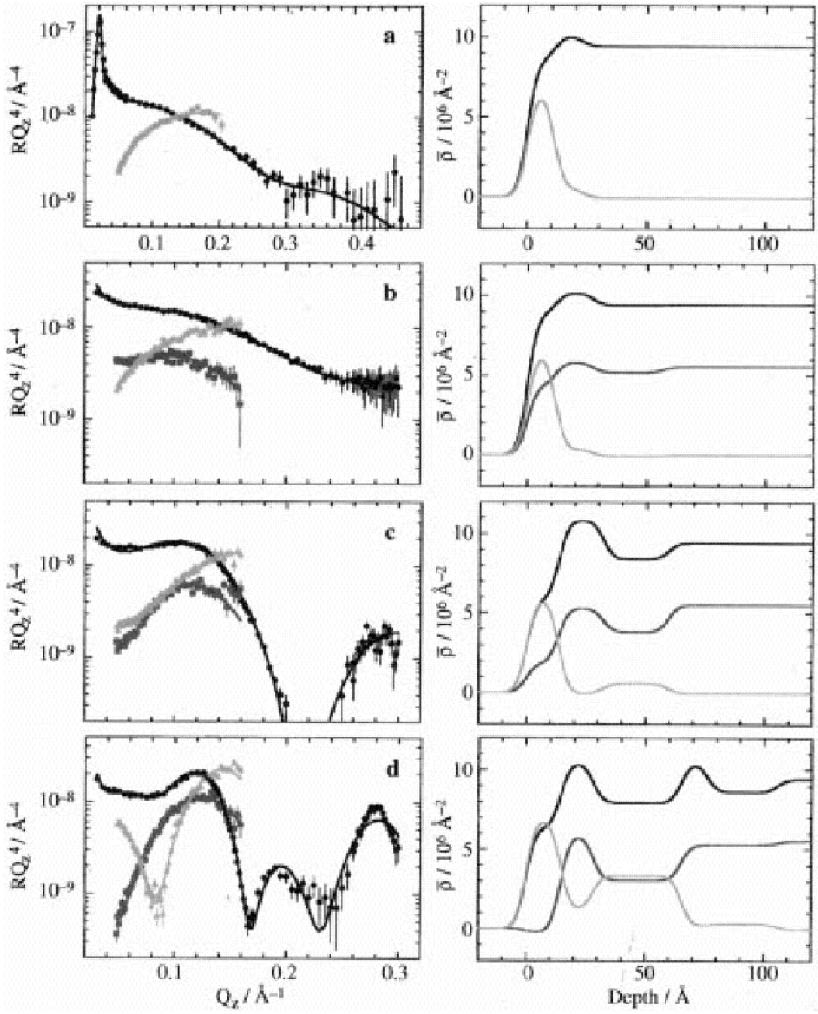

Figure 23. RQ_z^4 versus Q_z (left) and model scattering length density profiles (right) for (*a*) surfactant-only solutions, (*b*)–(*d*) silicate–surfactant solutions after (*b*) 25%, (*c*) 75% and (*d*) 90% of the time required for the diffraction peaks to appear. They show the increasing development of high-scattering-length-density silica-filled regions between lower-scattering-length-density surfactant-filled regions at the interface: (——), X-ray data for h_{33}-C_{P16}TACl in H_2O; (⋯⋯), for contrast-matched water neutron data for d_{33}-C_{16}TAB in air; (⋯⋯), neutron data for h_{33}-C_{16}TACl in D_2O. The lines in the RQ_z^4 versus Q_z plots are best fits to the data. The neutron data for $Q_z > 0.16\,\text{Å}^{-1}$ represents the sample-dependent background and have been excluded from the figure for clarity. (Reprinted with permission from Brown *et al.* (1998). © American Chemical Society 1998.)

layered structure perpendicular to the interface that was composed of alternating layers of silica and surfactant. Initially the interface resembled that for a C_{16}TAB solution in the absence of silica in the subphase, but with increasing density in the head-group region of the surfactant layer over time, followed by further accretion of a surfactant layer below this, eventually forming five layers prior to the sudden growth of diffraction peaks belonging to the composite film (figure 23). It was noted

that the subphase was also present in the surfactant layers, but changes in the scattering from these layers with time indicated that the subphase was successively excluded from this layer as it became more complete. Changing the counterion from bromide to chloride made no significant difference to the observed growth patterns, although raising the temperature from 25 to 30°C increased the rate of reaction by a factor of four. Microanalytical analysis of the final films indicated the presence of $C_{16}TA^+$, silica species and halide present in the approximate molar ratio 1:2:1, consistent with the counterion-mediated $S^+X^-I^+$ mechanism proposed for surfactant-templated silicate formation in acidic media.

Diffraction from fully grown films harvested from the surface of the synthesis solutions on to substrates or into capillaries was also studied by this group (Ruggles *et al.* 1999). Films were lifted on to silicon substrates while wet so that either the film–air interface or the film–solution interface was uppermost. The observed patterns were described in terms of five components:

(*a*) a primitive cubic cell of approximate size 100 Å called *Pm*3*n*;
(*b*) a primitive cubic cell of approximate size 100–108 Å;
(*c*) a series of three orders from a *d* spacing of about 41 Å called hexagonal;
(*d*) the known C_{16}TAB unit cell;
(*e*) the broad peak characteristic of amorphous silica at about $Q = 1.5\text{Å}^{-1}$.

Fresh wet films prepared with C_{16}TAB as the template were reported to have patterns that were indexed with the large *Pm*3*n* unit cell and also the smaller cubic subcell. Wet films stored in capillaries without the synthesis liquor showed only the larger cubic unit cell, as did the bottom surface of the same film mounted on silicon, while the top surface showed the three peaks of the hexagonal phase with 41 Å *d* spacing. The hexagonal peaks from the top surface were noted to appear at the same position as the (120), (240) and (360) cubic Bragg peaks from the bottom surface. A film from the same preparation allowed to dry before mounting in a capillary showed only the hexagonal phase peaks. These results were interpreted to suggest that the freshly formed and harvested films consisted of a highly ordered cubic array of spherical micelles in the silica framework including a subcell indicating silica organization, which evolved during drying towards a less ordered hexagonal phase through loss of the subcell and then the higher-order cubic peaks. The absence of cubic peaks in *in-situ* reflectivity experiments, however, suggested that the formation of the cubic phase occurred as a response to the disturbance of the film caused by harvesting, and that the structure of the initially grown and undisturbed films could be neither cubic nor hexagonal but some precursor structure capable of forming either symmetry as the film evolved under different conditions. It proved possible to stabilize the cubic phases via the addition of glycerol or polyethylene glycol into the synthesis mixture. The addition of glycerol promoted the formation of the cubic phase plus cubic subcell, resulting in many more diffraction peaks in the patterns that could be assigned to these phases. The initial film appeared to incorporate little glycerol but later slowly incorporated the glycerol, swelling slightly while the subcell peaks developed. Polyethylene glycol containing samples also showed well-developed cubic subcell peaks.

Variation in the chain length of the primary template surfactant and the ionic strength of the synthesis solutions were then also investigated by Ruggles *et al.* (2000) to test the generality of their proposed mechanism of structure transformation and to investigate processes occurring during the induction period. Induction times

were reported to be much shorter for longer-chain C_nTAB and C_nTACl surfactants, and the induction period was not observed at all for C_{18}TAB-templated syntheses at 25°C. Ordering of the micellar structure within the film resulted in *in-situ* diffraction peaks in X-ray reflectivity measurements only for alkyl chain lengths longer than C_{12}, although only in the presence of NaCl in the subphase for C_{14}TACl solutions. C_{12}-containing films removed from the surface contained only a broad maximum at 37 Å consistent with a glass of touching micelles. The amount of NaCl required to cause immediate formation of structure in the C_{14}TACl films was equivalent to that which caused a spherical-to-cylindrical micellar phase transition in aqueous solutions of C_{14}TACl in the absence of silica. Lower amounts of salt (NaCl added to C_{14}TACl or NaBr to C_{14}TAB solutions) added to the polymerizing silica-containing solution reduced the length of the induction period and higher amounts of salt increased the number of observed diffraction peaks. The effect of salt on a C_{16}TAB-containing synthesis had similar results. Temperature cycling of a C_{18}TAB-templated silica–surfactant film synthesis showed that it was possible for the growing film to change symmetries from a hexagonal (high-temperature) phase to a lamellar (low-temperature) phase repeatedly during film growth, indicating a low degree of silica polymerization at this stage of film formation. As well as the expected increase in unit-cell size with increasing chain length, it was also observed that films grown from the bromide anion syntheses were consistently larger in cell size, although this effect decreased with increasing chain length, and had shorter induction periods. The bromide anion is less hydrated than the chloride anion and may bind to the micelle surface more strongly than the chloride, becoming incorporated in the silica–surfactant structure and increasing the apparent micelle size. The bromide-containing surfactant also undergoes a sphere-to-rod micellar transition at lower concentrations and is more sensitive to the salt concentration than is the chloride analogue. From these results it was proposed that the rapid nucleation of the film observed at the end of the induction period is due to a sphere-to-rod micellar transition occurring in the subphase, induced by the reduction in ethanol concentration due to evaporation, the increasing polymerization of the silicate species in solution and, in some cases, to the addition of salt which promotes that transition.

3.2.4. *Formation of structure through a disorder–order transition*

Another detailed study on the formation of mesoscopic silica thin films was carried out using electron microscopy by Yang *et al.* (2000). In this report, films were grown at the air–water interface under dilute acidic (pH less than 2) conditions from TEOS and C_{16}TACl solutions with one solution split between several containers and the growing film harvested on to TEM grids at intervals, air dried over a few minutes, calcined embedded in resin and ultramicrotomed for inspection by SEM and TEM. Under the conditions used, a continuous film that was observed visually developed after about 5 h and was measured to be about 20 nm thick. These films could be extracted whole from their containers after about 1 day. The solution turned cloudy after 8–10 h owing to the formation of suspended particles that settled to the bottom of the container within a day. The films were initially smooth but developed wrinkles over several days (one to ten per centimetre and 10–30 mm in length), and the size of these wrinkles increased with time. Sample collection disrupted the surface film, leaving a small hole where the grid penetrated the surface, even for the earliest time samples collected (immediately after pouring solution into containers). The film regrew over the holes, but they remained visible as a defect

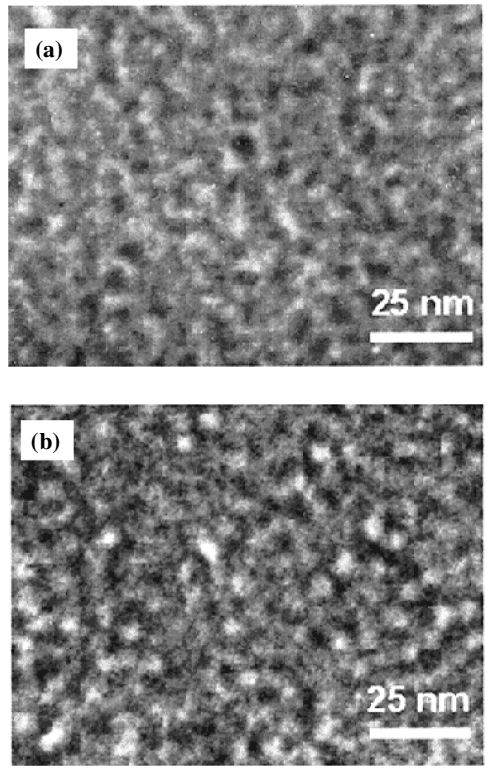

pattern with the same size and shape as the TEM grid. This suggests that some structure was present at the earliest stages of growth to record this perturbation. Film regrowth occurred throughout the first 2 days of growth, and further growth could be induced by adding more TEOS to the subphase. Samples taken at the earliest times were found to contain a disordered structure (figures 24 (*a*) and (*b*)). After 9 h a mixture of both ordered and disordered regions were observed with regions of hexagonal order surrounded by regions where the channels remained disordered (figure 24 (*c*)). Films grown for 2 days showed a thin disordered region (about 20 nm thick) at the film–water interface but regular hexagonal order was present in the film bulk with an average channel spacing of 4 nm (figure 24 (*d*)).

Cross-sectional TEM images showed that the tubules were roughly parallel to the interface; however, they were not always straight. The films were made up of larger areas of distinct tubule organization with a transition region between them, but no gross defects such as dislocations or massive faults. These results indicated that the silicate and surfactant moieties begin to accumulate at the surface immediately upon mixing in an initially amorphous film, which then grew through the accretion of silica-coated micelles. Order arose in the film through the reorganization of a disordered phase in which the micellar channels form organized regions within the amorphous structure. The delay associated with the initial appearance of these domains corresponded roughly to the induction period observed in the work of Brown *et al.* (1997, 1998) (see above). Ordered domains then promoted the organization of surrounding material, and interfacial interactions imposed an energy constraint on the orientation of the channels, causing them to be aligned parallel to

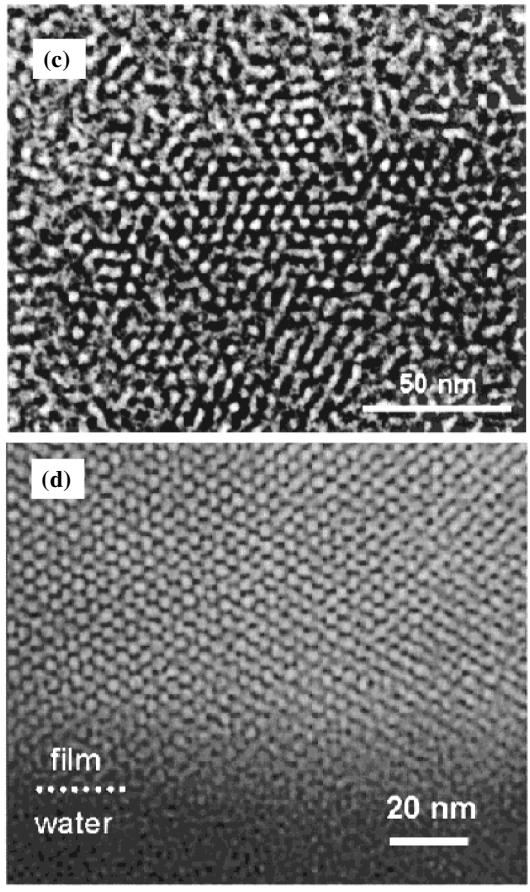

Figure 24. TEM images collected on gold grids at elapsed times of (*a*) 0 and (*b*) 4 h, indicating the disordered structure that can be observed throughout the induction period. (*c*) Cross-sectional TEM image of a film collected at the end of the induction period. Regions with hexagonal packing order are surrounded by disordered material. (*d*) Cross-sectional TEM image of the final film near the water–film interface. The film was collected after growth for 2 days. (Reprinted in part with permission from Yao *et al.* (2000). © 2000 American Chemical Society.)

the interface. The air–water interface was assumed to be an environment intermediate in energy between strongly interacting solid surfaces and bulk solution where, in the absence of a surface, particles are formed. Disorder-to-order transitions have also been observed in the formation of films from dip coating (Lu *et al.* 1997), as discussed above. It was also noted that, while the hexagonally packed channels oriented parallel to the interface was a strongly preferred organization, this was not always observed. Areas of cubic phase ordering, and of channels perpendicular to the interface were also reported, and ascribed to more energetically unfavourable configurations trapped by the disorder-to-order transition.

The air–film interface was also reported to be smoother than the film–water surface. Both surfaces appeared to consist of smooth ribbons which, for the air–film side, lie in the plane of the film (figure 25). On the film–water side these ribbons protrude out of the plane of the surface. This may be because the energy interaction

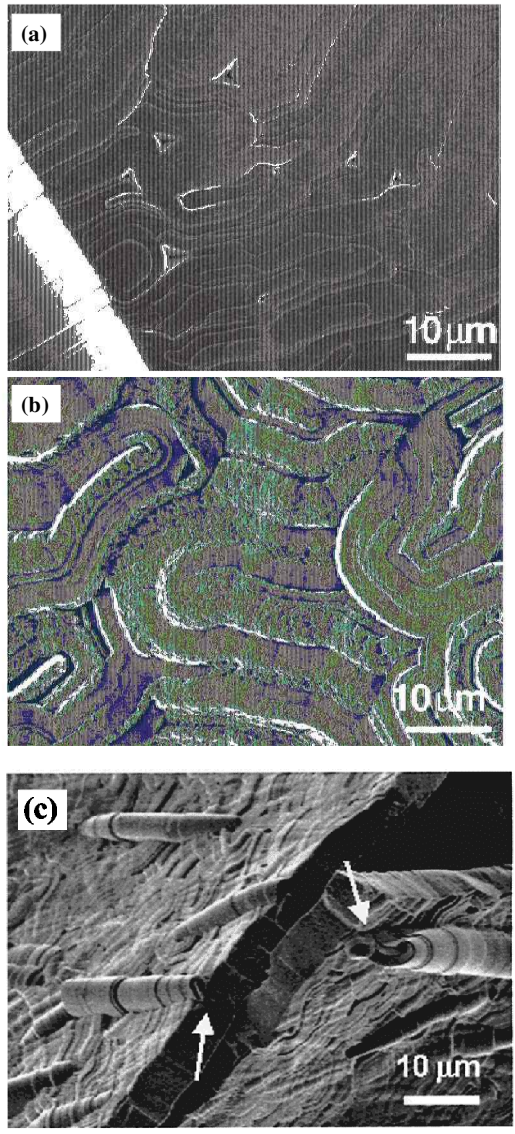

Figure 25. SEM images of the film grown at the air–water interface: (*a*) air–film surface; (*b*) film–water surface. (*c*) Cross-sectional SEM image of a film viewed nearly parallel to the surface, revealing that the particle like-ribbons are a continuous part of the film and showing more pronounced ribbon protrusions. The image is taken from a film grown at pH 0. (Reprinted in part with permission from Yao *et al.* (2000). © 2000 American Chemical Society.)

imposed by the interface diminishes as the film grows thicker, so that at some critical thickness (1–2 μm) the ribbon of channels is no longer confined to the plane of the film and begins to curl in three dimensions. The critical thickness was expected to be larger for strongly interacting surfaces such as mica and smaller for the air–water interface, and this was indeed observed. In more acidic solutions the ribbon protrusions were longer, but in all cases they appeared to begin within the bulk of

the film and not at the air–film interface. On both sides, microindentations and triangular pits were seen and were suggested to be due to the densification of the mesoporous silica during the rearrangement of disordered material into packed channels around multiple nucleation sites as well as the continuing polymerization of the silicate. This densification leads to the formation of voids within the body. Particles recovered from the same growth solutions showed similar ribbon morphologies, although not confined by the presence of an interface and also microindentations. The particles showed a disordered internal structure with some evidence that ordered domains developed after longer periods of growth, so that these also underwent a disorder-to-order transition sharing a common mechanism with the film growth process.

3.2.5. *Formation through accumulation of mesostructured particles at the interface:* in-situ *studies*

Off-specular X-ray reflectivity (Edler *et al.* 2001) and Brewster angle microscopy (BAM) (Edler *et al.* 2000), however, revealed a more complex film growth mechanism. These techniques were used by Edler *et al.* to study the *in-situ* growth of mesostructured films grown from dilute acidic solutions of TMOS in the presence of C_{16}TAB with higher time resolution than was reported by earlier groups. In the earlier paper (Edler *et al.* 2000), BAM images of the air–solution interface showed the rapid development of a solid film after a lengthy induction period. During the induction period, rapidly moving high contrast point features were observed on the liquid surface. These point features were 5–10 μm in size and increased slightly in number with time, although similar features were also observed on the surface of a

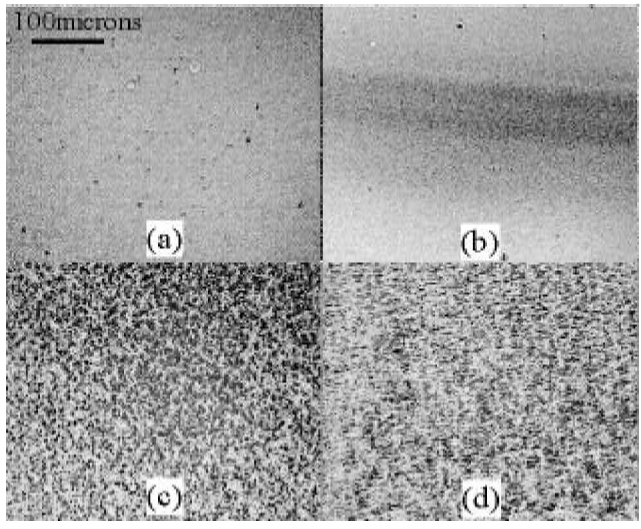

Figure 26. BAM pictures following the evolution of a silica–surfactant composite film at the air–water interface (*a*) during the induction period, (*b*) just after the onset of film growth and (*c*), (*d*) after growth and coarsening of the film at the interface. (Reprinted from Microporous Mesoporous Mater., 44–45, Edler, K. J., Goldar, A., Hughes, A.V., Roser, S. J. and Mann, S. "Structural studies on surfactant templated silica films grown at the air/water interface", 661–670 © (2001), with permission from Elsevier Science.)

solution of CTAB in 0.2 M HCl in the absence of TMOS. The appearance of these features was suggested to be consistent with a model in which the surfactant formed a monolayer owing to a surface excess at the air–water interface with polysilicate binding to the head groups in discrete regions, causing the formation of local domains with modified thickness or molecular orientation, which were visible by BAM. At the end of the induction period, a brief homogenizing of the surface was observed together with the cessation of movement of features on the surface, followed by the rapid development of many small areas of higher contrast, of similar size to the original point features. These small bright spots increased rapidly in number until the interface was covered, when they started to merge, forming a continuous fibrous network structure, which continued to grow and coarsen with time (figure 26). Overnight the film developed macroscopic wrinkling, possibly because of drying of the film and further silica condensation. X-ray reflectometry showed this film to contain two Bragg peaks that were attributed to an oriented lattice of hcp cylindrical channels aligned parallel to the air–solution interface. Surface pressure was also used to follow the film formation process, showing a reproducible surface pressure rise and fall during the induction period which did not correspond to structures visible by BAM, and a sharp rise at the onset of visible film formation followed by an equally sharp fall as the growing film became attached to the surface pressure sensor plate.

The later paper (Edler *et al.* 2001) continued work on the film growth from TMOS–C_{16}TAB in 0.2 M HCl using off-specular synchrotron X-ray reflectivity to follow the reaction at the air–solution interface. The use of the off-specular geometry allowed measurements to be taken with 1 min time resolution, allowing investigation of the rapid film development phase as well as the induction phase. In these measurements it was found that diffraction peaks appeared after an induction period, on time scales similar to that observed for the appearance of a visible film using BAM. The diffraction peaks were assigned to a layered structure with a repeat distance of 44 Å. At the end of the induction period the peaks appeared and grew in intensity, but not in peak width. This suggested that the structure did not form from small ordered domains that grew to cover the surface, but from the aggregation of preformed ordered particles at the interface. It was also observed that the specularly reflected intensity decreased as the diffraction peaks increased, indicating an increasing mesoscale roughness at the surface. This was also indicated by the increase in the intensity in the Yoneda wing, a feature due to scattering from the surface at the critical angle. A model based on the packing of ordered particles at the interface was used to fit the increase in intensity for the first-order diffraction peak. The results of this fit were then used to describe the behaviour of the second-order diffraction peak, the decay in the specularly reflected intensity and the increase in the Yoneda wing scattering, showing that the model was consistent with all the observed scattering features. Prior to the end of the induction period, one further peak was observed to develop, which appeared unrelated to the diffraction peaks that grew in at the end of the induction period. It was suggested that this peak may have indicated the presence of a precursor layered structure at the interface which developed on the same time scale as the increase in surface pressure noted in the previous paper, but which did not correspond to visible film growth in the Brewster angle microscope. This layered structure may have had some structure-directing role in the further development of the film but further work was required to determine its role.

3.2.6. *Spontaneous film formation from alkaline solutions*

X-ray reflectivity was also used in the study of silica–surfactant structures grown at the air–water interface in an alkaline solution of TEOS and C_{16}TAB (Roser *et al.* 1998). For a solution with an unmodified interface, a single micellar layer of a silicate–surfactant film was reported to be present from the earliest stage of the reaction. For an interface modified with a spread monolayer of an insoluble surfactant, phosphatidylcholine, a similar single micellar layer was observed, with a slightly higher density, suggesting that the monolayer promoted the nucleation of a more densely packed layer of silica-coated micelles. It was not possible to fit the data with a layer of hemispherical micelles such as had been proposed as the initial stage for nucleation of surfactant-templated films from acidic solutions. Film growth was followed for 3 days. After this time the film grown under the phosphatidylcholine monolayer showed five distinct peaks in the fitted scattering length density profile, which resulted in a broad Bragg peak centred on a *d* spacing of 39 Å in the X-ray pattern. The calculated density was less than that expected from a perfectly ordered structure, but the observed *in-situ* Bragg peak in the reflectivity was consistent with powder XRD and electron diffraction data from the same film harvested from the surface, confirming formation of hexagonally packed cylinders in the mesophase. In contrast the silica–surfactant structure grown at the unmodified interface showed a less well-developed reflectivity pattern and no Bragg peak after 48 h, indicating significantly less ordering in this system. The time dependence of the development of the Bragg peak under the phosphotidylcholine monolayer was measured, with the peak discernible after 4 h and clearly visible after 1 day. After this point the peak did not change further in position, width or intensity; however, the study showed that the presence of a secondary template of insoluble surfactant at the air–water interface could nucleate a surfactant–silicate mesostructure which otherwise did not form.

4. Other methods of film growth

4.1. *Pulsed-laser deposition*

Pulsed-laser deposition of previously templated surfactant-containing oxides has been used as a method of creating continuous thin (tens of nanometres to several micrometres) films of mesophase material on to a variety of solid substrates. This also has the advantage of being able to coat non-flat surfaces. The process involves striking a molecular sieve target with an intense laser beam, which results in the ejection of atoms, ions and fragments containing template that deposit on to a substrate. Continuous well-adhered films of nanometre-scale particles result, although some rearrangement takes place during the subsequent processing steps. A number of papers on this method have been published by Gimon-Kinsel and Balkus (1998, 1999) and Balkus *et al.* (2000). The earlier work concerns films made from niobium oxide mesophases prepared by the covalent S—I route from niobium(V) ethoxide and dodecylamine. These films were deposited on to a TiN-coated silicon substrate and were initially disordered. Following hydrothermal treatment in the presence of the bulk niobium oxide mesophase used for the pulsed-laser deposition a worm-like interconnected pore structure (32 Å diameter from TEM) that was stable to template removal by washing was formed. The high-surface-area film was tested as a sensor for capacitance changes owing to changes in humidity.

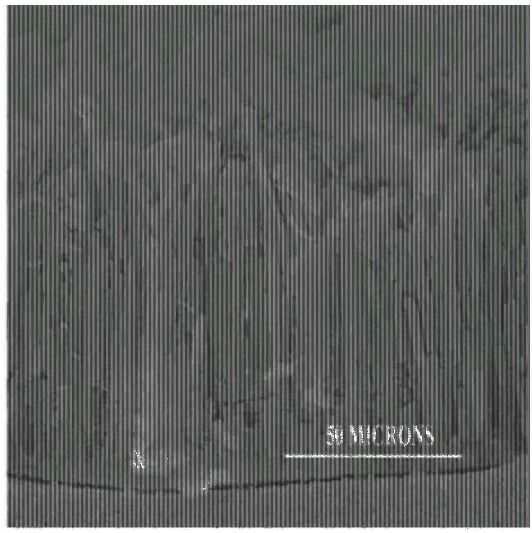

Figure 27. SEM cross-section of an oriented MCM-41 mesoporous molecular sieve film after pulsed-laser deposition and hydrothermal treatment having a worm-like morphology. (Reprinted from Microporous Mesoporous Mater., 38, Balkus, Jr K. J., Scott, A. S., Gimon-Kinsel, M. E. and Blanco, J. H. "Oriented films of mesoporous MCM-41 macroporous tubules via pulsed laser deposition," 97–105 © (2000) with permission from Elsevier Science.)

Pure silica MCM-41 was also deposited on to polished silicon wafer substrates in this manner, resulting in films with a tubule structure of hexagonally packed cylindrical micelle structure that is oriented perpendicularly to the substrate (Balkus *et al.* 2000). To achieve this, the precursor MCM-41 material was synthesized from an alkaline solution of sodium silicate and C_{16}TAB under conditions that would result in a hollow tubular morphology. Ferrocene was adsorbed into the as-prepared MCM-41 to act as a UV adsorbant to adsorb the eximer laser radiation and to prevent formation of defects in the silicate framework during deposition (guest-assisted laser ablation). This composite was pressed into a pellet and pulsed-laser deposited on to silicon wafers or stainless steel porous substrates followed by hydrothermal treatment in the presence of an MCM-41 synthesis gel of the same composition as used to create the original MCM-41 material. This synthesis gel was pH adjusted to between 9.5 and 10 every 24 h for 5 days, a procedure which has been shown to improve the long-range order of bulk MCM-41 materials (Ryoo and Kim 1995, Edler and White 1997). The initially deposited films were about 1.0 μm thick, continuous and tightly packed with no evidence of the worm-like morphology. For films placed face up in the synthesis gel during the hydrothermal treatment, no preferred orientation of the tubules was observed, but a random worm-like morphology formed on the surface. Only when the substrate was placed face down in the synthesis gel did orientation of the tubules making up the film occur. The tubules of approximately 3 μm diameter formed a close-packed layer about 200 μm thick perpendicular to the silicon wafer substrate for distances close to the substrate, but curling over at the surface of the film (figure 27). Reducing the hydrothermal treatment to less than 3 days resulted in non-oriented films, and treatments for 3 days or longer showed oriented films, but also the curling of the tubules at the surface. Physically restricting the film thickness to 19 μm did not prevent formation of the

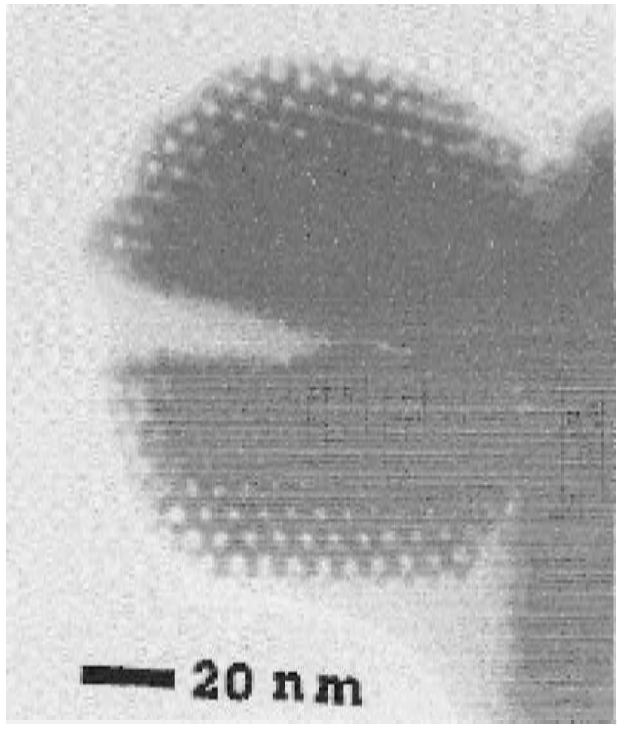

(*a*)

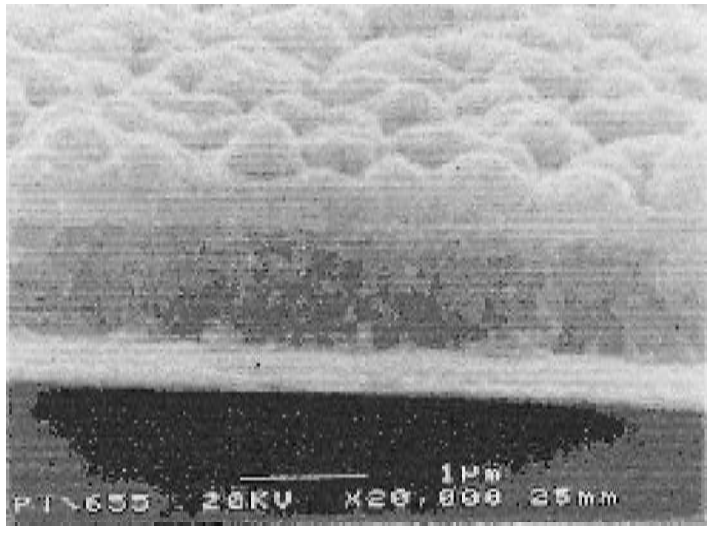

(*b*)

Figure 28. (*a*) TEM image of nanostructured platinum deposited at +0.1 V versus a saturated calomel electrode (SCE), at 25°C, showing the pores end on. (*b*) Cross-sectional SEM image through the electrode of the platinum film deposited at −0.1 V versus SCE; the deposition temperature was 65°C. The films were both deposited with a charge density of about 6.37 C cm^{-2}. (Reprinted in part with permission from Elliott *et al.* (1999a). © 2000 American Chemical Society.)

curved tubules. Precipitate also occurred on a clean silicon wafer suspended in the synthesis gel during the hydrothermal treatment but this did not adhere to the substrate. The deposited films showed XRD patterns corresponding to a well-ordered 2D hexagonal phase with no preferential orientation.

4.2. *Electrodeposition*

Another application of the principle of surfactant templating to create thin films is the electrodeposition method of Attard *et al.* (1997), Elliott *et al.* (1999a,b) and Gollas *et al.* (2000). This group used the direct templating route rather than the co-assembly mechanism, requiring surfactant concentrations of greater than 30 wt% to ensure that a homogeneous liquid crystal phase was obtained and maintained throughout the electrodeposition process. Non-ionic octaethylene glycol monohexadecyl ether ($C_{16}EO_8$) surfactant was used to create a 2D, hexagonally packed cylindrical micelle phase and a platinum film was formed through the reduction of hexachloroplatinic acid in an electroplating solution containing this micelle phase. The pore diameters were found to be about 25 Å and the pores were aligned at 20° to the substrate normal. Pore diameters could be varied by changing the surfactant chain length or by swelling the tail region with a hydrophobic solvent such as heptane. Factors such as electrodeposition temperature, deposition potential and the amount of charge passed were found to change the properties of the resulting porous platinum films (Elliott *et al.* 1999a). Films with highly ordered well-controlled porosity (figure 28) were obtained only when the electrodeposition conditions were controlled to eliminate unwanted side reactions; deposition was carried out at −0.1 V versus SCE and above. The inner walls of the pore structure were rough, and TEM indicated that the channels were not straight, although they extended over several hundred nanometres in length. Polystyrene latex spheres have also been used as templates for the electrodeposition of platinum, palladium and cobalt films to produce polycrystalline films with a macroporous structure (Bartlett *et al.* 2000).

5. Conclusion

The two broad classes of mesophase silicate–surfactant films, namely those created by solvent evaporation methods and those that grow spontaneously at surfaces, appear to have very different formation mechanisms. In the solvent evaporation case, significant silicate polymerization has occurred before the solutions become sufficiently concentrated for surfactant micelles to form. The extent of silicate polymerization is an important factor in controlling the degree of order in the final film as the fractal silicate clusters must be incorporated into the walls separating surfactant micelles without disturbing their developing long-range order. However, contrasting reports of the development of structure occurring initially at the evaporating surface or at the substrate indicate that the details of the mechanism have not been fully worked out, although substantial control over the mesophase structures formed has been achieved.

Films that grow spontaneously at substrate–solution or solution–air interfaces develop out of solutions containing both surfactant micelles and polymerizing silicate species. The formation mechanism for these materials is more directly related to that of the formation of other bulk morphologies of silicate–surfactant materials from solution preparations using similar pH conditions. The film structure formed is

highly dependent upon synthesis conditions and work continues on the details of the self-assembly mechanisms in these systems.

References

Aksay, I. A., Trau, M., Manne, S., Honma, I., Yao, N., Zhou, L., Fenter, P., Eisenberger, P. M., and Gruner, S. M., 1996, *Science*, **273**, 892.

Anderson, M. T., Martin, J. E., Odinek, J. G., and Newcomer, P., 1996, *Microporous and Macroporous Materials*, *Materials Research Society Symposium Proceedings*, Vol. 431, edited by R. F. Lobo, J. S. Beck, S. L. Suib, D. R. Corbin, M. E. Davis, L. E. Iton, and S. I. Zones (Pittsburgh, Pennsylvania: Materials Research Society), pp. 217–223).

Antonelli, D. M., Nakahira, A., and Ying, J. Y., 1996, *Inorg. Chem.*, **35**, 3126.

Antonelli, D. M., and Ying, J. Y., 1996a, *Chem. Mater.*, **8**, 874; 1996b, *Angew. Chem. Int. Edn Engl.*, **35**, 426.

Attard, G. S., Bartlett, P. N., Coleman, N. R. B., Elliott, J. M., Owen, J. R., and Wang, J. H., 1997, *Science*, **278**, 838.

Attard, G. S., Edgar, M., and Göltner, C. G., 1998, *Acta mater.*, **46**, 751.

Attard, G. S., Glyde, J. C., and Göltner, C. G., 1995, *Nature*, **378**, 366.

Auvray, L., Ayral, A., Dabadie, T., Cot, L., Guizard, C., and Ramsay, J. D. F., 1995, *Discuss. Faraday Soc.*, **101**, 235.

Bagshaw, S. A., Prouzet, E., and Pinnavaia, T. J., 1995, *Science*, **269**, 1242.

Balkus, K. J., Jr, Scott, A. S., Gimon-Kinsel, M. E., and Blanco, J. H., 2000, *Microporous Mesoporous Mater.*, **38**, 97.

Bartlett, P. N., Birkin, P. R., and Ghanem, M. A., 2000, *Chem. Commun.*, 1671.

Baskaran, S., Liu, J., Domansky, K., Kohler, N., Li, X., Coyle, C., Fryxell, G. E., Thevuthasan, S., and Williford, R. E., 2000, *Advd Mater.*, **12**, 291.

Beck, J. S., Vartuli, J. C., Roth, W. J., Leonowicz, M. E., Kresge, C. T., Schmitt, K. D., Chu, C. T.-W., Olson, D. H., Sheppard, E. W., McCullen, S. B., Higgins, J. B., and Schlenker, J. L., 1992, *J. Am. chem. Soc.*, **114**, 10834.

Behrens, P., 1996, *Angew. Chem., Int. Edn Engl.*, **35**, 515.

Bekiari, V., Ferrer, M.-L., and Lianos, P., 1999, *J. phys. Chem.* B, **103**, 9085.

Besson, S., Gacoin, T., Jacquiod, C., Ricolleau, C., Babonneau, D., and Boilot, J. P., 2000a, *J. Mater. Chem.*, **10**, 1331.

Besson, S., Ricolleau, C., Gacoin, T., Jacquiod, C., and Boilot, J.-P., 2000b, *J. phys. Chem.* B, **104**, 12095.

Brinker, C. J., and Scherer, G. W., 1990, *Sol–Gel Science. The Physics and Chemistry of Sol–Gel Processing* (San Diego, California: Academic Press).

Brown, A. S., Holt, S. A., Dam, T., Trau, M., and White, J. W., 1997, *Langmuir*, **13**, 6363.

Brown, A. S., Holt, S. A., Reynolds, P. A., Penfold, J., and White, J. W., 1998, *Langmuir*, **14**, 5532.

Chen, C. Y., Burkett, S. L., Li, H.-X., and Davis, M. E., 1993, *Microporous Mater.*, **2**, 22.

Chen, C.-Y., Xiao, S.-Q., and Davis, M. E., 1995, *Microporous Mater.*, **4**, 1.

Cheng, C.-F., He, H., Zhou, W., and Klinowski, J., 1995a, *Chem. Phys. Lett.*, **244**, 117.

Cheng, C.-F., Luan, Z., and Klinowski, J., 1995b, *Langmuir*, **11**, 2815.

Chia, S., Urano, J., and Tamanoi, F., 2000, *J. Am. chem. Soc.*, **122**, 6488.

Coombs, N., Khushalani, D., Oliver, S., Ozin, G. A., Shen, G. C., Sokolov, I., and Yang, H., 1997, *J. chem. Soc., Dalton Trans.*, 3941.

Corma, A., 1997, *Chem. Rev.*, **97**, 2373.

Cot, L., Ayral, A., Durand, J., Guizard, C., Hovnanian, N., Julbe, A., and Larbot, A., 2000, *Solid St. Sci.*, **2**, 313.

Dabadie, T., Ayral, A., Guizard, C., Cot, L., and Lacan, P., 1996, *J. Mater. Chem.*, **6**, 1789.

Dag, ö., Ozin, G. A., Yang, H., Reber, C., and Bussiére, G., 1999a, *Advd Mater.*, **11**, 474.

Dag, ö., Verma, A., Ozin, G. A., and Kresge, C. T., 1999b, *J. Mater. Chem.*, **9**, 1475.

DAVIS, M. E., CHEN, C.-Y., BURKETT, S. L., and LOBO, R. F., 1994, *Better Ceramics Through Chemistry VI*, Materials Research Society Symposium, Vol. 346, edited by A. K. C. J. B. Cheetham, M. L. Mccartney and C. Sanchez (Pittsburgh, Pennsylvania: Materials Research Society), pp. 831–842.

DI RENZO, F., CAMBON, H., and DUTARTRE, R., 1997, *Microporous Mater.*, **10**, 283.

DI RENZO, F., TESTA, F., CHEN, J. D., CAMBON, H., GALARNEAU, A., PLEE, D., and FAJULA, F., 1999, *Microporous Mesoporous Mater.*, **28**, 437.

DOSHI, D. A., HUESING, N. K., LU, M., FAN, H., LU, Y., SIMMONS-POTTER, K., POTTER, B. G., JR., HURD, A. J., and BRINKER, C. J., 2000, *Science*, **290**, 107.

EDLER, K. J., GOLDAR, A., HUGHES, A. V., ROSER, S. J., and MANN, S., 2001, *Microporous Mesoporous Mater.*, **44–45**, 661.

EDLER, K. J., ROSER, S. J., and MANN, S., 2000, *J. chem. Soc., chem. Commun.*, 773.

EDLER, K. J., and WHITE, J. W., 1997, *Chem. Mater.*, **9**, 1226.

ELLIOTT, J. M., ATTARD, G. S., BARTLETT, P. N., and COLEMAN, N. R. B., 1999a, *Chem. Mater.*, **11**, 3602.

ELLIOTT, J. M., BIRKIN, P. R., BARTLETT, P. N., and ATTARD, G. S., 1999b, *Langmuir*, **15**, 7411.

FAN, H., LU, Y., STUMP, A., REED, S. T., BAER, T., SCHUNK, R., PEREZ-LUNA, V., LÓPEZ, G. P., and BRINKER, C. J., 2000, *Nature*, **405**, 56.

FENG, J., HUO, Q., PETROFF, P. M., and STUCKY, G. D., 1997, *Appl. Phys. Lett.*, **71**, 1887.

FERRER, M., and LIANOS, P., 1996, *Langmuir*, **12**, 5620.

FERRER, M. L., BEKIARI, V., LIANOS, P., and TSIOURVAS, D., 1997, *Chem. Mater.*, **9**, 2652.

FIROUZI, A., ATEF, F., OERTLI, A. G., STUCKY, G. D., and CHMELKA, B. F., 1997, *J. Am. chem. Soc.*, **119**, 3596.

FIROUZI, A., KUMAR, D., BULL, L. M., BESIER, T., SIEGER, P., HUO, Q., WALKER, S. A., ZASADZINSKI, J. A., GLINKA, C., NICOL, J., MARGOLESE, D., STUCKY, G. D., and CHMELKA, B. F., 1995, *Science*, **267**, 1138.

FLANIGEN, E. M., 1980, *Pure appl. Chem.*, **52**, 2191.

FRASCH, J., LEBEAU, B., SOULARD, M., PATARIN, J., and ZANA, R., 2000, *Langmuir*, **16**, 9049.

GALARNEAU, A., DI RENZO, F., FAJULA, F., MOLLO, L., FUBINI, B., and OTTAVIANI, M. F., 1998, *J. Colloid Interface Sci.*, **201**, 105.

GIMON-KINSEL, M. E., and BALKUS, K. J., JR, 1998, *Mesoporous Molecular Sieves, 1998*, Vol. 117, edited by L. Bonneviot, F. Béland, C. Danymah, S. Giasson and, S. Kaliaguine (Amsterdam: Elsevier), pp. 111–118; 1999, *Microporous Mesoporous Mater.*, **28**, 113.

GLINKA, C. J., NICOL, J. M., STUCKY, G. D., RAMLI, E., MARGOLESE, D., HUO, Q., HIGGINS, J. B., and LEONOWICZ, M. E., 1996, *J. Porous Mater.*, **3**, 93.

GOLLAS, B., ELLIOTT, J. M., and BARTLETT, P. N., 2000, *Electrochim. Acta*, **45**, 3711.

GÖLTNER, C. G., and ANTONIETTI, M., 1997, *Advd Mater.*, **9**, 431.

GÖLTNER, C. G., BERTON, B., KRÄMER, E., and ANTONIETTI, M., 1998a, *J. chem. Soc., chem. Commun.*, 2287; 1999, *Advd Mater.*, **11**, 395.

GÖLTNER, C. G., HENKE, S., WEISSENBERGER, M. C., and ANTONIETTI, M., 1998b, *Angew. Chem., Int. Edn*, **37**, 613.

GROSSO, D., BALKENENDE, A. R., ALBOUY, P. A., LAVERGNE, M., MAZEROLLES, L., and BABONNEAU, F., 2000, *J. Mater. Chem.*, **10**, 2085.

HAAG, W. O., 1994, *Zeolites and Related Microporous Materials: State of the Art 1994*, Vol. 84, edited by J. Weitkamp, H. G. Karge, H. Pfeifer, and W. Hölderich (Amsterdam: Elsevier), pp. 1375–1394.

HILLHOUSE, H. W., OKUBO, T., VAN EGMOND, J. W., and TSAPATSIS, M., 1997, *Chem. Mater.*, **9**, 1505.

HILLHOUSE, H. W., VAN EGMOND, J. W., and TSAPATSIS, M., 1999, *Langmuir*, **15**, 4544.

HILLHOUSE, H. W., VAN EGMOND, J. W., TSAPATSIS, M., HANSON, J. C., and LARESE, J. Z., 2000, *Chem. Mater.*, **12**, 2888.

HOLMES, S. M., ZHOLOBENKO, V. L., THURSFIELD, A., PLAISTED, R. J., CUNDY, C. S., and DWYER, J., 1998, *J. chem. Soc., Faraday Trans.*, **94**, 2025.

HOLT, S. A., FORAN, G. J., and WHITE, J. W., 1999, *Langmuir*, **15**, 2540.

HOLT, S. J., REYNOLDS, P. A., and WHITE, J. W., 2000, *Phys. Chem., chem. Phys.*, **2**, 5667.

Honma, I., and Zhou, H. S., 1998, *Advd Mater.*, **10**, 1532.
Honma, I., Zhou, H. S., Kundu, D., and Endo, A., 2000, *Advd Mater.*, **12**, 1529.
Hozumi, A., Yokogawa, Y., Kameyama, T., Hiraku, K., Sugimura, H., Takai, O., and Okido, M., 2000, *Advd Mater.*, **12**, 985.
Hrubesh, L. W., 1990, *Chem. Ind.*, **24**, 824.
Huang, M. H., Dunn, B. S., Soyez, H., and Zink, J. I., 1998, *Langmuir*, **14**, 7331.
Huang, M. H., Dunn, B. S., and Zink, J. I., 2000, *J. Am. chem. Soc.*, **122**, 3739.
Huo, Q., Margolese, D. I., Ciesa, U., Feng, P., Gier, T. E., Sieger, P., Leon, R., Petroff, P. M., Schüth, F., and Stucky, G. D., 1994a, *Nature*, **368**, 317.
Huo, Q., Margolese, D. I., Ciesla, U., Demuth, D. G., Feng, P., Gier, T. E., Sieger, P., Firouzi, A., Chmelka, B. F., Schüth, F., and Stucky, G. D., 1994b, *Chem. Mater.*, **6**, 1176.
Huo, Q., Margolese, D. I., and Stucky, G. D., 1996, *Chem. Mater.*, **8**, 1147.
Inagaki, S., Fukushima, Y., and Kuroda, K., 1993, *J. chem. Soc., chem. Commun.*, 680; 1994, *Zeolites and Related Microporous Materials: State of the Art 1994*, Vol. 84A, edited by J. Weitkamp, H. G. Karge, H. Pfeifer, and W. Hölderich (Amsterdam: Elsevier), pp. 125–132.
Inagaki, S., Koiwai, A., Suzuki, N., Fukushima, Y., and Kuroda, K., 1996, *Bull. chem. Soc. Japan*, **69**, 1449.
Israelachvili, J. N., 1985, *Physics of Amphiphiles: Micelles, Vesicles and Microemulsions*, edited by X. C. Corso (Bologna: Societa Italiana di Fisica), pp. 24–58; 1987, *Surfactants in Solution* (New York: Plenum).
Israelachvili, J. N., Mitchell, D. J., and Ninham, B. W., 1976, *J. chem. Soc., Faraday Trans.* II, **72**, 1527.
Karthaus, O., Cieren, X., Maruyama, N., and Shimomura, M., 1999, *Mater. Sci. Engng*, **C10**, 103.
Kim, J. M., Kim, S. K., and Ryoo, R., 1998, *J. chem. Soc., chem. Commun.*, 259.
Klotz, M., Albouy, P.-A., Ayral, A., Ménager, C., Grosso, D., Van der Lee, A., Cabuil, V., Babonneau, F., and Guizard, C., 2000a, *Chem. Mater.*, **12**, 1721.
Klotz, M., Ayral, A., Guizard, C., and Cot, L., 2000b, *J. Mater. Chem.*, **10**, 663.
Ko, C. H., Kim, J. M., and Ryoo, R., 1998, *Microporous Mesoporous Mater.*, **21**, 235.
Kolodziejski, W., Corma, A., Navarro, M.-T., and Pérez-Pariente, J., 1993, *Solid St. nucl. magn. Resonance*, **2**, 253.
Kresge, C. T., Leonowicz, M. E., Roth, W. J., Vartuli, J. C., and Beck, J. S., 1992, *Nature*, **359**, 710.
Kuroda, K., 1996, *J. Porous Mater.*, **3**, 107.
Lebeau, B., Fowler, C. E., Hall, S. R., and Mann, S., 1999, *J. Mater.*, **9**, 2279.
Liu, J., Bontha, J. R., Kim, A. Y., and Baskaran, S., 1996, *Microporous and Macroporous Materials*, Materials Research Society Symposium Proceedings, Vol. 431, edited by R. F. Lobo, J. S. Beck, S. L. Suib, D. R. Corbin, M. E. Davis, L. E. Iton, and S. I. Zones (Pittsburgh, Pennsylvania: Materials Research Society), pp. 245–250.
Liu, J., Kim, A. Y., Virden, J. W., and Bunker, B. C., 1995, *Langmuir*, **11**, 689.
Lu, Y., Ganguli, R., Drewien, C. A., Anderson, M. T., Brinker, C. J., Gong, W., Guo, Y., Soyez, H., Dunn, B., Huang, M. H., and Zink, J. I., 1997, *Nature*, **389**, 364.
Manne, S., Schäffer, T. E., Huo, Q., Hansma, P. K., Morse, D. E., Stucky, G. D., and Aksay, I. A., 1997, *Langmuir*, **13**, 6382.
Martin, J. E., Anderson, M. T., Odinek, J., and Newcomer, P., 1997, *Langmuir*, **13**, 4133.
Maschmeyer, T., 1998, *Curr. Op. Colloid Interface Sci.*, **3**, 71.
Matijasic, A., Voegtlin, A.-C., Patarin, J., Guth, J. L., and Huve, L., 1996, *J. chem. Soc., chem. Commun.*, 1123.
Melosh, N. A., Davidson, P., and Chmelka, B. F., 2000, *J. Am. chem. Soc.*, **122**, 823.
Miyata, H., and Kuroda, K., 1999a, *Chem. Mater.*, **11**, 1609; 1999b, *Advd Mater.*, **11**, 1448; 1999c *J. Am. chem. Soc.*, **121**, 7618; 2000, *Chem. Mater.*, **12**, 49.
Mokaya, R., and Jones, W., 1996, *J. chem. Soc., chem. Commun.*, , 981.
Moller, K., and Bein, T., 1998, *Chem. Mater.*, **10**, 2950.

MONNIER, A., SCHÜTH, F., HUO, Q., KUMAR, D., MARGOLESE, D., MAXWELL, R. S., STUCKY, G. D., KRISHNAMURTY, M., PETROFF, P., FIROUZI, A., JANICKE, M., and CHMELKA, B. F., 1993, *Science*, **261**, 1299.

NISHIYAMA, N., KOIDE, A., EGASHIRA, Y., and UEYAMA, K., 1998, *J. chem. Soc., chem. Commun.*, 2147.

O'BRIEN, S., FRANCIS, R. J., PRICE, S. J., O'HARE, D., CLARK, S., OKAZAKI, N., and KURODA, K., 1995, *J. chem. Soc., chem. Commun.*, 2423.

OGAWA, M., 1994, *J. Am. chem. Soc.*, **116**, 7941; 1995, *Langmuir*, **11**, 4639; 1996, *J. chem. Soc., chem. Commun.*, 1149; 1997, *Langmuir*, **13**, 1853; 1998, *Supramolec. Sci.*, **5**, 247.

OGAWA, M., IGARASHI, T., and KURODA, K., 1997, *Bull. chem. Soc. Japan*, **70**, 2833.

OGAWA, M., ISHIKAWA, H., and KIKUCHI, T., 1998, *J. Mater. Chem.*, **8**, 1783.

OGAWA, M., and KIKUCHI, T., 1998, *Advd Mater.*, **10**, 1077.

OGAWA, M., KURODA, K., and MORI, J.-I., 2000, *Chem. Commun.*, 2441.

OGAWA, M., and MASUKAWA, N., 2000, *Microporous Mesoporous Mater.*, **38**, 35.

OLSON, D. H., 1970, *J. phys. Chem.*, **74**, 2758.

ORTLAM, A., RATHOUSKY, J., SCHULZ-EKLOFF, G., and ZUKAL, A., 1996, *Microporous Mater.*, **6**, 171.

OZIN, G. A., YANG, H., SOKOLOV, I., and COOMBS, N., 1997, *Advd Mater.*, **9**, 662.

PLYUTO, Y., BERQUIER, J.-M., JACQUIOD, C., and RICOLLEAU, C., 1999, *Chem. Commun.*, 1653.

RAMAN, N. K., ANDERSON, M. T., and BRINKER, C. J., 1996, *Chem. Mater.*, **8**, 1682.

RATHOUSKY, J., SCHULZ-EKLOFF, G., HAD, J., and ZUKAL, A., 1999, *Phys. Chem. chem. Phys.*, **1**, 3053.

REGEV, O., 1996, *Langmuir*, **12**, 4940.

ROSER, S., PATEL, H. M., LOVELL, M. R., MUIR, J. E., and MANN, S., 1998, *J. chem. Soc., chem. Commun.*, 829.

RUGGLES, J. L., HOLT, S. A., REYNOLDS, P. A., BROWN, A. S., CREAGH, D. C., and WHITE, J. W., 1999, *Phys. Chem. chem. Phys.*, **1**, 323.

RUGGLES, J. L., HOLT, S. A., REYNOLDS, P. A., and WHITE, J. W., 2000, *Langmuir,* **16**, 4613.

RYOO, R., and KIM, J. M., 1995, *J. chem. Soc., chem. Commun.*, 711.

RYOO, R., KIM, J. M., KO, C. H., and SHIN, C. H., 1996, *J. phys. Chem.*, **100**, 17718.

RYOO, R., KO, C. H., CHO, S. J., and KIM, J. M., 1997, *J. phys. Chem.* B, **101**, 10610.

SCHACHT, S., HUO, Q., VOIGT-MARTIN, I. G., STUCKY, G. D., and SCHÜTH, F., 1996, *Science*, **273**, 768.

SELLINGER, A., WEISS, P. M., NGUYEN, A., LU, Y., ASSINK, R. A., GONG, W., and BRINKER, J. C., 1998, *Nature*, **394**, 256.

SHIMOJIMA, A., SUGAHARA, Y., and KURODA, K., 1998, *J. Am. chem. Soc.*, **120**, 4528.

SOKOLOV, I., YANG, H., OZIN, G. A., and KRESGE, C. T., 1999, *Advd Mater.*, **11**, 636.

STEEL, A., CARR, S. W., and ANDERSON, M. W., 1994, *J. chem. Soc., chem. Commun.*, 1571.

STUCKY, G. D., MONNIER, A., SCHÜTH, F., HUO, Q., MARGOLESE, D., KUMAR, D., KRISHNAMURTY, M., PETROFF, P., FIROUZI, A., JANICKE, M., and CHMELKA, B. F., 1994, *Molec. Crystals liq. Crystals*, **240**, 187.

SUIB, S. L., 1993, *Chem. Rev.*, **93**, 803.

TANEV, P. T., and PINNAVAIA, T. J., 1995a, *Science*, **267**, 865.; 1995b, *Access in Nanoporous Materials,* edited by T. J. Pinnavaia and M. F. Thorpe (New York: Plenum Press).

TEMPLIN, M., FRANCK, A., DUCHESNE, A., LEIST, H., ZHANG, Y. M., ULRICH, R., SCHADLER, V., and WIESNER, U., 1997, *Science*, **278**, 1795.

TOLBERT, S. H., SCHAFFER, T. E., FENG, J., HANSMA, P. K., and STUCKY, G. D., 1997, *Chem. Mater.*, **9**, 1962.

TRAU, M., YAO, N., KIM, E., XIA, Y., WHITESIDES, G. M., and AKSAY, I. A., 1997, *Nature*, **390**, 674.

VARTULI, J. C., SCHMITT, K. D., KRESGE, C. T., ROTH, W. J., LEONOWICZ, M. E., MCCULLEN, S. B., HELLRING, S. D., BECK, J. S., SCHLENKER, J. L., OLSON, D. H., and SHEPPARD, E. W., 1994a, *Zeolites and Related Microporous Materials: State of the Art 1994*, Vol. 84A, edited by J. Weitkamp, H. G. Karge, H. Pfeifer and W. Hölderich (Amsterdam: Elsevier), pp. 53–60; 1994b, *Chem. Mater.*, **1994**, 2317.

WIRNSBERGER, G., SCOTT, B. J., and STUCKY, G. D., 2001, *Chem. Commun.*, 119.

YANG, H., COOMBS, N., DAG, O., SOKOLOV, I., and OZIN, G. A., 1997a, *J. Mater. Chem.*, **7**, 1755.
YANG, H., COOMBS, N., and OZIN, G. A., 1997b, *Advd Mater.*, **9**, 811; 1997c, *Nature*, **386**, 692; 1998a, *J. Mater. Chem.*, **8**, 1205.
YANG, H., COOMS, N., SOKOLOV, I., and OZIN, G. A., 1996a, *Nature*, **381**, 589; (1997d), *J. Mater. Chem.*, **7**, 1285.
YANG, H., KUPERMAN, A., COOMBS, N., MAMICHE-AFARA, S., and OZIN, G. A., 1996b, *Nature*, **379**, 703.
YANG, H., OZIN, G. A., and KRESGE, C. T., 1998b, *Advd Mater.*, **10**, 883.
YANG, H., VOVK, G., COOMBS, N., SOKOLOV, I., and OZIN, G. A., 1998c, *J. Mater. Chem.*, **8**, 743.
YANG, P., DENG, T., ZHAO, D., FENG, P., PINE, D., CHMELKA, B. F., WHITESIDES, G. M., and STUCKY, G. D., 1998d, *Science*, **282**, 2244.
YANG, P. D., WIRNSBERGER, G., HUANG, H. C., CORDERO, S. R., MCGEHEE, M. D., SCOTT, B., DENG, T., WHITESIDES, G. M., CHMELKA, B. F., BURATTO, S. K., and STUCKY, G. D., 2000, *Science*, **287**, 465.
YANG, S. M., SOKOLOV, I., COOMBS, N., KRESGE, C. T., and OZIN, G. A., 1999a, *Advd Mater.*, **11**, 1427.
YANG, S. M., YANG, H., COOMBS, N., SOKOLOV, I., KRESGE, C. T., and OZIN, G. A., 1999b, *Advd Mater.*, **11**, 52.
YAO, N., KU, A. Y., NAKAGAWA, N., LEE, T., SAVILLE, D. A., and AKSAY, I. A., 2000, *Chem. Mater.*, **12**, 1536.
ZANA, R., FRASH, J., SOULARD, M., LEBEAU, B., and PATARIN, J., 1999, *Langmuir*, **15**, 2603.
ZHANG, J., LUZ, Z., and GOLDFARB, D., 1997, *J. phys. Chem.* B, **101**, 7087.
ZHAO, D., FENG, J., HUO, Q., MELOSH, N., FREDRICKSON, G. H., CHMELKA, B. F., and STUCKY, G. D., 1998a, *Science*, **279**, 548.
ZHAO, D., HUO, Q., FENG, J., CHMELKA, B. F., and STUCKY, G. D., 1998b, *J. Am. chem. Soc.*, **120**, 6024.
ZHAO, D., YANG, P., CHMELKA, B. F., and STUCKY, G. D., 1999, *Chem. Mater.*, **11**, 1174.
ZHAO, D., YANG, P., MARGOLESE, D. I., CHMELKA, B. F., and STUCKY, G. D., 1998c, *J. chem. Soc., chem. Commun.*, 2499.
ZHAO, D., YANG, P., MELOSH, N., FENG, J., CHMELKA, B. F., and STUCKY, G. D., 1998d, *Advd Mater.*, **10**, 1380.
ZHAO, X. S., LU, G. Q., and MILLAR, G. J., 1996, *Ind. Engng chem. Res.*, **35**, 2075.
ZHOU, H. S., KUNDU, D., and HONMA, I., 1999, *J. Eur. Ceram. Soc.*, **19**, 1361.
ZHOU, W., HUNTER, H. M. A., WRIGHT, P. A., GE, Q., and THOMAS, J. M., 1998, *J. phys. Chem.* B, **102**, 6933.
ZHOU, W., and KLINOWSKI, J., 1998, *Chem. Phys. Lett.*, **292**, 207.